

January 01, 2010

Precoding and equalization for MIMO broadcast channels with applications in spread spectrum systems

Jin He

Northeastern University

Recommended Citation

He, Jin, "Precoding and equalization for MIMO broadcast channels with applications in spread spectrum systems" (2010). *Computer Engineering Dissertations*. Paper 9. <http://hdl.handle.net/2047/d20002063>

This work is available open access, hosted by Northeastern University.

**PRECODING AND EQUALIZATION FOR MIMO
BROADCAST CHANNELS WITH APPLICATIONS IN
SPREAD SPECTRUM SYSTEMS**

A Dissertation Presented

by

Jin He

to

The Department of Electrical and Computer Engineering

in partial fulfillment of the requirements

for the degree of

Doctor of Philosophy

in

Communications and Digital Signal Processing

Northeastern University

Boston, Massachusetts

September 2010

Abstract

Proliferation of mobile data applications has increased the demand for wireless communication systems offering high throughput, wide coverage, and improved reliability. The main challenges in the design of such systems are the limited resources—such as constrained transmission power, scarce frequency bandwidth, and limited implementation complexity—and the impairments of the wireless channels, including noise, interference, and fading effects. Multiple-Input Multiple-Output (MIMO) communication has been shown to be one of the most promising emerging wireless technologies that can efficiently boost the data transmission rate, improve system coverage, and enhance link reliability. MIMO is now widely adopted by many mainstream wireless industry standards including 3GPP WCDMA/HSDPA, LTE, EVDO, WiFi, and WiMAX. By employing multiple antennas at both transmitter and receiver sides, MIMO techniques enable a new dimension—the spatial dimension—that can be utilized in different ways to combat the impairments of wireless channels. Spatial diversity provided by multiple antennas is one of the diversity techniques, which are known to be the most effective tool against fading effects of wireless channels. Spatial multiplexing exploits independent fading effects to create additional degrees of freedom, thus achieving higher capacity. Spatial diversity benefits different systems and channel types, from single user systems to multi-user systems, and from flat-fading to frequency-selective channels.

This thesis focuses on precoding and equalization techniques, for flat-fading MIMO broadcast channels, with their applications in spread spectrum communication systems. First, a novel linear precoding technique, Coordinated Interference-aware Beamforming (CIB) that utilizes channel side information at the transmitter for transmit beamforming is introduced in Chapter 2. With constrained transmitted

power, CIB balances multi-user interference, spatial channel interference, and noise effects. Both analysis and the simulation results show that the achievable sum-rate of CIB bridges the rates of zero-forcing precoding and matched filtering techniques at high and low signal to noise ratios, respectively. The complexity of CIB is similar to that of other linear non-adaptive techniques, however, in addition to featuring a closed-form solution, it also allows flexible configurations on the number of antennas at the transmitter and receiver sides. In Chapter 3, we show that for the more complicated spread-spectrum systems with frequency-selective broadcast channels, the properly extended CIB can precode the signals well and inherits the some of the benefits of CIB for flat-fading channels. The role of CIB in maximizing the signal to interference plus noise ratio results in improved performance in error rates compared with other linear techniques. In Chapter 4 we introduce an innovative non-linear eigenvalue-decomposition based lattice precoding technique (EDLP), designed for precoding and equalization for single user flat-fading channels. EDLP is a variant of dirty-paper coding and benefits from the lattice reduction, Tomlinson-Harashima precoding (THP), and linear precoding/equalization techniques. EDLP achieves full diversity and a significant power gain with an implementation complexity similar to linear techniques. In Chapter 5, we discuss linear and nonlinear precoding and equalization techniques used in flat-fading multi-user MIMO broadcast channels. We propose a BDZF-EDLP technique based on EDLP and block-diagonal zero-forcing linear precoding. This technique offers a tradeoff among the uncoded error probability, the transmitted power, and the computational complexity at the transmitter and receiver. As a result, it achieves full receive diversity with a significantly lower complexity. It also features flexible scalability thanks to its linearly growth of its complexity. Finally, in Chapter 6, a novel finger placement strategy, Maximum Weight Placement (MWP) for the generalized RAKE (GRAKE) receivers is proposed. The MWP strategy offers a good balance between the computational complexity of the finger location placement and the resulting performance.

Summarizing, this thesis discusses linear and nonlinear techniques for precoding and equalization in different channel models that include flat-fading, frequency-selective fading, MIMO, single user, and multi-user channels. A number of novel techniques are proposed witch improve the error rate performance, throughput, and

computational complexity of the communication system. These techniques include CIB for flat-fading MIMO broadcast channels, CIB-CDMA for frequency-selective fading MIMO broadcast channels, EDLP for flat-fading MIMO single-user channels and BDZF-EDLP for flat-fading MIMO broadcast channels, and MWP for spread-spectrum frequency-selective multi-user channels.

Acknowledgements

Any thanks should start with my advisor, Professor Masoud Salehi. His luminous guidance, generous encouragement and steady support make him my endless source of ideas, enthusiasm and faith throughout the course of my PhD program.

I want to extend my appreciation to many faculty members of the Department of Electrical and Computer Engineering, Professor David Brady, Professor Bahram Shafai, Professor Dana Brooks, Professor Gilead Tadmor, Professor Vinay Ingle, Professor Amir Farhat, Professor Stefano Basagni, Professor Bradley Lehman, Professor Bruce McDonald and many others who offered me their excellent teaching and invaluable discussions during the time with Northeastern University.

It is my good fortune to have Professor John Proakis, Professor Hanoch Lev-Ari and Dr. Zoran Zvonar as members of my thesis committee. I own them many thanks for their high standards of excellence and precious advices which profoundly influenced me and taught me on not only this work but also my future research.

My developing career path is always accompanied fortunately by great help from a number of wonderful supervisors and mentors, Professor Fang, Shiliang from Southeast University, Vice President Wu, Weihong and Min, Youli from China Mobile and Dr. Aiguo Yan, Dr. Marko Kocic from Analog Devices Inc. I am also grateful It is my pleasure to appreciate Analog Devices Inc. and the group of Dr. Zoran Zvonar for their consistent financial support.

My association with Communications and Digital Signal Processing lab has been also a source of invaluable experience and friendship for me. It was so enjoyable to work with so many talented and successful people, including Joan Pratt, Dr. Frantz Bouchereau, Dr. Reza Marandian Hagh, Dr. Oguz Bayat, Dr. Hamid Satarboroujeni, Dr. Michele Battelli, Demetris Galatopoullos, Dr. Yalcin Bulut, Anshuman Mishra

and etc.

Finally I am greatly indebted to my wife for her unconditional support and to my parents for giving me the opportunities to live, to learn, to love, to be loved, and everything they have done for me.

Contents

Abstract	ii
Acknowledgements	v
1 Introduction	1
1.1 MIMO Channel Capacity	2
1.1.1 Preliminary Works	2
1.1.2 Deterministic MIMO Channel Capacity	5
1.1.3 Random Channel Capacity	9
1.2 Diversity and Multiplexing Tradeoff	15
1.3 Equalization Techniques	19
1.3.1 Zero-Forcing Nulling	19
1.3.2 Linear MMSE	20
1.3.3 Successive Interference Cancellation	21
1.3.4 Lattice Reduction Based Detection	22
1.4 Nonlinear Precoding Techniques	24
1.4.1 The Tomlinson-Harashima Precoding	24
1.4.2 Dirty Paper Coding	25
1.5 Main Contributions of the Dissertation	30
2 Coordinated Interference-Aware Beamforming (CIB)	35
2.1 System and Channel Model	37
2.2 SVD-MMSE Precoding	40
2.3 Zero-Forcing Precoding	42
2.4 Block-Diagonal Zero-Forcing Precoding	45

2.5	Coordinated Interference-Aware Beamforming	48
2.5.1	Full Diversity Mode	48
2.5.2	Spatial Multiplexing Mode	52
2.5.3	Interference Equivalence	53
2.5.4	Optimality Analysis	54
2.6	Performance Analysis	55
2.7	Conclusions	57
3	A Linear Beamforming Technique for MIMO CDMA	58
3.1	The Single User MIMO-CDMA Channel	59
3.2	Single User Linear Chip-Level Transceiver	62
3.2.1	The RAKE Receiver	63
3.2.2	Pre-RAKE Transmitter	64
3.2.3	Decorrelator and LMMSE Receivers	64
3.2.4	Eigenprecoder and Selection Combiner	65
3.3	Multi-User MIMO-CDMA System Model	66
3.4	Coordinated Interference-Aware Beamforming	69
3.5	Performance Analysis	72
3.6	Conclusions	75
4	Eigenvalue Decomposition Based Lattice Precoding	76
4.1	Introduction	76
4.2	System Model	78
4.3	An Eigenvalue Decomposition Based Lattice Precoding (EDLP)	81
4.4	Performance and Complexity Analysis	86
4.4.1	Simulation Results	87
4.4.2	Complexity	90
4.4.3	Channel Estimation Error	94
4.4.4	Diversity Order When More Antennas Are Available	96
4.5	Conclusions	98
5	Lattice Precoding for MIMO Broadcast Channels	99
5.1	General System Structure	101

5.2	MISO Broadcast Channel and the WFH Scheme	103
5.3	Block-Diagonal ZF and EDLP	107
5.4	Block-Diagonalization ZF and LR	112
5.5	Comparative Analysis	112
5.6	Conclusions	116
6	Advanced Equalization Techniques for CDMA Receivers	118
6.1	Introduction	119
6.2	The Generalized RAKE Receiver	121
6.3	GRAKE Parameter Estimation	131
6.4	Other Types of Linear Equalizations	133
6.5	GRAKE and LMMSE-CE Equivalence	135
6.6	Finger Placement Algorithms	137
6.6.1	The Greedy Search Algorithm	137
6.6.2	GRAKE Symmetric Placement Algorithm	137
6.6.3	The Maximum Weight Placement Algorithm	140
6.7	Simulation Results	142
6.8	Conclusions	144
7	Future Work	145
	Bibliography	147

List of Tables

3.1	Similarity of ISI and MIMO equalizations	60
4.1	Types of computations needed for the EDLP and comparable techniques	91
4.2	Estimated numbers of flops	92
5.1	Average flops of lattice precoding for MIMO broadcast channels . . .	114

List of Figures

1.1	Single user MIMO system	5
1.2	Vertical bell labs space time (V-BLAST) architecture	12
1.3	Ergodic capacity varies with SNR	14
1.4	Diversity-multiplexing optimal tradeoff, for $l \geq N_r + N_t - 1$	17
1.5	Diversity-multiplexing optimal tradeoff: give one more transmit antenna and receive antenna	18
1.6	Zero-forcing SIC architecture	21
1.7	Lattice reduction based detection	23
1.8	THP system block diagram	26
1.9	Dirty paper channel model	26
1.10	Transmit 4 PAM with interference	28
1.11	2-D constellation replication	29
1.12	MIMO broadcast channel precoding and equalization	31
2.1	System model of coordinated interference-aware beamforming (CIB)	38
2.2	Spatial multiplexing mode: 10 users each has 2 receive antennas	55
2.3	Total throughput varies with number of users each has two receive antennas	56
3.1	CIB-CDMA system model	60
3.2	Transceiver block diagram and signal flow for a MIMO-CDMA frequency-selective channel with CSI available at both transmitter and receiver	66
3.3	Average achievable throughput of CIB, SVD-RAKE, and SVD-MMSE	73
3.4	Uncoded average symbol error rate of CIB, SVD-RAKE, and SVD-MMSE	74

4.1	Example of periodically extended signal constellation by the two dimensional real lattice	79
4.2	Sketch for finding solutions of minimizing transmitted power	84
4.3	The block diagram for the EDLP transceiver	87
4.4	BER calculation with extended constellation	88
4.5	Error rate performance comparison of different techniques	90
4.6	A performance comparison of different techniques with 1% channel estimation error variance	95
4.7	EDLP with different antenna settings	97
5.1	The WFH scheme	105
5.2	BER vs Tx-power performance comparison of the WFH Scheme, BDZF-EDLP and BDZF-LR	115
6.1	Error probability performance with finger placements: RAKE, GRAKE, and MWP	143

List of Conventions

Acronyms

ACF	Auto-Correlation Function
AWGN	Additive White Gaussian Noise
BC	Broadcast Channel
BER	Bit Error Rate
BPSK	Binary Phase-Shift Keying
CDMA, WCDMA	Code Division Multiple Access, Wideband CDMA
CIB	Coordinated Interference-aware Beamforming
CCF	Cross-Correlation Function
CSI, CSIT, CSIR	Channel State Information, CSI at Transmitter, CSI at Receiver
DFE	Decision Feedback Equalizer
DPC	Dirty Paper Coding
DSP	Digital Signal Processing
EDLP	Eigenvalue Decomposition based Lattice Precoding
EVD	Eigen-Value Decomposition
FDD	Frequency Division Duplex
GBC	Gaussian Broadcast Channel
GRAKE	Generalized RAKE
HSDPA	High Speed Data Packet Access
ICI	Inter-Chip Interference
IE	Interference Equivalency
i.i.d.	Identically and Independently Distributed
ISI	Inter-Symbol Interference
LHS	Left Hand Side
LR	Lattice Reduction
LRAP	LR Aided Precoding

LRAPR	LR Aided Precoding and Reception
LTE	Long Term Evolution
MAC	Multiple Access Channel
MAI	Multiple Access Interference
MIMO	Multiple Input Multiple Output
MISO	Multiple Input Single Output
ML	Maximum Likelihood
MLD	Maximum Likelihood Detection
MMSE, LMMSE	Minimum Mean Square Error, Linear MMSE
MRC	Maximum Ratio Combining
MSE	Mean Square Error
MWP	Maximum Weight Placement
OVSF	Orthogonal Variable Spreading Factor
PIC	Parallel Interference cancellation
PSD	Power Spectral Density
PSK	Phase-Shift Keying
QAM	Quadratic Amplitude Modulation
QoS	Quality of Service
QPSK	Quadratic Phase Shift Keying
QRD	QR Decomposition
RHS	Right Hand Side
RF	Radio Frequency
RRC	Root-Raised Cosine
SER	Symbol Error Rate
SINR	Signal to Interference plus Noise Ratio
SISO	Single Input Single Output
SIMO	Single Input Multiple Output
SNR	Signal to Noise Ratio
STBC	Space-Time Block Codes
STC	Space-Time Coding
SVD	Singular Value Decomposition
TDD	Time Division Duplex
THP	Tomlinson-Harashima Precoding
ZF, ZFBF, BDZF	Zero-Forcing, ZF Beamforming, Block-Diagonal ZF

Notations

$ x $	Absolute value for real x and complex modulus for complex x
$\mathcal{W}_t(r, \mathbf{X})$	Central complex Wishart matrix
C	Channel capacity
$\mathcal{CN}(\mathbf{m}, \mathbf{X})$	Circular symmetric complex Gaussian distribution with mean \mathbf{m} and covariance \mathbf{X}
$\nabla f(x)$	Gradient of $f(x)$
$\mathbb{Q}_{\mathbb{Z}^n}$	Per-component modulo with respect to n dimensional lattice \mathbb{Z}
$\det(\mathbf{X})$	Determinant of \mathbf{X}
$\text{diag}(\mathbf{X})$	Diagonal matrix whose diagonal elements are \mathbf{x}
$\mathbb{E}[x]$	Expected value of the random variable x
$\exp(x)$	Exponential function of x
$\mathcal{N}(\mathbf{m}, \mathbf{X})$	Gaussian distribution with mean \mathbf{m} and covariance \mathbf{X}
N_0	Noise power spectral density
\mathbf{X}	Matrix \mathbf{X}
x^+	$\max(x, 0)$
$\max A$	Maximum of the set A
$\min A$	Minimum of the set A
\mathbb{C}^n	n dimensional complex space
\mathbb{R}^n	n dimensional real space
K	Number of active users in downlink channel
N_r	Number of receive antennas for single user channel
N_t	Number of transmit antennas for single user channel
\mathbb{R}^+	Positive real space
$\mathbb{P}[\text{event}]$	Probability of the event
\propto	Proportional to
$\Re(x), \Im(x)$	Real and imaginary parts of x , respectively
\mathbf{H}	Single user channel matrix with dimension $N_r \times N_t$
$\text{argmax}_{\{x:x \in A\}} f(x)$	The argument of the maximum of f given $x \in A$
$\text{argmin}_{\{x:x \in A\}} f(x)$	The argument of the minimum of f given $x \in A$
$\mathbf{x}^T, \mathbf{x}^H, \bar{\mathbf{x}}$	Transpose, Hermitian transpose, conjugate of \mathbf{x} , respectively
$\text{tr}(\mathbf{X})$	Trace of matrix \mathbf{X}
$a \in \{m_i\}_{i=1}^k$	Variable a is in the set of m_1 through m_k
\mathbf{x}	Vector \mathbf{x}
$\ \mathbf{x}\ $	vector norm 2 unless specified, respectively

Chapter 1

Introduction

Using multiple antenna systems in wireless communications has a long history which spans a number of decades. Multiple antennas used in either receiver or transmitter side can provide diversity gain which is the main tool used against fading effects in wireless channels [1]. With manufacturing techniques getting more and more advanced, communication devices can be made much smaller and accommodate more sophisticated hardware with affordable price. As a result, hardware complexity can be exchanged for more power and spectrum efficiency, two very precious and highly limited resources. Multiple Input Multiple Output (MIMO) systems were gradually introduced from the middle of 1990s through the research on the capacity of transmit diversity channels and the development of Space-Time Coding (STC).

MIMO shows its benefits in many directions [2] [3] among which some key features are listed here. With N_t transmit and N_r receive antennas, MIMO system can achieve a diversity order of $N_t N_r$. Therefore, to achieve the same diversity order, total number of antennas required in MIMO systems can be less than the number of antennas in previously used receive diversity systems. When the diversity order requirement is large, the saving on the number of antennas is significant. In addition to the diversity gain, MIMO systems can also support spatial multiplexing, which divides the point-to-point wireless channel into up to $\min(N_t, N_r)$ spatial sub-channels. Independent data stream can be transmitted over each of these spatial channels in parallel. Spatial multiplexing provides significant gain in transmission data rate [2] [3] [4] exploiting the the multi-path effects and random fading of the wireless channel,

which once were considered as impairments, thus creating additional spatial degrees of freedom. Furthermore, spatial multiplexing, similar to other multiplexing techniques, such as time multiplexing, frequency multiplexing and code multiplexing, is capable of separating different users by their signature (distinguished spatial characteristics) [5] and therefore can support many-to-one (MAC) and one-to-many (BC) communication [6]. The use of multiple transmit antennas allows flexible sharing of hardware complexity between communication terminals and therefore, makes system design more flexible.

In this introductory chapter, our objective is to briefly introduce certain basic aspects of MIMO systems. We start our treatment with theoretical analysis of MIMO channel capacities in Sections 1.1. The fundamental description of the diversity order and multiplexing gain of the spatial channel and their relation are described in Section 1.2. Section 1.3 discusses linear and non-linear equalization techniques and how these techniques are used to exploit possible gains outlined in Section 1.1 and the optimum tradeoff discussed in Section 1.2. Precoding techniques are discussed in Section 1.4 to show how equalization techniques are enhanced, when channel side information at the transmitters is available. Main contributions of this thesis are introduced in Section 1.5.

1.1 MIMO Channel Capacity

1.1.1 Preliminary Works

A memoryless, discrete-time complex Additive White Gaussian Noise (AWGN) channel with noise Power Spectral Density (PSD) $N_0/2$ per dimension, can be represented as an equivalent baseband channel

$$y = x + n,$$

where x and y are the complex channel input and output respectively, and noise n has a complex circular Gaussian distribution $n \sim \mathcal{CN}(0, N_0)$. The capacity of this

channel is given by

$$C = \log \left(1 + \frac{P}{N_0} \right), \quad (1.1)$$

where P is the energy per symbol transmitted into the channel and P/N_0 is the Signal to Noise Ratio (SNR) per symbol. Equation (1.1) can also be written as

$$C = \log(1 + \text{SNR}). \quad (1.2)$$

We consider various forms of channel complex gain h , where we assume that both transmitter and receiver have perfect knowledge of h . First suppose h is a deterministic scalar and the corresponding channel is an ideal time-invariant Gaussian Single-Input-Single-Output (SISO) channel, represented by

$$y = hx + n$$

where the effect of the channel is to scale the input signal by h and the corresponding equivalent SNR is scaled by $|h|^2$. Following Equation (1.2) the capacity of the channel is given by

$$C = \log \left(1 + \frac{P|h|^2}{N_0} \right). \quad (1.3)$$

For the traditional receive diversity, the channel can be modeled as a Single-Input-Multiple-Output (SIMO) channel with N_r receive antennas and one transmit antenna [6]. We consider the time-invariant, memoryless deterministic AWGN channel,

$$\mathbf{y} = \mathbf{h}x + \mathbf{n},$$

where

$$\begin{aligned} \mathbf{y} &= [y_1, \dots, y_{N_r}]^T \\ \mathbf{h} &= [h_1, \dots, h_r]^T \\ \mathbf{n} &= [n_1, \dots, n_r]^T \text{ and} \\ \mathbf{n} &\sim \mathcal{CN}(\mathbf{0}, N_0 \mathbf{I}_{N_r}). \end{aligned}$$

Assuming that we use linear Maximum Ratio Combining (MRC)

$$r = \frac{\mathbf{h}^H}{\|\mathbf{h}\|^2} \mathbf{y} = x + n',$$

where

$$n' = \frac{\mathbf{h}^H}{\|\mathbf{h}\|^2} \mathbf{n}, \quad \text{and} \quad n' \sim \mathcal{CN}(0, N_0/\|\mathbf{h}\|^2).$$

The equivalent SNR is $P\|\mathbf{h}\|^2/N_0$ and the capacity is given by

$$C_{SIMO} = \log \left(1 + \frac{P\|\mathbf{h}\|^2}{N_0} \right). \quad (1.4)$$

In this case only the receive antennas need to have access to the Channel Side Information (CSI).

For transmit diversity case, the channel is called Multiple-Input-Single-Output (MISO), using N_t transmit antennas and one receive antenna. Here

$$y = \mathbf{h}^H \mathbf{x} + \mathbf{n},$$

where

$$\begin{aligned} \mathbf{h} &= [h_1, \dots, h_{N_t}]^T \\ \mathbf{x} &= [x_1, \dots, x_{N_t}]^T \end{aligned}$$

where \mathbf{x} denotes the input signals on N_t transmit antennas and $\mathbf{n} \sim \mathcal{CN}(0, N_0 \mathbf{I}_{N_t})$. The energy per symbol of the signals transmitted on total N_t transmit antennas is constrained by P . Suppose that before transmission, the transmit side transforms the data modulated signals by

$$\mathbf{x} = \frac{\mathbf{h}}{\|\mathbf{h}\|} x',$$

where x' is the original data modulated signals. Then,

$$y = \mathbf{h}^H \mathbf{x} + \mathbf{n} = \|\mathbf{h}\| x' + \mathbf{n},$$

which is similar to the deterministic scalar channel coefficient case. Therefore, SNR =

$P\|\mathbf{h}\|^2/N_0$ and

$$C_{MISO}^{CSI} = \log \left(1 + \frac{P\|\mathbf{h}\|^2}{N_0} \right). \quad (1.5)$$

To achieve this capacity the transmitter should have the CSI and use waterfilling technique to allocate energy to each antenna. This scheme uses channel gain to allocate more energy to signals transmitted over better channels. In other words, similar to the way that SIMO projects the received vector on the channel coefficient vector to suppress Gaussian noise projected on the orthogonal plane, MISO pre-projects its signals on the channel coefficient vector and then transmits them to combat noise.

When the transmitter has no CSI, it can be proved that the optimal way is to allocate power equally among transmit antennas and the resulting channel capacity is

$$C_{MISO}^{no-CSI} = \log \left(1 + \frac{P\|\mathbf{h}\|^2}{N_0 N_t} \right). \quad (1.6)$$

In both SIMO and MISO channels with CSI, $\|\mathbf{h}\|^2$ is the power gain obtained by the use of multiple antennas, whereas in MISO channel without CSI, the power gain is only $\|\mathbf{h}\|^2/N_t$.

1.1.2 Deterministic MIMO Channel Capacity

Consider a time-invariant, deterministic MIMO AWGN channel with N_t transmit antennas and N_r receive antennas as shown in Figure 1.1, and

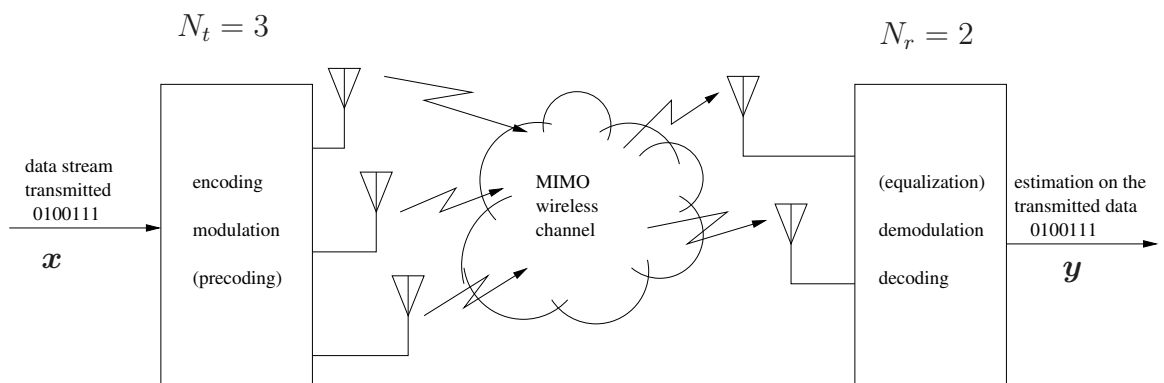


Figure 1.1: Single user MIMO system

$$\mathbf{y} = \mathbf{H}\mathbf{x} + \mathbf{n}, \quad (1.7)$$

where \mathbf{H} is a deterministic $N_r \times N_t$ complex matrix, $\mathbf{y} \in \mathbb{C}^{N_r}$, $\mathbf{x} \in \mathbb{C}^{N_t}$, $\mathbf{n} \in \mathbb{C}^{N_r}$, and $\mathbf{n} \sim \mathcal{CN}(\mathbf{0}, N_0 \mathbf{I}_{N_r})$. To maximize the capacity, we can transform such channel to many parallel channels and use the existing results. We first assume that \mathbf{H} is known at both sides [7].

Using Singular Value Decomposition (SVD), any complex matrix \mathbf{H} can be decomposed as

$$\mathbf{H} = \mathbf{U}\mathbf{\Lambda}\mathbf{V}^H,$$

where $\mathbf{U} \in \mathbb{C}^{N_r \times N_r}$ and $\mathbf{V} \in \mathbb{C}^{N_t \times N_t}$ are unitary matrices and $\mathbf{\Lambda} \in (\mathbb{R}^+)^{N_r \times N_t}$ is a diagonal matrix with nonnegative diagonal elements. Furthermore, columns of \mathbf{U} and \mathbf{V} are eigenvectors of $\mathbf{H}\mathbf{H}^H$ and $\mathbf{H}^H\mathbf{H}$, respectively. The diagonal entries of $\mathbf{\Lambda}$ are the nonnegative square roots of the eigenvalues of $\mathbf{H}\mathbf{H}^H$ or $\mathbf{H}^H\mathbf{H}$. Note that $\mathbf{H}\mathbf{H}^H$ and $\mathbf{H}^H\mathbf{H}$ have the same eigenvalues and as Hermitian matrices have real and non-negative eigenvalues. We denote the positive eigenvalues of $\mathbf{H}\mathbf{H}^H$ as $\{\lambda_i^2\}_{i=1}^m$ where m is the rank of $\mathbf{H}\mathbf{H}^H$.

Now if we rewrite Equation (1.7) as

$$\mathbf{U}\mathbf{U}^H\mathbf{y} = \mathbf{U}\mathbf{\Lambda}\mathbf{V}^H\mathbf{x} + \mathbf{U}\mathbf{U}^H\mathbf{n},$$

and multiply both sides by \mathbf{U}^H , we obtain

$$\mathbf{U}^H\mathbf{y} = \mathbf{\Lambda}\mathbf{V}^H\mathbf{x} + \mathbf{U}^H\mathbf{n}. \quad (1.8)$$

Substituting

$$\tilde{\mathbf{y}} = \mathbf{U}^H\mathbf{y}, \quad \tilde{\mathbf{x}} = \mathbf{V}^H\mathbf{x}, \quad \tilde{\mathbf{n}} = \mathbf{U}^H\mathbf{n} \quad (1.9)$$

into Equation (1.8), we have

$$\tilde{\mathbf{y}} = \mathbf{\Lambda}\tilde{\mathbf{x}} + \tilde{\mathbf{n}}. \quad (1.10)$$

Here the role of \mathbf{U} and \mathbf{V} is to rotate the output and input signals in such a way that the resulting channels are independent and the role of the diagonal elements of $\mathbf{\Lambda}$ is to provide the real channel gains and give the real channel gain to the transformed independent parallel Gaussian channels.

Since $\mathbf{\Lambda}$ is a diagonal matrix, Equation (1.10) can be reduced to

$$\tilde{y}_i = \lambda_i \tilde{x}_i + \tilde{n}_i, \quad i = 1, 2, \dots, m,$$

i.e., we have a total of m parallel channels. Note that the transformations in Equation (1.9) are unitary so the power of $\tilde{\mathbf{x}}$ is equal to the power of \mathbf{x} , i.e., $\|\tilde{\mathbf{x}}\|^2 = \|\mathbf{x}\|^2$. It can also be easily proved that $\tilde{\mathbf{n}}$ and \mathbf{n} have the same distribution $\mathcal{CN}(\mathbf{0}, N_0 \mathbf{I}_{N_r})$ indicating that the noise is white across these parallel channels. The capacity of the resulting channel is given by

$$C_{MIMO}^{full-CSI} = \sum_{i=1}^m \log \left(1 + \frac{P_i \lambda_i^2}{N_0} \right), \quad (1.11)$$

where $\{P_i\}_{i=1}^m$ are selected to maximize C , i.e.,

$$C = \operatorname{argmax}_{\{P_1, P_2, \dots, P_m\}} \sum_{i=1}^m \log \left(1 + \frac{P_i \lambda_i^2}{N_0} \right),$$

subject to

$$\sum_{i=1}^m P_i = P,$$

where P denotes the total power constraint. The solution for this optimization problem is the waterfilling power allocation obtained by using *Lagrangian* optimization method which results in

$$P_i = \left(\mu - \frac{N_0}{\lambda_i^2} \right)^+,$$

where $x^+ = \max(x, 0)$, μ^{-1} is the Lagrange multiplier and is selected such that

$$\sum_{i=1}^m \left(\mu - \frac{N_0}{\lambda_i^2} \right)^+ = P.$$

Now consider the case that the receiver has access to CSI but the transmitter has no CSI, then total power P is allocated equally to each transmitter antenna,

$$P_1 = P_2 = \dots = P_{N_t} = \frac{P}{N_t},$$

and

$$C_{MIMO}^{Rx-CSI} = \sum_{i=1}^m \log \left(1 + \frac{P\lambda_i^2}{mN_0} \right). \quad (1.12)$$

Since function \log is concave, by applying Jensen's inequality

$$\frac{\sum_{i=1}^n f(x_i)}{n} \leq f \left(\frac{\sum_{i=1}^n x_i}{n} \right),$$

where equality holds iff

$$x_1 = x_2 = \dots = x_n,$$

from Equation (1.12) we obtain

$$\sum_{i=1}^m \log \left(1 + \frac{P\lambda_i^2}{mN_0} \right) \leq m \log \left(1 + \frac{P}{m^2 N_0} \sum_{i=1}^m \lambda_i^2 \right),$$

with equality when

$$\lambda_1^2 = \lambda_2^2 = \dots = \lambda_m^2 \quad \text{and} \quad m = \min(N_r, N_t).$$

Then, from Equation (1.12),

$$C_{MIMO}^{Rx-CSI} = m \log \left(1 + \frac{P\lambda_1^2}{N_t N_0} \right). \quad (1.13)$$

From Equations (1.12) and (1.13) the total power gain for this matrix channel is approximately $\sum_{i=1}^m \lambda_i^2$ when $\mathbf{H}\mathbf{H}^H$ has rank $m = \min(N_r, N_t)$ and has identical eigenvalues. Let us define

$$\kappa_2(\mathbf{H}) = \frac{\max(\{\lambda_i\}_{i=1}^m)}{\min(\{\lambda_i\}_{i=1}^m)}$$

as the *condition number* of the matrix \mathbf{H} and say matrix \mathbf{H} is *well conditioned* if the condition number is close to 1. With this definition we conclude that if the transmitter allocate energy evenly across all transmit antennas, and $\mathbf{H}\mathbf{H}^H$ has rank m , well conditioned channel has its capacity maximized.

When SNR, defined as P/N_0 , is relatively high, Equation (1.12) can be approximated as

$$C_{MIMO}^{Rx-CSI} \approx m \log \text{SNR} + \sum_{i=1}^m \log \frac{\lambda_i^2}{m},$$

and in the low SNR case

$$C_{MIMO}^{Rx-CSI} \approx \frac{P}{N_0} \max(\{\lambda_i^2\}_{i=1}^m).$$

An equivalent form of (1.11) can be found using information theoretical arguments given in [8] and [9]. Denoting the covariance matrix of \mathbf{x} by \mathbf{Q} , and normalizing noise power so that the variance of noise is unity, we have

$$C_{MIMO} = \max_{\mathbf{Q}: \text{tr}(\mathbf{Q}) \leq P} \log [\det (\mathbf{I}_{N_r} + \mathbf{H}\mathbf{Q}\mathbf{H}^H)]. \quad (1.14)$$

For equal power uncorrelated sources

$$\mathbf{Q} = \frac{P}{N_t N_0} \mathbf{I}_{N_t},$$

and we have

$$C_{MIMO}^{Rx-CSI} = \log \left[\det \left(\mathbf{I}_{N_r} + \frac{P}{N_t} \mathbf{H}\mathbf{H}^H \right) \right]. \quad (1.15)$$

1.1.3 Random Channel Capacity

In this section we will consider fading channels. By a fading channel we mean the channel is random and is represented as a random channel matrix \mathbf{H} . Since \mathbf{H} is random, the resulting channel capacity becomes random too. There are two metrics used to evaluate this random variable, ϵ -Outage Capacity C_ϵ and Ergodic Capacity $C_{\mathbb{E}}$ which are used in slow-fading and fast-fading channels, respectively.

For slow fading channel, we assume the channel coherence time is sufficiently large so that the channel gain is random but remains the same during the transmission. If the transmitter does not know the channel realization but only knows the distribution of this random variable, then we cannot guarantee that reliable communication, at any given rate $R > 0$ is possible, therefore, the Shannon channel capacity is zero.

However, given a rate R , we can determine the probability of reliable transmission from the distribution of the channel.

We define the outage probability to be

$$p(R) = \mathbb{P} [\log(1 + |\mathbf{h}|^2 \text{SNR}) \leq R] = \mathbb{P} \left[\|\mathbf{h}\|^2 \leq \frac{2^R - 1}{\text{SNR}} \right].$$

For any probability ϵ , the outage capacity C_ϵ is the largest transmission rate such that the outage probability is less than or equal to ϵ

$$p(C_\epsilon) \leq \epsilon.$$

Suppose the transmitter encodes data at a rate R . If the realization of the channel is such that $\log(1 + |\mathbf{h}|^2 \text{SNR}) \leq R$, then regardless of the code, the decoding error probability cannot be made arbitrarily small and the system is said to be *in outage*.

For example, in Equation (1.3), if the channel is in Rayleigh slow fading, $h \sim \mathcal{CN}(0, 1)$, given the outage probability ϵ ,

$$p(R) = \mathbb{P} [\log(1 + |h|^2 \text{SNR}) \leq R] = \mathbb{P} \left[|h|^2 \leq \frac{2^{C_\epsilon} - 1}{\text{SNR}} \right] = \epsilon,$$

and the outage capacity is

$$C_\epsilon = \log \left[1 + \log \left(\frac{1}{1 - \epsilon} \right) \text{SNR} \right].$$

In SIMO channels where the channel gain is a random vector \mathbf{h} , from Equation (1.4) the outage probability is

$$p(R) = \mathbb{P} [\log(1 + \|\mathbf{h}\|^2 \text{SNR}) \leq R] = \mathbb{P} \left[\|\mathbf{h}\|^2 \leq \frac{2^R - 1}{\text{SNR}} \right].$$

With only receiver CSI, Equation (1.6), the outage probability is

$$p(R) = \mathbb{P} \left[\log \left(1 + \frac{\|\mathbf{h}\|^2}{N_t} \text{SNR} \right) \leq R \right] = \mathbb{P} \left[\|\mathbf{h}\|^2 \leq N_t \frac{2^R - 1}{\text{SNR}} \right].$$

The general form of the outage capacity for the cases above is introduced in [6] as

$$C_\epsilon = \log (1 + F^{-1}(1 - \epsilon)\text{SNR}),$$

where F is the complementary cumulative distribution function of $\|\mathbf{h}\|^2$, i.e., $F(x) = \mathbb{P}[\|\mathbf{h}\|^2 > x]$. Here \mathbf{h} is a sum of the squares of $2N_t$ independent Gaussian random variables and is distributed as Chi-square with $2N_t$ degrees of freedom,

$$f(x) = \frac{1}{(N_t - 1)!} x^{N_t - 1} e^{-x}, \quad x \geq 0.$$

In MIMO channels, following Equation (1.14), we have

$$p(C_\epsilon) = \mathbb{P}[\log \det(\mathbf{I}_{N_r} + \mathbf{H}\mathbf{Q}\mathbf{H}^H) \leq C_\epsilon] = \epsilon,$$

where the choice of \mathbf{Q} is determined by the allocation of power over transmitter antennas and can be considered as a parameter that can minimize the outage probability. In [8], it is shown that with receive CSI, the optimal \mathbf{Q} is of the form

$$\mathbf{Q}_{opt} = \frac{P}{k} \text{diag}(\underbrace{1, \dots, 1}_k, \underbrace{0, \dots, 0}_{N_t - k})$$

for some $k = 1, \dots, N_t$. Such form helps us to understand the important trade-off between diversity gain and the transmission rate. Lower values of k means using fewer transmit antennas. We will discuss this issue more later on.

The *Ergodic Capacity* is the statistic average of the deterministic channel capacity over the ergodic channel realizations. The *Ergodic Capacity* is the expected value of the Shannon capacity over all channel realizations and has the form

$$C_{\mathbb{E}} = \mathbb{E}[\log(1 + \|\mathbf{h}\|^2 \text{SNR})]$$

for SIMO and

$$C_{\mathbb{E}} = \mathbb{E}\left[\log\left(1 + \frac{\text{SNR}}{N_t} \|\mathbf{h}\|^2\right)\right]$$

for MISO with receiver CSI. If full CSI is available to MISO, the factor N_t in above

expression disappears.

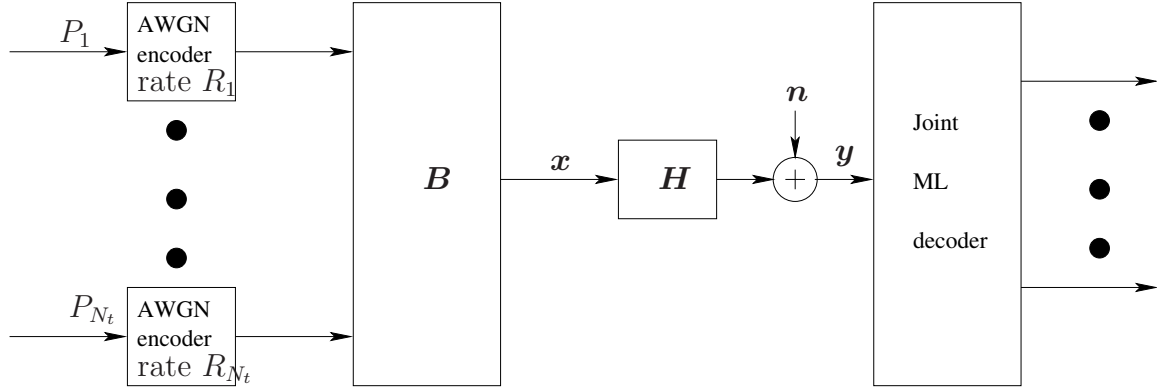


Figure 1.2: Vertical bell labs space time (V-BLAST) architecture

To make our discussion more general, we follow the Vertical Bell Labs Space Time Architecture (V-BLAST), as shown in Figure 1.2. Here \mathbf{Q} is defined to be the covariance matrix of the transmitted signal \mathbf{x} and

$$\mathbf{Q} = \mathbf{B} \text{diag}(P_1, P_2, \dots, P_{N_t}) \mathbf{B}^H,$$

where the series P_1, P_2, \dots, P_{N_t} denote the power allocation among the transmit antennas, \mathbf{B} is called the multiplexing coordinate system and has two special cases. If the transmitter has access to CSI and employs waterfilling to allocate power, then $\mathbf{B} = \mathbf{V}$. If not, same rate and independent data streams are transmitted and $\mathbf{B} = \mathbf{I}_{N_t}$. By this definition, we can express the outage probability of a MIMO system as

$$p(R) = \underset{\{\mathbf{K}_x: \text{tr}(\mathbf{K}_x) \leq P\}}{\text{argmin}} \mathbb{P} \left[\log \det \left(\mathbf{I}_{N_r} + \frac{1}{N_0} \mathbf{H} \mathbf{K}_x \mathbf{H}^H \right) \leq R \right].$$

The optimal selection of \mathbf{K}_x is found to be $\frac{P}{N_t} \mathbf{I}_{N_t}$ and the resulted outage probability

$$p(R) = \mathbb{P} \left[\log \det \left(\mathbf{I}_{N_r} + \frac{\text{SNR}}{N_t} \mathbf{H} \mathbf{H}^H \right) \leq R \right].$$

When the MIMO channel is in fast fading, the ergodic capacity can be used to

evaluate the maximum transmission rate and has the form of

$$C_{\mathbb{E}} = \mathbb{E} \left[\sum_{i=1}^{N_t} \log \left(1 + \frac{P\lambda_i^2}{N_t N_0} \right) \right]$$

or using Equation (1.14) equivalently,

$$C_{\mathbb{E}} = \mathbb{E} \left[\log \det \left(\mathbf{I}_r + \frac{\text{SNR}}{N_t} \mathbf{H} \mathbf{H}^H \right) \right]. \quad (1.16)$$

This expression is elaborated by Telatar [8] as follows. Define

$$\mathbf{W} = \begin{cases} \mathbf{H} \mathbf{H}^H & N_r < N_t \\ \mathbf{H}^H \mathbf{H} & N_r \geq N_t \end{cases},$$

to be an $m \times m$ random non-negative definite matrix, called the Wishart matrix, whose eigenvalues $\lambda_1, \dots, \lambda_m \geq 0$ are also random. The joint distribution and marginal distribution for the eigenvalues are found, based on which we can easily express Equation (1.16) as

$$C_{\mathbb{E}} = \mathbb{E} \left[\sum_{i=1}^m \log \left(1 + \frac{P}{N_t} \lambda_i \right) \right] = m \mathbb{E} \left[\log \left(1 + \frac{P}{N_t} \lambda_1 \right) \right]. \quad (1.17)$$

Resulting in

$$C_{\mathbb{E}} = \int_0^{\infty} \log(1 + P\lambda/t) \sum_{k=0}^{m-1} \frac{k!}{(k+n-m)!} [L_k^{n-m}(\lambda)]^2 \lambda^{n-m} e^{-\lambda} d\lambda$$

where

$$L_k^{n-m}(\lambda) = \frac{1}{k!} e^{\lambda} \lambda^{m-n} \frac{d^k}{d\lambda^k} (e^{-\lambda} \lambda^{n-m+k})$$

is the associated Laguerre polynomial of order k .

Figure 1.3 shows how the ergodic capacity varies with SNR in different settings of the MIMO system. As we can see from Figure 1.3, increasing the number of transmit antennas has a lower impact on increasing the capacity than increasing the number of receive antennas. This holds only for the case when CSI is available at receiver.

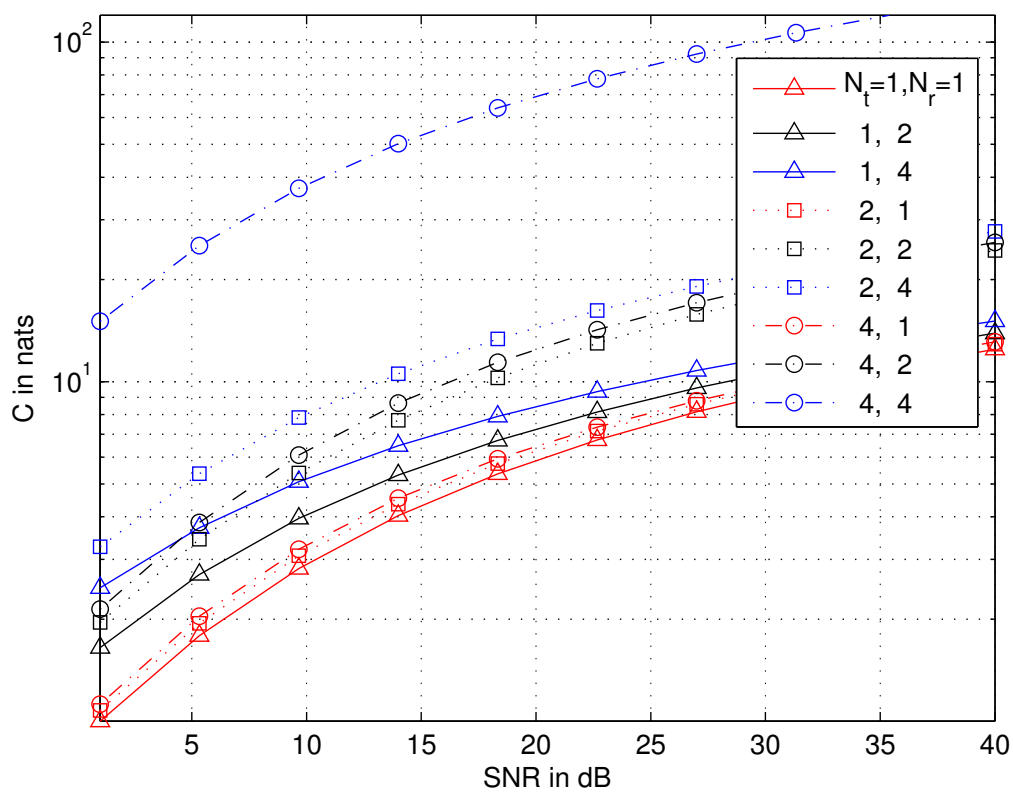


Figure 1.3: Ergodic capacity varies with SNR

When the number of both transmit and receive antennas increase the capacity greatly increases, and at high SNR values the capacity becomes proportional to the minimum of the number of transmit and receive antennas. This will be further discussed in Section 1.2.

1.2 Diversity and Multiplexing Tradeoff

The diversity-multiplexing tradeoff is indeed the tradeoff between the error probability and the data rate of the system [10]. In [11] and [12] an upper bounds for the pairwise error probability of space-time codes is derived as

$$P_{c \rightarrow e} \leq \alpha_c \left(\frac{E_s}{4N_0} \right)^{-N_t N_r} \quad (1.18)$$

where α_c is a function of the channel and the codeword, and do not depend on the SNR. From Equation (1.18) we see that the maximum diversity gain of the channel is $N_t N_r$. Besides providing diversity to improve the error probability, i.e., reliability, MIMO channels can also support a higher data rate than SISO channels. Consider an ergodic fading channel with capacity (1.17), at high SNR,

$$C_{\mathbb{E}} = m \log \frac{\text{SNR}}{N_t} + \sum_{i=|N_r - N_t| + 1}^n \mathbb{E}[\log \chi_{2i}^2] + o(1) \quad (1.19)$$

where χ_{2i}^2 is chi-square distributed with $2i$ degrees of freedom. We can observe that the channel capacity increases with SNR as $m \log \text{SNR}$, i.e., m times faster than the capacity of SISO channels. This indicates that the MIMO channels can be viewed as m parallel channels where m is the number of degrees of freedom. One can transmit independent information symbols in parallel through m channels. Equation (1.19) indicates that instead of transmitting one data stream on all equivalent spatial parallel channels, we can transmit independent data streams onto each Eigenmode channels to achieve maximum transmission rate, i.e., the capacity. This leads to a different system design from the last section.

We define the *multiplexing gain* γ and *diversity gain* d of a system as

$$\gamma = \lim_{\text{SNR} \rightarrow \infty} \frac{R(\text{SNR})}{\log(\text{SNR})}$$

and

$$d = - \lim_{\text{SNR} \rightarrow \infty} \frac{\log P_e(\text{SNR})}{\log(\text{SNR})}$$

where $R(\text{SNR})$ is the transmission rate and P_e is the average error probability. A system designer's goal is to design systems that achieve maximal multiplexing gain for a given diversity gain or achieve maximal diversity gain for a given multiplexing gain. For example, the well-known Alamouti scheme and repetition scheme both achieve maximal diversity gain. But Alamouti scheme achieves twice the transmission rate of the repetition scheme.

The optimal tradeoff curve between diversity and multiplexing gain is derived in [10] as

$$d(i) = (N_r - i)(N_t - i),$$

for $i = 0, \dots, m$ and $l \geq N_r + N_t - 1$, where l denotes the transmitted block length. In particular,

$$d_{\max} = N_r N_t \quad \text{and} \quad \gamma_{\max} = m.$$

As in Figure 1.4, the optimal tradeoff curve shows the compensation between the two design criteria discussed earlier, by connecting the two extreme points, $(0, d_{\max})$ and $(\gamma_{\max}, 0)$. This result shows that diversity gain and multiplexing gain can be achieved simultaneously. Fixing one of the gains, one can get the optimal value of the other gain from the curve. Increasing the diversity gain comes at the price of decreasing the multiplexing gain and vice versa.

Now if we increase N_r and N_t each by 1, the channel gains one more degree of freedom and as we see in Figure 1.5, given a fixed diversity gain d , the multiplexing gain is increased. Note that in the extreme case when the diversity gain is maximized while the spatial multiplexing gain is zero, does not correspond to zero transmission rate because in this case $\log \text{SNR}$ goes to infinity. One scheme that can achieve such optimal tradeoff can be found in [13].

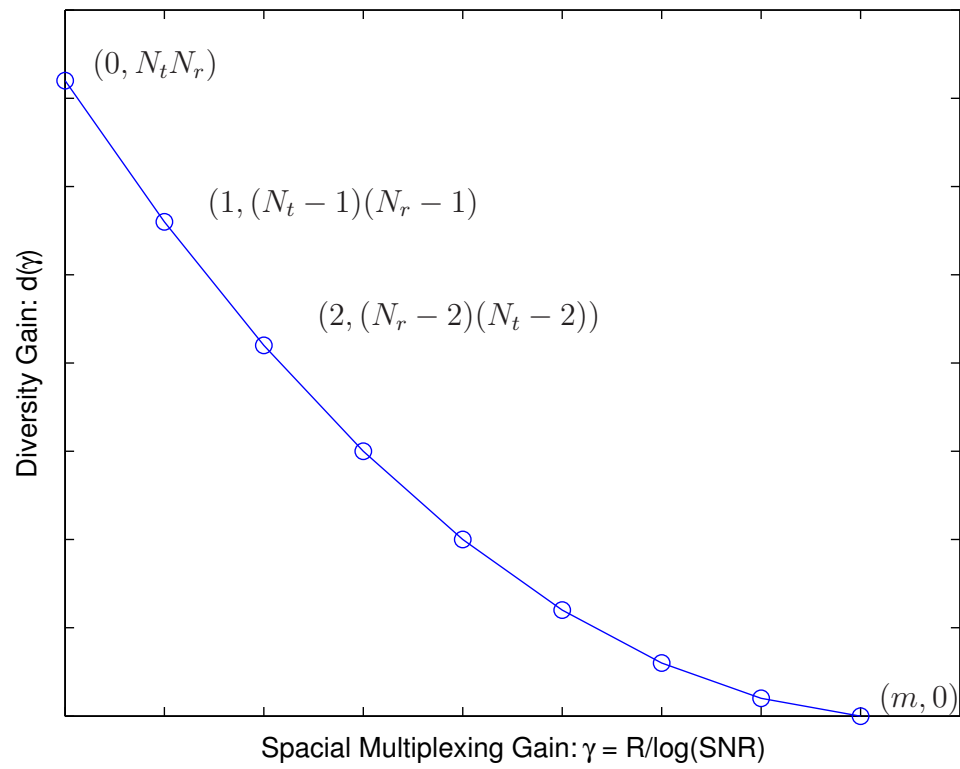


Figure 1.4: Diversity-multiplexing optimal tradeoff, for $l \geq N_r + N_t - 1$

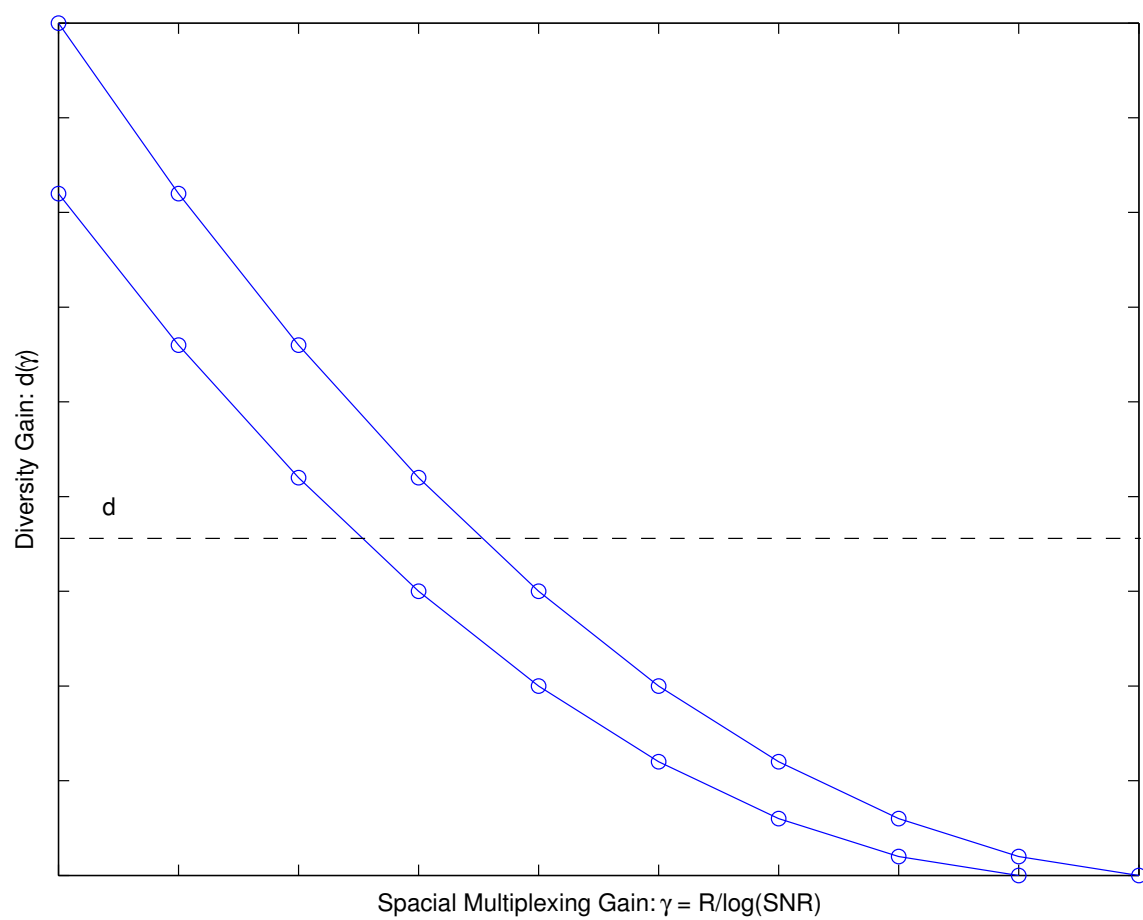


Figure 1.5: Diversity-multiplexing optimal tradeoff: give one more transmit antenna and receive antenna

1.3 Equalization Techniques

When transmit antennas of MIMO systems transmit different symbols simultaneously, on each receive antenna signals are summed and the receiver has to separate them in order to detect each signal. If we consider each transmit antenna as a user, the system can be thought of as a multiple access system and multi-user detection techniques can be employed by the MIMO system. In this section, first we review the two basic linear multi-user detectors and then consider some non-linear techniques.

1.3.1 Zero-Forcing Nulling

The received signal vector has the form

$$\mathbf{y} = \sum_{i=1}^{N_t} \mathbf{h}_i x_i + \mathbf{n} \quad (1.20)$$

where \mathbf{h}_i 's are the columns of \mathbf{H} and the data streams x_i transmitted on the i^{th} antenna, $1 \leq i \leq N_t$ are independent. Focusing on the k^{th} data stream, we can rewrite Equation (1.20) as

$$\mathbf{y} = \mathbf{h}_k x_k + \sum_{i \neq k} \mathbf{h}_i x_i + \mathbf{n}$$

where the second term on the right hand side is the interference part. The k^{th} data stream is subject to interference from other data streams. A simple approach is to project the received signal vector \mathbf{y} onto the subspace orthogonal to the one spanned by the vectors $\mathbf{h}_i, i = 1 \dots t$ and $i \neq k$, thus nullifying the inter-stream interference. Such projection operation followed by the matched filter is called the decorrelation, interference nulling, or zero-forcing given by the Moore-Penrose pseudo-inverse,

$$\mathbf{H}^- \equiv (\mathbf{H}^H \mathbf{H})^{-1} \mathbf{H}^H.$$

The received SNR at the k^{th} antenna is therefore equal to

$$\frac{P_k \|\mathbf{h}_k\|^2}{N_0} \quad (1.21)$$

where P_k is the transmitted energy per symbol on the k^{th} antenna. If we denote the k^{th} row of \mathbf{H}^{-1} by \mathbf{w}_k , we can write (1.21) as

$$\frac{P_k}{N_0 \|\mathbf{w}_k\|^2}. \quad (1.22)$$

Although this simple decorrelation can successfully null the interference from other data streams, the additive noise is amplified by the nulling vectors. In the absence of noise, i.e., when N_0 goes to zero, this is the optimal detection scheme.

1.3.2 Linear MMSE

If the mean square error between the transmitted symbols and the outputs of the detected symbols, or equivalently, the received SINR is taken as the performance criteria, the MMSE detector is the optimal detection that seeks to balance between cancelation of the interference and reduction of noise enhancement. Let us denote the linear MMSE detector as K_k and the detection operation by

$$\hat{x}_k = \text{sgn}[K_k \mathbf{y}]$$

for the bit transmitted at the k^{th} antenna. The K_k that maximizes the SINR and minimizes the mean square error $E[(\hat{x}_k - K_k \mathbf{y})^T (\hat{x}_k - K_k \mathbf{y})]$ is derived as

$$K_x = \left(N_0 \mathbf{I}_{N_r} + \sum_{i \neq k}^{N_t} P_i \mathbf{h}_i \mathbf{h}_i^H \right)^{-1} \mathbf{h}_k$$

and the corresponding output SINR is

$$P_k \mathbf{h}_k^H \left(N_0 \mathbf{I}_{N_r} + \sum_{i \neq k}^{N_t} P_i \mathbf{h}_i \mathbf{h}_i^H \right)^{-1} \mathbf{h}_k.$$

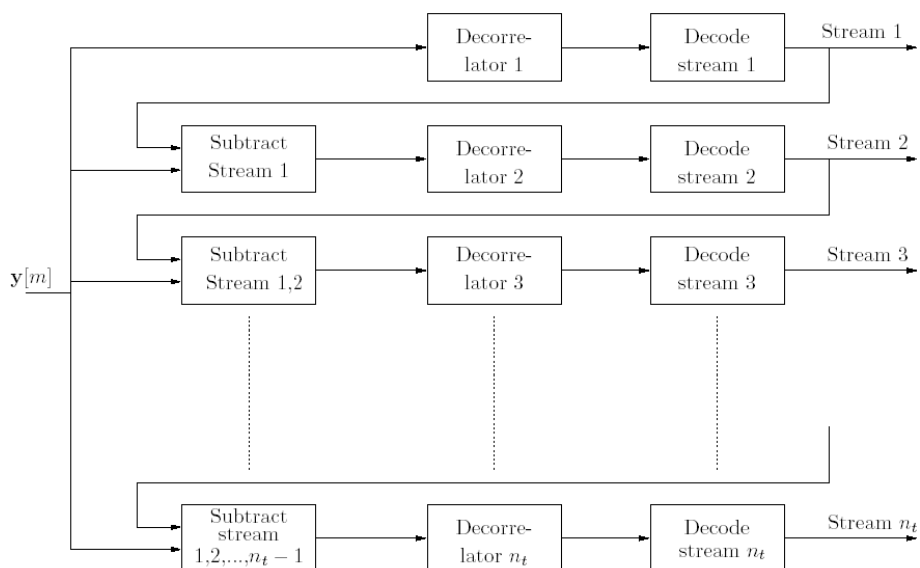


Figure 1.6: Zero-forcing SIC architecture

It can be shown that this linear MMSE detector works strictly better than the linear decorrelator when noise is present and has a better performance than the matched filter when the interference is large.

1.3.3 Successive Interference Cancellation

We have just considered two detection schemes that include banks of separate filters to estimate the data streams. However, when signals are detected successively, the outputs of previous detectors can be used to aid the operations of next ones which leads to the decision directed detection algorithms including SIC, Parallel Interference cancellation (PIC), and multistage detection. In this section we will focus on the SIC as depicted in Figure 1.6. The V-BLAST detection scheme is a good example that employs ZF SIC with optimal ordering, whereas MMSE-SIC with equal power allocation approaches the capacity of the i.i.d. Rayleigh fading channel. After the first bit is detected by the decorrelator the result is used to cancel the interference from the received signal vector assuming the decision of the first stream is correct. For the ZF-SIC, since the interference is already nulled, the significance of SIC is to reduce the noise amplification by the nulling vector. The nulling vector \mathbf{w}_1 filters the

received vector \mathbf{y} as

$$\hat{x}_1 = \text{sgn}[\mathbf{w}_1^T \mathbf{y}].$$

Assuming $\hat{x}_1 = x_1$, by substituting x_1 from the received vector \mathbf{y} , we obtain a modified received vector \mathbf{y}_1 given by

$$\mathbf{y}_1 = \mathbf{y} - \hat{x}_1(\mathbf{H})_1$$

where $(\mathbf{H})_1$ denotes the first column of \mathbf{H} . We then repeat this operation until all N_t bits are detected. Note that the nulling vector for the first stream has full dimension N_r . Once the first stream is detected, the first row of \mathbf{H} is useless and will be eliminated. Therefore after the first cancelation the nulling vector for the second stream need only $N_r - 1$ dimensions. A simple consequence of the Cauchy-Schwartz inequality is that if a particular \mathbf{w}_k is constrained to be orthogonal to fewer rows of \mathbf{H} , its norm will be smaller and thus, by the SNR expression given in Equation (1.22), its post-detection SNR will be larger.

For the MMSE detector the significance of SIC is not only to minimize the amplification of noise but also the cancelation of the interference from other antennas.

In addition, there is another opportunity to improve the performance by optimal ordering the SIC process. The ordering is based on the norm of the nulling vector. At each stage of cancelation, instead of randomly selecting the stream to detect, we choose the nulling vector that has the smallest norm to detect the corresponding data stream. This scheme is proved to be the globally optimum ordering [14].

Although SIC has many advantages, the need for measurement of the received amplitudes makes it more complex.

Some authors [15], [16] have tried to improve the performance of the MIMO receivers using multi-stage parallel-interference cancelation or a combination of these techniques which all result in more complex systems.

1.3.4 Lattice Reduction Based Detection

All lattice reduction based detection methods can be expressed using lattice basis transformation. Lattice basis transformation transforms one lattice basis to another. Usually transformed lattice basis is selected to be the lattice basis that has the shortest, and therefore closest to orthogonal, lattice basis. Suppose we have an arbitrary

lattice basis \mathbf{H} and it is transformed to \mathbf{H}' as $\mathbf{H}' = \mathbf{H}\mathbf{P}$, where \mathbf{P} is the transformation matrix. \mathbf{P} has to be a unimodular matrix to make this transformation valid. A unimodular matrix is defined as an invertible square matrix that has determinant $+1$ or -1 and all of its elements are integers or Gaussian integers, depending whether the matrix is real or complex. The algorithms that compute this unimodular matrix \mathbf{P} are referred to as the lattice reduction algorithms [17].

Finding the reduced shortest basis is in general difficult. Currently there are no polynomial-time algorithms that guarantee finding such basis [18]. In [19], Lenstra, Lenstra and Lovasz (LLL) proposed a lattice reduction algorithm that reduces a lattice basis to a so-called LLL-reduced lattice basis.

There are many proposed lattice detection algorithms such as the very early one in [17], based on zero-forcing, and [20], based on MMSE. The first technique is briefly introduced here and depicted in Figure 1.7. The baseband signal is passed through

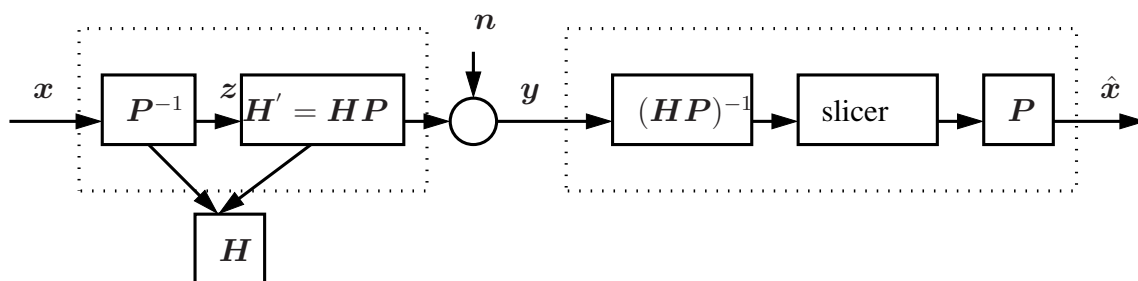


Figure 1.7: Lattice reduction based detection

two concatenated channels \mathbf{P}^{-1} and \mathbf{H}' . The transformed signal, after \mathbf{x} passed through the first channel \mathbf{P}^{-1} is denoted by \mathbf{z} . Since \mathbf{H}' is LLL-reduced lattice basis, as a channel, it is more orthogonal and conditioned. The zero-forcing detection $(\mathbf{H}\mathbf{P})^{-1}$ is used to recover \mathbf{z} . This process involves less noise enhancement than using \mathbf{H}^{-1} directly to recover \mathbf{x} . The rest of the receiver is a reverse transformation from the estimate of \mathbf{z} to the estimate of \mathbf{x} . By doing so, the channel noise enhancement due to the ill-conditioned channel is largely reduced and the detection performance is greatly improved.

1.4 Nonlinear Precoding Techniques

In interference channels linear equalizers may suffer from noise enhancement and ZF based equalizers may suffer from error propagations. For channels whose characteristics vary slowly compared to the transmitted frame duration, the CSI can be fed back to the transmitter, in which case, it is possible to avoid these problems by placing equalizers at the transmitter [21]. Employing equalization techniques at the transmitter is referred to as precoding. Tomlinson-Harashima Precoding (THP) [22] [23] is a precoding technique proposed in early 1970s for ISI channels with CSI known at the transmitter. From early 1980s Dirty Paper Coding (DPC) [24] precoding techniques indicate that when CSI in the form of interference is present at the transmitter, the channel capacity is the same as the capacity of a channel with no interference. These results motivate us to investigate applications of precoding for MIMO channels and MIMO BC.

1.4.1 The Tomlinson-Harashima Precoding

In THP the transmitter selects the transmitted signal based on the CSI and the previously transmitted symbols such that the receiver sees no ISI.

Assume the channel impulse response of an ISI channel with L taps is

$$h(t) = 1 + \sum_{l=1}^{L-1} h_l \delta(t - lT_s)$$

where T_s is the symbol duration. Information bits are modulated using M -QAM as complex symbols s_i . Without THP, at time 0, the received signal is $s_i + I_i + n_i$ where n_i is the noise term and

$$I_i = \sum_{l=1}^{L-1} h_l x_{i-l},$$

where x_{i-l} 's are the previously transmitted baseband discrete signals. Since the transmitter has access to CSI and x_{i-l} 's, it can transmit $x_i = s_i - I_i$ to pre-cancel the ISI. In this way the receiver receives no interference from the previously transmitted signals.

The transfer function of the THP operation can be described in the transform

domain as

$$X(z) = S(z) - (X(z)H(z) - X(z)),$$

or

$$X(z) = H^{-1}(z)S(z)$$

where $H(z)$ is the z -transform of the normalized channel impulse response, written as

$$H(z) = 1 + \sum_{l=1}^{L-1} h_l z^{-l}.$$

Since the natural channel does not guarantee the stability of this system, i.e., $H(z)$ is not bounded-input-bounded-output, a modulo operation has to be applied to the signal at the output of the filter, before the signal being fed back to the filter and transmitted, i.e.,

$$x'_i = (s_i - I_i) \bmod 2M = s_i - I_i + 2m_i M$$

where m_i is some Gaussian integer.

The received signal then can be written as

$$r_i = s_i + 2m_i M + n_i.$$

If the same modulo operation is applied in the receiver to r_i ,

$$r'_i = s_i + (n_i \bmod 2M).$$

In this way the communication becomes ISI free. The THP system block-diagram is depicted in Figure 1.8.

1.4.2 Dirty Paper Coding

THP is an early development of methods dealing with interference channels. DPC approaches the precoding for interference cancelation problem from an information theoretical point of view. Some practical DPC algorithms share many common ideas with THP.

A Gaussian channel model has one transmitter, one receiver and is subject to

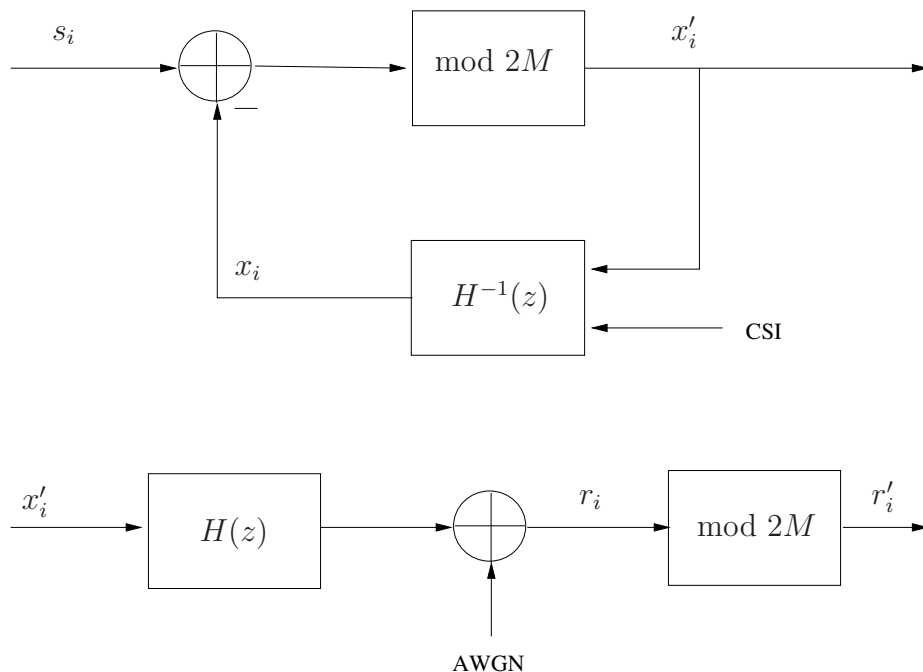


Figure 1.8: THP system block diagram

additive Gaussian noise. When there exists a power constraint P on the input, the capacity of this channel is well-known. In some applications the channel is corrupted by two independent additive disturbances, one of which is known non-causally at the transmitter representing the interference. This interference can be modeled as a random parameter of the channel which is known at the transmitter. Therefore, we can model this communication situation as a Gaussian channel with side information at the transmitter.

A variation of the standard AWGN channel model is depicted in Figure 1.9. In

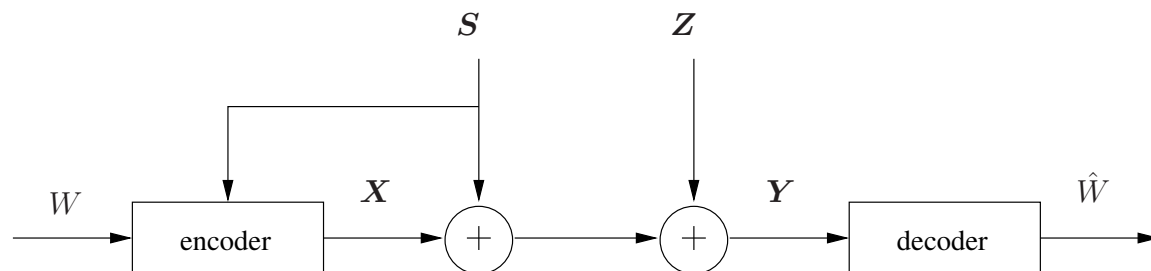


Figure 1.9: Dirty paper channel model

this channel an independent Gaussian interference, which is unknown to the receiver and known non-causally to the transmitter is added to the transmitted signal. The output of the channel is

$$\mathbf{Y} = \mathbf{X} + \mathbf{S} + \mathbf{Z}, \quad (1.23)$$

where the interference state $\mathbf{S} \sim N(\mathbf{0}, \beta \mathbf{I})$ is a sequence of i.i.d. Gaussian random variables. The noise is i.i.d. Gaussian $\mathbf{Z} \sim N(0, N_0 \mathbf{I})$ and is independent of \mathbf{S} . We want to send an index W of 2^{nR} messages to the receiver by n transmissions over this channel. We assume all messages are equally likely. The input codeword sequence $\mathbf{X} \in \mathcal{R}^n$ must satisfy the power constraint $\frac{1}{n} \mathbf{X}^T \mathbf{X} \leq P$. With the knowledge of \mathbf{S} , encoder designs codeword \mathbf{X} based on W and \mathbf{S} . The decoder receives sequence \mathbf{Y} and make an estimate of W , denoted by \hat{W} .

This channel model is defined by Costa in [24] and the coding schemes that are suitable for the dirty paper channel model are usually called dirty paper precoding schemes. The name comes from the title of that paper, “Writing on Dirty Paper”. The writer writes a message on a dirty paper and knows the location and density of the dirt. The reader cannot distinguish the dirt from the ink marks applied by the writer and to distinguish the message. A good writer can adapt his writing with those dirt so that the reader has a good understanding of his writing. The dirty-paper channel capacity problem was first suggested by Cover who conjectured the answer, while in 1983 Costa in [24] actually proved the conjecture.

Although the capacity of dirty paper channel with i.i.d. Gaussian interference and independent noise and transmit power constraint is found in early 1980s, intensive research on this topic started only recently from 2000 due to the work of digital watermarking and interference channel communications.

Before the dirty paper channel, Gel’fand and Pinsker in [25] had shown that the capacity of a discrete memoryless channel with random state \mathbf{S} known only to the encoder is given by

$$C = \max_{p(u, x|s)} \{I(U; Y) - I(U; S)\}, \quad (1.24)$$

where the maximum is over all joint distributions of the form $p(s)p(u, x|s)p(y|x, s)$,

and U is a finite alphabet auxiliary random variable

$$\|U\| \leq \min(\|X\|, \|Y\|) + \|S\| - 1.$$

In general cases when β is comparable with or much larger than P , the scheme introduced in [25] has poor performance since the transmit power is not enough to reduce the total noise significantly. A new approach is used here. First we define a one dimensional uniform quantizer

$$\mathbb{Q}_u = \mathbb{Q}_{(AZ+A/2)} = \left(\cdots, -\frac{3A}{2}, -\frac{A}{2}, \frac{A}{2}, \frac{3A}{2}, \cdots \right)$$

where $A^2 \gg N_0$. The interference is quantized to \mathbb{Q}_u . The encoder spends part of the transmitter power P^{conc} to concentrate the interference to \mathbb{Q}_u , i.e. the closest point in the set of \mathbb{Q}_u to the interference. The rest of the transmitted power is used for signal transmission. Now the transmitted signal can be considered as the quantization error, i.e., the difference between the interference S and the quantized value $\mathbb{Q}_u(S)$. At the receiver end, decoder matches the received signal to the quantizer q_u grid, the decision is made not based on the whole real line but within one segment between two consecutive quantization points that the received signal falls into. This scheme is also very similar to the modulo operation described in the discussion of Tomlinson-Harashima precoding. A more explicit interpretation is depicted in figure (1.10). Suppose we would like to modulate information to 4-PAM constellation. In

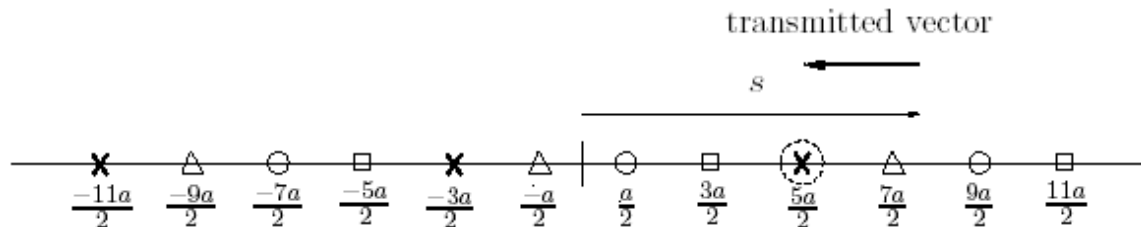


Figure 1.10: Transmit 4 PAM with interference

the presence of additive interference, this 4-PAM constellation is replicated along the entire real line. The original constellation points are located at $-\frac{3a}{2}$, $-\frac{a}{2}$, $\frac{a}{2}$ and $\frac{3a}{2}$. Points marked by the same sign in the figure (1.10) correspond to the same symbol.

Transmitter wants to transmit the cross sign and knows that the interference exceeds the $7a/2$ point. The closest cross sign is located at $5a/2$, therefore the difference $5a/2 - S$ is transmitted so that receiver sees the received signal around the point $5a/2$ and if without noise, the symbol that cross sign represents can be recovered without error. Unlike the compensation scheme used previously, the transmit power $\mathbb{Q}_u(S) - S$ can be much smaller and does not depend on S . The received signal becomes

$$Y = (\mathbb{Q}_u(S) - S) + S + Z = X' + Z.$$

This simple but luminous approach is called symbol-by-symbol precoding in [6].

There is still plenty of space to improve the above scheme. Instead of uncoded one-dimension transmission, for block coding, we can replicate the original constellation into n -dimensional space to form a n -dimensional uniform quantizer. A two-dimensional replicated constellation is depicted in figure (1.11). The transmit signal

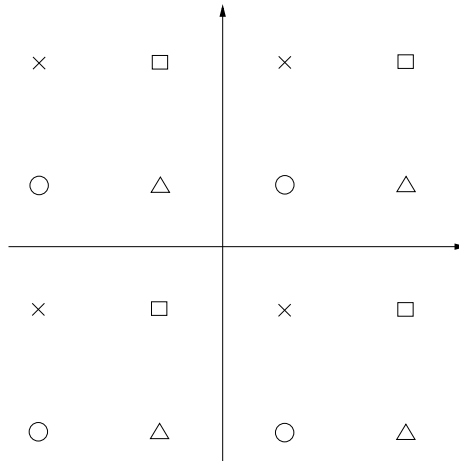


Figure 1.11: 2-D constellation replication

becomes the difference vector

$$\mathbf{X} = \mathbb{Q}_u(\mathbf{S}) - \mathbf{S}.$$

The maximum achievable rate of reliable communication for such scheme is estimated

using sphere packing and sphere covering. If the total power constraint is P ,

$$R \leq \frac{1}{2} \log_2 \frac{P}{N_0},$$

which is strictly suboptimal in the sense that it does not meet the AWGN capacity. The performance of such scheme can be enhanced via MMSE estimation which reduces the radius of the decoding uncertainty sphere. Details can be found in [6]. Actually, the involved multi-dimensional lattice quantization and MMSE scaling techniques are proved to be necessary tools to achieve full DPC capacity [26], [27]. Another newly proposed transmitter interference cancelation scheme is presented in [28].

The developing multi-user multiple input multiple output (MIMO) systems can achieve very high data rates. However, the inter-user, inter-antenna and inter-symbol interference cancelation become critical in these systems. The initial connection between DPC and MIMO-GBC was introduced in [29] with arbitrary interference. Zero-forcing beamforming is combined with single user DPC to simulate the DPC in multi-user MIMO-GBC. Using this approach, the capacity region of the MIMO-GBC is found to be equivalent to the DPC rate region under the same total power constraint in [30].

1.5 Main Contributions of the Dissertation

In a broadcast multiple antenna wireless communication system, as shown in Figure 1.12, utilizing multiple transmit and receive antennas in the downlink is of great interest due to the demand for high data rates and large user capacity. The capacity region for the degraded BC, for instance the Gaussian BC (GBC) with one transmit antenna and multiple receivers each with a single receive antenna, is well-known [31]. However, the GBC with multiple antennas is generally non-degraded and cannot be reduced to equivalent parallel degraded BCs. The capacity of MIMO-GBC was first considered in [32] where its sum-rate capacity was also derived. In [30], [33] the capacity region of MIMO-GBC is proved to be equivalent to the rate region achievable by Dirty Paper Coding (DPC).

The DPC interference channel model was introduced in [24] with the assumption

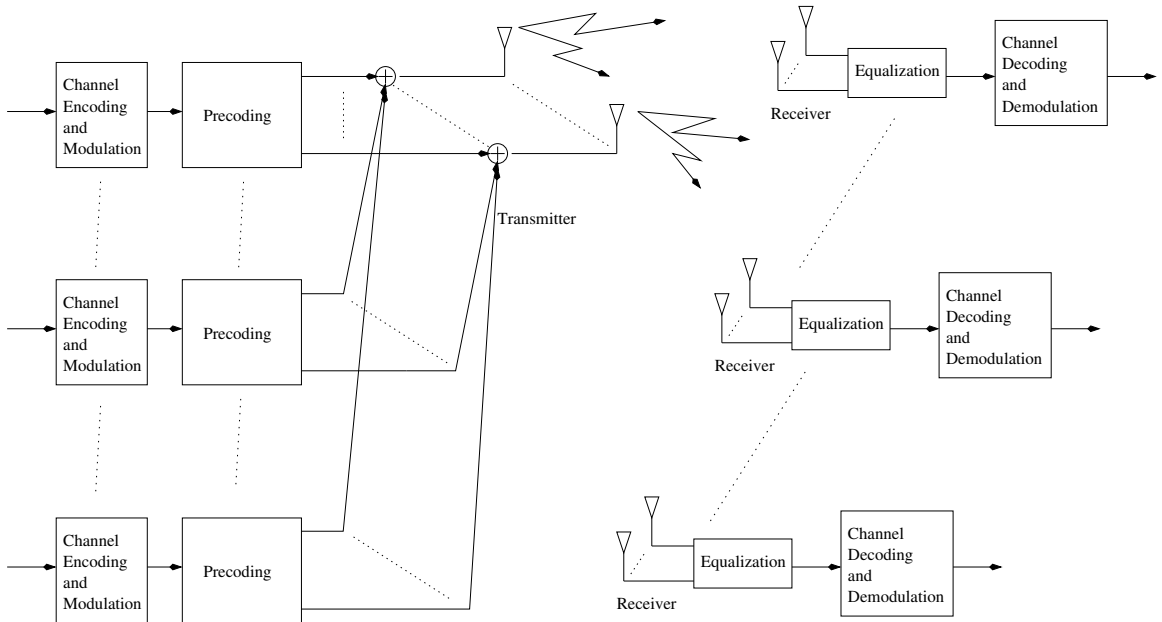


Figure 1.12: MIMO broadcast channel precoding and equalization

that the interference is known at the transmitter in advance and the interference and the channel noise are independent Gaussian processes. The assumptions in [24] were then extended to various scenarios in [34] [35] [36]. A number of works have pointed out the connection between DPC and information embedding and digital watermarking [37] [38]. DPC was first utilized in communication systems in [39] based on quantization of the interference. A close to capacity DPC scheme based on multidimensional lattice quantization and MMSE scaling was proposed in [27] for the case of general interference. In MIMO-BC, a number of practical DPC techniques such as ZF DPC [29], Ranked Known Interference (RKI) [29], Tomlinson-Harashima precoding [40] have been proposed. However, DPC schemes generally have high computational complexity, and many alternatives to DPC have been proposed which balance performance versus complexity.

Equalization and precoding are concepts usually treated separately from channel coding and modulation. At the transmitter, after channel encoding and modulation, the coded and modulated signals from different users are processed, usually multiplying by user-dependent matrices, and then summed to construct the equivalent transmit signal before pulse shaping. The user-dependent matrices are computed

according to the user's channel conditions and possibly other concerns. At each receiver, the baseband equivalent received signal, which is the sum of the low-pass equivalents of the transmitted signal and the channel noise, is processed again to construct the statistics for symbol detection or the soft output for demodulation and channel decoding.

If in equalization and precoding linear processing is employed, then the equalization and precoding are called linear. For example, in [41], coded signals for different users are multiplied by a set of user-dependent matrices, added and transmitted over the channel. The set of linear precoding matrices are selected so that the corresponding mutual information is maximized. A similar idea is used in [42] using STBC. A widely considered equalization technique is ZF based beamforming, working either at the receiver or at the transmitter [43]. Beamforming is an antenna technique for controlling electro-magnetic wave emission to achieve directional signal transmission, detection or reception. In this context, we refer to it as a spatial signal processing technique used to improve spatial selectivity when omnidirectional antennas are used in transmission/reception. In the MIMO case, it is also capable of supporting multiple data streams over spatial sub-channels and can be classified as a type of equalization. With the CSI available at the transmitter, ZF precoding can nullify interuser interference so that the users would not experience any interference from other users, resulting in improved performance when interference to noise ratio is large. This is a suboptimal strategy but can achieve the same asymptotic sum-rate capacity as DPC when the number of users is large. The problem with this equalizer is that when it nullifies the interuser interference, the noise gets enhanced. There are other types of linear equalization and precoding techniques such as LMMSE that have different advantages and disadvantages.

Linear equalization can be implemented with low computational complexity and has been widely studied and used. However, the linearity constraint limits the performance of these systems, resulting in increased interest in research on non-linear equalization techniques. For instance, LR aided MIMO detection [17] is a receive equalization technique that combines non-linear LR operation and linear equalization to achieve near MLD performance. Many of these non-linear equalization techniques increase complexity in exchange for enhanced performance gain.

In this thesis, a novel linear joint precoding-equalization technique, Coordinated Interference-aware Beamforming (CIB) is proposed. This technique is sub-optimal but has a closed-form solution for the equalization and precoding matrices. The Bit Error Rate (BER) performances and achievable rates of CIB under different scenarios are investigated using analytical and simulation results.

Next, we extend CIB to chip-level equalization in MIMO broadcast and spread-spectrum frequency-selective channels. The interuser interference, inter-symbol interference and inter-chip interference can be modeled in similar way as the interference presents in frequency non-selective MIMO broadcast channels. This motivates the research on using CIB in the spread-spectrum frequency-selective MIMO broadcast channels.

In Chapter 4, a new non-linear precoding system for MIMO single user flat-fading channel is proposed. As a novel Eigenvalue Decomposition based Lattice Precoding (EDLP), a linear-complexity non-linear precoding technique for single user MIMO flat-fading channels is developed. Similar to other nonlinear precoding or equalization techniques, such as lattice reduction based techniques, the EDLP algorithm also achieves full diversity order ($\max(N_t, N_r)$) in the presence of spatial multiplexing. However, unlike other lattice precoding or equalization techniques, EDLP does not require complex lattice reduction algorithms. Even more interestingly, EDLP enjoys a power gain over other lattice precoding techniques through its coordinated transmission.

In Chapter 5, we propose a coordinated precoding and equalization technique, BDZF-EDLP, for flat-fading MIMO broadcast channels. This technique uses block-diagonal zero-forcing precoding techniques and the proposed EDLP technique. The BDZF technique through a coordinated precoding and equalization mechanism can nullify different users' block MIMO channel with linear complexity. After the multi-user interference is muted, EDLP takes place to efficiently utilize the transmitted power and minimize the bit error rate. In this way, this new technique takes advantages of both techniques and is able to provide a good balance between complexity and performance.

Another approach to deal with the spread-spectrum frequency-selective MIMO broadcast channel is to have two composite stage of equalizations. The first stage

consists of a bank of single-user spread-spectrum frequency selective channel equalizers, that combat with the ISI brought by the channel to certain extent. And the second stage is a normal multi-user MIMO flat-fading broadcast channel equalizer. In the first stage, for the channel it deals with, RAKE receiver is a widely used architecture, which is equivalent to matched filter detection. Although it has a simple implementation but its performance gain is also limited. In high speed channels, more advanced receive equalization technique are needed. After 3GPP release 5, receivers with better performance are assumed to support High Speed Downlink Packet Access. Generalized RAKE (G-RAKE) receiver equalization is therefore proposed and is expected to achieve better performance compared to RAKE by improved channel probing techniques and better estimation and cancelation on interference correlation. After analyzing G-RAKE technique in detail in Chapter 6, a novel finger placement algorithm is proposed. This algorithm serves an important part of GRAKE equalization and provides a better performance with similar complexity comparing to the originally used finger placement algorithm.

Chapter 2

Coordinated Interference-Aware Beamforming (CIB)

In this chapter a number of linear techniques for spatial precoding and equalization in MIMO single-user and broadcast channels are discussed. Moreover, a new linear technique, using spatial precoding at the transmitter and spatial equalization at the receiver is introduced. Since this technique uses channel side information (CSI) at both sides, it is called a coordinated technique.

The ultimate goal of all techniques used in broadcast channels is to maximize the capacity. As we have seen in Section 1.1.2, the ergodic capacity, i.e., the average capacity over all possible channel realizations, can be used to evaluate the performances of precoding and equalization techniques.

We assume that there are K active users (clients) in the broadcast channels and each client has $N_{r,i}$ receive antennas, i.e., the total number of independent data streams can be up to $\sum_{i=1}^K N_{r,i}$ and therefore the capacity region of the broadcast channel has up to $\sum_{i=1}^K N_{r,i}$ dimensions. An intuitive and tractable metric for evaluation of the transmission capability of this channel is its sum-rate capacity, defined as the sum of the capacities of all the spatial channels, $\sum_{i=1}^K \sum_{j=1}^{N_{r,i}} C_{i,j}$. Such capacity metric conceptually is close to the downlink throughput of a cell in cellular networks. Sum-rate capacity is used in this chapter as the performance metric to evaluate linear techniques proposed for MIMO broadcast channels.

A number of transmission techniques have been proposed to utilize MIMO in

practical systems for broadcast channels, where the interference is the major impairment compared to the channel noise [44]. For such applications DPC [33], [27],[26] is a capacity achieving and theoretically optimal technique that can transmit signal transparently through the interference. Techniques using Ranked Known Interference (RKI) [29] and Tomlinson-Harashima precoding [40] are proposed as practical alternatives to DPC. However, practical low-complexity alternatives to DPC for BCs are still under development.

Single-user MIMO SVD precoding [8] [45] is a natural candidate that can be easily extended to broadcast channels. However, in this approach the inter-user interference, which is known at the base station, is modeled as unknown noise, thus preventing it from achieving good performance in multi-user scenarios. Well addressed low complexity techniques which can nullify the inter-user interference are Zero Forcing BeamForming (ZFBF) [43] and Block Diagonal Zero Forcing (BDZF) [46] techniques. In ZFBF, each precoded data stream is designed to be orthogonal to the channels of all other streams so that the interference from other spatial channels is completely canceled. In BDZF, after precoding, each user's signal space lies in the null space of all other users' signal space, hence nullifying the inter-user interference.

These ZF techniques lead to closed form solutions for MIMO BC capacities. Furthermore, the ergodic sum capacity scales similar to DPC as a function of the number of users for Rayleigh fading channels [46]. Some more advanced techniques, for instance user scheduling, can be based on ZF. But before moving to such upper layer techniques, we need to make sure that the base technique is good enough. Actually, similar to the cases when ZF is applied to receive equalization which results in noise enhancement, the use of ZFBF and BDZF at the transmitter side attenuates the signal power. We can consider ZF and SVD as two extreme cases where SVD optimizes the received SNR regardless of the inter-user interference, and ZF nullifies the inter-user interference without being concerned about the received SNR. Indeed, SVD-MMSE outperforms ZF techniques at low SNR values but at high SNR its performance is dominated by interference and reaches an upper ceiling. Sum capacity of ZFBF and BDZF converge at high SNR region and both monotonically increase with the SNR. In this chapter we propose CIB which can be used with any number of transmit and receive antennas and interpolates between the sum-rates of SVD-MMSE at low SNR

and ZF at high SNR values. CIB can be used as a base technique upon which more complicated scheduling techniques can be developed.

Optimal linear transmit precoding design involves joint optimization of all users' beamformers and their power allocation. The large number of parameters, the interdependency amongst the beamformers, and the power constraint make this optimization problem difficult to solve, even though the duality of MIMO-MAC and MIMO-BC studied in [47] helps to convert this non-convex optimization problem to a convex problem. The suboptimal CIB, developed in this chapter, breaks the inter-dependency of the beamformers, thus making the optimization more tractable. Furthermore, the CIB chooses the beamforming direction to balance the signal power of each user and the interference introduced by that user. Each user sacrifices part of its signal power to reduce the interference it causes to other users. The asymptotic optimality of the CIB in terms of SNR and number of users is evaluated through analytical and simulation results.

Notice that in this model during the channel estimation phase we cannot use a common pilot for estimating the precoded channel because each user uses a different precoding filter and thus the effective channel matrix contains the precoding filter as well as the raw channel matrix.

2.1 System and Channel Model

Our system model is basically a downlink flat-fading broadcast channel with multiple antennas at both transmitter and receiver sides. Suppose there are K active users in the system at a given time slot. Let N_t denote the number of transmit antennas at the base station and $N_{r,k}$ the number of receive antennas at each user k , $1 \leq k \leq K$ as shown in Figure 2.1. Each user operates in either full diversity mode or spatial multiplexing mode; depending on the wireless MIMO channel condition it experiences and/or client demands. In the spatial multiplexing mode, the base station transmits L_k information symbols per channel use for user k , where $1 \leq L_k \leq \min(N_{r,k}, N_t)$. For user k , $\min(N_{r,k}, N_t)$ is the maximum number of independent data streams that a $N_{r,k}$ -by- N_t MIMO channel can accommodate. The method by which the system selects L_k for each user can depend on different criteria, for instance, minimizing total

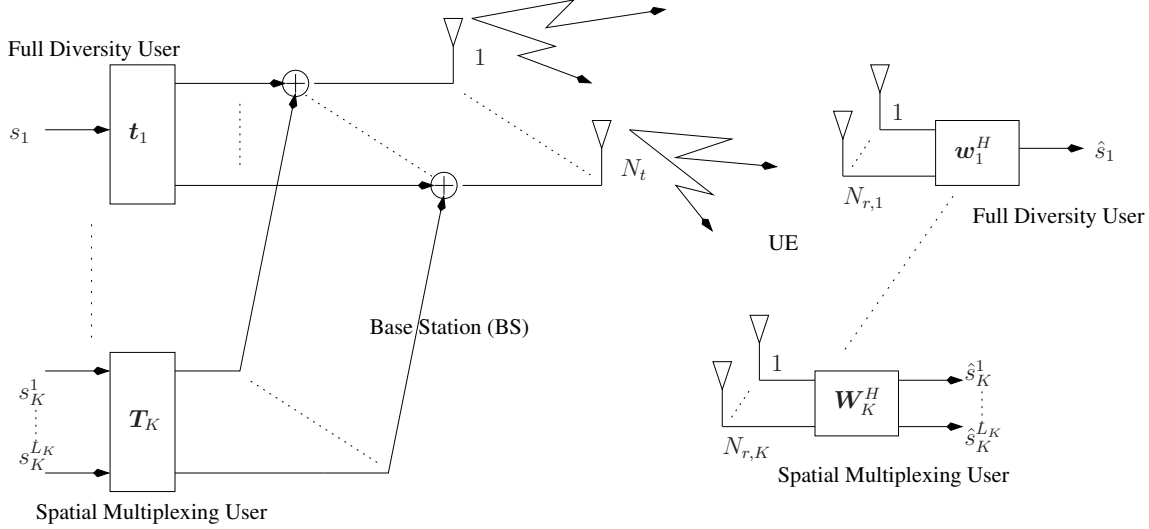


Figure 2.1: System model of coordinated interference-aware beamforming (CIB)

transmit-receive error or maximizing multi-user diversity. In cases when error rate is critical, or the channel for one user is ill-conditioned and therefore is hardly able to support multiple stream transmission, full diversity mode is used to transmit only one symbol per channel use in exchange for higher diversity order. Therefore, full diversity mode can be considered as a special case of spatial multiplexing mode. The choice of L_k 's is left for further optimization. We first present our analysis assuming a given set of L_k 's.

We assume the rank of each user's channel matrix is equal to $\min(N_t, N_{r,k})$, indicating that maximum spatial multiplexing order is possible.

Transmitted symbols are assumed to be independent, complex random variables with unit power selected, for example, from a PSK constellation. We denote the index of the spatial subchannel of user k by l_k , $1 \leq l_k \leq L_k$. User k 's l_k th symbol, $s_k^{l_k}$ is precoded by an assigned beamforming vector $\mathbf{t}_k^{l_k}$. Every beamforming vector $\mathbf{t}_k^{l_k}$ is normalized and has unit L^2 norm. The transmitter is total-power limited. The total transmit power constraint is denoted by P and is referred to as the total SNR based on the following settings. Each spatial sub-channel data is allocated certain amount

of power $\alpha_k^{l_k}$ which add up to P over spatial channels of all users,

$$\sum_{k=1}^K \sum_{l_k=1}^{L_k} \alpha_k^{l_k} = P.$$

This means the beamforming signal of each spatial channel is the data symbol distributed over N_t transmit antennas by $\mathbf{t}_k^{l_k}$ and scaled by $\alpha_k^{l_k}$. The transmit signal at the N_t transmit antennas of the base station is the sum of all precoded symbol vectors

$$\mathbf{x} = \sum_{k=1}^K \sum_{l_k=1}^{L_k} \alpha_k^{l_k} \mathbf{t}_k^{l_k} s_k^{l_k} \quad (2.1)$$

and the received signal by user k is

$$\mathbf{y}_k = \mathbf{H}_k \mathbf{x} + \mathbf{n}_k = \mathbf{H}_k \sum_{l_k=1}^{L_k} \alpha_k^{l_k} \mathbf{t}_k^{l_k} s_k^{l_k} + \mathbf{H}_k \sum_{\substack{i=1 \\ i \neq k}}^K \sum_{l_i=1}^{L_i} \alpha_i^{l_i} \mathbf{t}_i^{l_i} s_i^{l_i} + \mathbf{n}_k \quad (2.2)$$

where the $N_{r,k}$ -by- N_t channel matrix \mathbf{H}_k for any user k is a random matrix whose entries are assumed to be i.i.d. circular complex Gaussian random variables with zero mean and variance $1/2$ per dimension. The channel matrices $\mathbf{H}_k, 1 \leq k \leq K$, are assumed to be known at the base station whereas user k knows only the realizations of its own channel matrix \mathbf{H}_k at the receiver end. The noise \mathbf{n}_k is an $N_{r,k} \times 1$ vector with i.i.d. circular complex Gaussian components each with zero mean and unit variance, independent of the signal and the channel fading.

Linear spatial equalization is assumed to be employed in coordination with the transmit precoding. The received signal vector at user k , consisting of signal elements on each receive antenna is equalized by \mathbf{w}_k , the l_k th receiver equalizer. The result provides a decision variable for symbol detection of $s_k^{l_k}$, given by

$$\hat{s}_k^{l_k} = (\mathbf{w}_k^{l_k})^H \mathbf{y}_k \quad (2.3)$$

$$= (\mathbf{w}_k^{l_k})^H \mathbf{H}_k \alpha_k^{l_k} \mathbf{t}_k^{l_k} s_k^{l_k} + (\mathbf{w}_k^{l_k})^H \mathbf{H}_k \sum_{\substack{(i,l_i)=(1,1) \\ (i,l_i) \neq (k,l_k)}}^{(K,L_k)} \alpha_i^{l_i} \mathbf{t}_i^{l_i} s_i^{l_i} + (\mathbf{w}_k^{l_k})^H \mathbf{n}_k \quad (2.4)$$

where the three terms in Equation (2.4) can be considered as the desired signal, the interference, and the noise, respectively. The receiver equalizer $\mathbf{w}_k^{l_k}$ can be arbitrarily scaled without affecting the performance.

2.2 SVD-MMSE Precoding

SVD-MMSE technique uses SVD decomposition at the transmitter as a precoding technique and linear MMSE at the receiver for equalization [48].

This scheme performs SVD decomposition on the individual channel matrices of each user k , \mathbf{H}_k , at the transmitter side,

$$\mathbf{H}_k = \mathbf{U}_k \mathbf{D}_k \mathbf{V}_k^H.$$

The precoding vectors for each individual user signal is selected as the column vectors of the matrix \mathbf{V}_k . Therefore, by Equation 2.1, the precoding vectors of the spatial channels of user k in SVD-MMSE technique are set to be

$$\left[\mathbf{t}_k^1, \dots, \mathbf{t}_k^{L_k} \right] = \left[\mathbf{v}_k^1, \dots, \mathbf{v}_k^{L_k} \right],$$

where $\mathbf{v}_k^1, \dots, \mathbf{v}_k^{L_k}$ are L_k column vectors of matrix \mathbf{V}_k . In this case the transmit signal becomes

$$\mathbf{x} = \sum_{k=1}^K \sum_{l_k=1}^{L_k} \alpha_k^{l_k} \mathbf{v}_k^{l_k} s_k^{l_k}. \quad (2.5)$$

For a more compact notation we define

$$\mathbf{V}_k^{L_k} = \left[\mathbf{v}_k^1, \dots, \mathbf{v}_k^{L_k} \right].$$

Using this notation the transmit signal of SVD-MMSE given by Equation 2.5 can be rewritten as

$$\mathbf{x} = \sum_{k=1}^K \mathbf{V}_k^{L_k} \mathbf{P}_k \mathbf{s}_k \quad (2.6)$$

where \mathbf{s}_k is a vector of size L_k , defined as

$$\mathbf{s}_k = [s_k^1, s_k^2, \dots, s_k^{L_k}]$$

and \mathbf{P}_k is a diagonal matrix representing power allocation, i.e.,

$$\mathbf{P}_k = \begin{bmatrix} \alpha_k^1 & 0 & \cdots & 0 \\ 0 & \alpha_k^2 & \cdots & 0 \\ \vdots & \vdots & \ddots & \vdots \\ 0 & 0 & 0 & \alpha_k^{L_k} \end{bmatrix}.$$

Note that when $L_k < \min(N_t, N_{r,k})$, in order to exploit the maximum channel gains, we select vectors $\mathbf{V}_k^{L_k}$ in \mathbf{V}_k that are corresponding to the L_k largest singular values.

When used with water-filling power allocation, this SVD transmit scheme is optimal in the sense that it maximizes the single user channel capacity and fully exploits the channel gain. However, in multi-user downlink case, where interference is the dominant impairment, this precoding technique does not address the problem of interference. That is, \mathbf{V}_k of user k is only a function of \mathbf{H}_k and is independent of all other users' precoded signals. Actually, the single user SVD scheme can be regarded as a matched filter matched to the orthonormal basis \mathbf{U}_k and \mathbf{V}_k from two sides. So if SVD scheme is used for each user, the demodulators will experience not only AWGN but also colored multi-user interference. A minor modification is to use MMSE at the receiver of each user due to the fact that the receiver of each user can observe the multi-user interference. By doing so, the multi-user interference seen by the receiver can be mitigated to a certain level.

The problem of power allocation for this scheme is more challenging than the single user case. Since the multi-user interference exists and moreover, the multi-user interference depends on the choice of precoding and power allocation, we cannot simply use water-filling or similar power allocation techniques in this case. Here, for comparison purposes, we allocate the total available power equally on every spatial channel of every user although this allocation is not optimal. This means that we set

$$\mathbf{P}_k = \frac{P}{\sum_{k=1}^K L_k} \mathbf{I}.$$

As a result, the received signal before equalization can be written as

$$\begin{aligned} \mathbf{y}_k &= \mathbf{H}_k \mathbf{x} + \mathbf{n} \\ &= \mathbf{H}_k \mathbf{V}_k^{L_k} \mathbf{P}_k \mathbf{s}_k + \mathbf{H}_k \sum_{\substack{i=1 \\ i \neq k}}^{i=K} \mathbf{V}_i^{L_i} \mathbf{P}_i \mathbf{s}_i + \mathbf{n}. \end{aligned} \quad (2.7)$$

The linear MMSE reception has the following form,

$$\begin{aligned} \mathbf{r}_k &= \mathbf{R}_k^H \mathbf{y}_k \\ &= \mathbf{R}_k^H \mathbf{H}_k \mathbf{V}_k^{L_k} \mathbf{P}_k \mathbf{s}_k + \mathbf{R}_k^H \mathbf{H}_k \sum_{\substack{i=1 \\ i \neq k}}^{i=K} \mathbf{V}_i^{L_i} \mathbf{P}_i \mathbf{s}_i + \mathbf{R}_k^H \mathbf{n} \end{aligned}$$

and \mathbf{R}_k is selected to maximize the MSE

$$\mathbf{R}_{k,opt} = \underset{\mathbf{R}_k}{\operatorname{argmax}} \mathbb{E}[\|\mathbf{r}_k - \mathbf{s}_k\|^2].$$

Since all data symbols $s_k^{l_k}, 1 \leq k \leq K, 1 \leq l_k \leq L_k$ and noise components are independent and zero mean random variables,

$$\mathbf{R}_k = \left[\sum_{\substack{i=1 \\ i \neq k}}^{i=K} \mathbf{H}_k \mathbf{V}_i^{L_i} \mathbf{P}_i \mathbf{P}_i^H (\mathbf{V}_i^{L_i})^H \mathbf{H}_k^H + \mathbf{I} \right]^{-1} \mathbf{H}_k \mathbf{V}_k^{L_k} \mathbf{P}_k.$$

2.3 Zero-Forcing Precoding

If we define $\mathbf{s} = [\mathbf{s}_1^T, \mathbf{s}_2^T, \dots, \mathbf{s}_K^T]^T$,

$$\mathbf{T} = \left[\mathbf{t}_1^1, \mathbf{t}_1^2, \dots, \mathbf{t}_1^{L_1}, \mathbf{t}_2^1, \dots, \mathbf{t}_2^{L_2}, \dots, \mathbf{t}_K^1, \dots, \mathbf{t}_K^{L_k} \right],$$

$$\mathbf{y} = [\mathbf{y}_1^T, \mathbf{y}_2^T, \dots, \mathbf{y}_K^T]^T,$$

$$\mathbf{n} = [\mathbf{n}_1^T, \mathbf{n}_2^T, \dots, \mathbf{n}_K^T]^T \quad \text{and}$$

and

$$\mathbf{H} = \begin{bmatrix} \mathbf{H}_1 \\ \mathbf{H}_2 \\ \vdots \\ \mathbf{H}_K \end{bmatrix},$$

then we have

$$\begin{aligned} \mathbf{x} &= \mathbf{T}\mathbf{s} \\ \mathbf{y} &= \mathbf{H}\mathbf{x} + \mathbf{n} \\ &= \mathbf{HT}\mathbf{s} + \mathbf{n}. \end{aligned}$$

Similar to an IIR channel inverse filter, ZF precoding has the form of $\mathbf{T} = \alpha\mathbf{H}^{-1}$, where \mathbf{H}^{-1} is the right pseudo-inverse of the channel matrix \mathbf{H} , and therefore, $\mathbf{HT} = \mathbf{I}$. The positive scalar α is to scale the power that \mathbf{H}^{-1} induces to meet the total power constraint, i.e.,

$$\alpha \sum_i \|(\mathbf{H}^{-1})_i\|^2 = P,$$

where $(\mathbf{X})_i$ denotes the i th column of \mathbf{X} .

Since here we assume the right pseudo-inverse of the channel matrix exists, we automatically assume that the channel \mathbf{H} has fewer rows than columns, this assumption is equivalent to the assumption that the sum of all users' receive antennas is less than the number of transmit antenna, i.e.,

$$\sum_{k=1}^K N_{r,k} \leq N_t.$$

This dimension limit on ZF precoding is different from SVD-MMSE technique where there is no such limit. In large systems this assumption is not realistic. Therefore, additional scheduling is required to exclude some users.

Based on the above, the received signal vector on all receive antennas is simply

$$\mathbf{y} = \alpha\mathbf{s} + \mathbf{n}. \quad (2.8)$$

Equation 2.8 looks like a typical parallel Gaussian channel. However, the average transmitted power is not the average power of \mathbf{s} but the average power of \mathbf{x} , i.e.,

$$\begin{aligned} P &= \alpha \mathbb{E}[\|\mathbf{x}\|^2 | \mathbf{H}] \\ &= \alpha \mathbb{E}[\|\mathbf{H}^{-1} \mathbf{s}\|^2 | \mathbf{H}]. \end{aligned} \quad (2.9)$$

ZF receivers are also referred as decorrelator and are well-known to cause noise amplification when the channel is nearly rank deficient. When decorrelation is used in precoding, the noise amplification effect at the receiver side becomes the transmitted power amplification effect at the transmitter side. In both cases the objective is to restore the orthogonality of the signal that is reshaped by the channel.

To elaborate, we can denote the SVD of \mathbf{H} as $\mathbf{H} = \mathbf{U} \mathbf{D} \mathbf{V}^H$ and rewrite the transmitted power in Equation 2.9 as

$$\begin{aligned} P &= \alpha \mathbb{E}[\|\mathbf{D}^{-1} \mathbf{U}^H \mathbf{s}\|^2 | \mathbf{H}] \\ &= \alpha \mathbb{E} \left[\sum_j \lambda_j^{-2} \|(\mathbf{U}^H)_j\|^2 \|s_j\|^2 | \mathbf{H} \right] \\ &= \alpha \mathbb{E} \left[\sum_j \lambda_j^{-2} \|s_j\|^2 | \mathbf{H} \right]. \end{aligned}$$

The last equation follows from the fact all the column vectors of the unitary matrix \mathbf{U} have unit norm. If we assume the signal constellation is designed such that all symbols has absolute unit power, we can further simplify the above equations to

$$P = \alpha \sum_j \lambda_j^{-2}.$$

From Equation 2.8 we note that since the total power constraint P is fixed, α becomes small when λ_j^{-2} becomes large and such α has a direct impact on the signal scaling. Larger values of α result in smaller error probabilities. However, recall that we have assumed that the distribution of all elements of the channel matrix are Rayleigh distributed [49], in some cases when the condition number $\kappa_2(\mathbf{H})$ is large, the quantity λ_j^{-2} is dominated by the largest singular values and therefore limit α to a small scaling

factor. As a result, channel orthogonalization by ZF precoding suffers from large transmitted power requirements.

2.4 Block-Diagonal Zero-Forcing Precoding

In ZF precoding, every receive antenna carries an independent data stream (spatial multiplexing). The receiver detects the transmitted signal from each receive antenna individually. However, some users may have more than one receive antenna, which means the detector of a certain user may collect information from a number of antennas and perform joint detection. Even for independent circular noise the performance of joint detection is always better than individual detection [50]. For example, the decision regions of the detection problem in Equation 2.8 in two dimensional BPSK signal case (corresponding to the two antennas) are squares for individual detection but are hexagons for joint detection.

In [51], a novel precoding technique is proposed based on ZF and collaboration among receive antennas so that the detection performance can be improved. Here we keep most of the assumptions made in previous sections. Define

$$\tilde{\mathbf{H}}_k = [\mathbf{H}_1^T, \dots, \mathbf{H}_{k-1}^T, \mathbf{H}_{k+1}^T, \dots, \mathbf{H}_K^T]^T$$

and SVD of $\tilde{\mathbf{H}}_k$, with the convention that singular values are placed in descending order, as

$$\tilde{\mathbf{H}}_k = \tilde{\mathbf{U}}_k \tilde{\mathbf{D}}_k [\tilde{\mathbf{V}}_k^{(1)}, \tilde{\mathbf{V}}_k^{(0)}]^H$$

where the column vectors of $\tilde{\mathbf{V}}_k^{(1)}$ are the first $N_t - L_k$ right singular vectors and the column vectors of $\tilde{\mathbf{V}}_k^{(0)}$ are the rest of right singular vectors. Assuming $\sum_{k=1}^K N_{r,k} = N_t$, the dimensions of $\tilde{\mathbf{H}}_k$ is $N_t - N_{r,k}$ -by- N_t . It is easy to see that L_k needs to satisfy the condition $1 \leq L_k \leq \text{rank}(\tilde{\mathbf{H}}_k) \leq (N_t - N_{r,k})$. The orthonormal basis $\tilde{\mathbf{V}}_k^{(0)}$ is the null space of $\tilde{\mathbf{H}}_k$, i.e.,

$$\tilde{\mathbf{H}}_k \tilde{\mathbf{V}}_k^{(0)} = \mathbf{0},$$

or,

$$\mathbf{H}_i \tilde{\mathbf{V}}_k^{(0)} = \mathbf{0}, \quad 1 \leq k \leq K \text{ and } i \neq k.$$

From above, if we use $\tilde{\mathbf{V}}_k^{(0)}$ as the precoding matrix for signal \mathbf{s}_k of user k , then for all users,

$$\mathbf{T}'' = \left[\tilde{\mathbf{V}}_1^{(0)}, \tilde{\mathbf{V}}_2^{(0)}, \dots, \tilde{\mathbf{V}}_K^{(0)} \right]$$

and

$$\mathbf{H}\mathbf{T}'' = \begin{bmatrix} \mathbf{H}_1 \tilde{\mathbf{V}}_1^{(0)} & \mathbf{0} & \dots & \mathbf{0} \\ \mathbf{0} & \mathbf{H}_2 \tilde{\mathbf{V}}_2^{(0)} & \dots & \mathbf{0} \\ \vdots & \vdots & \ddots & \vdots \\ \mathbf{0} & \mathbf{0} & \dots & \mathbf{H}_K \tilde{\mathbf{V}}_K^{(0)} \end{bmatrix}$$

In this way, the multi-user channel matrix \mathbf{H} is block-diagonalized. This method separates the signals of different users and thus eliminates the multi-user interference. Although the defined \mathbf{T}'' is a legitimate precoding matrix, in order to maximize the sum-rate capacity, further operations are needed. Using \mathbf{T}'' , signals from different users become parallel. Each of these parallel channels is a MIMO single user channel. Therefore, maximizing the sum-rate capacity based on the block diagonalization of the channel matrix is equivalent to maximizing the capacity of each users' MIMO channel under a total power constraint P . Similar to the analysis in [8], user k 's equivalent single user MIMO channel can be decomposed by SVD as

$$\mathbf{H}_k \tilde{\mathbf{V}}_k^{(0)} = \bar{\mathbf{U}}_k \bar{\mathbf{D}}_k \left[\bar{\mathbf{V}}_k^{(1)}, \bar{\mathbf{V}}_k^{(0)} \right]^H$$

where the number of column vectors in $\bar{\mathbf{V}}_k^{(1)}$ equals to L_k , the spatial multiplexing order of user k .

Now we define a new precoding matrix

$$\mathbf{T}' = \left[\tilde{\mathbf{V}}_1^{(0)} \bar{\mathbf{V}}_1^{(1)}, \tilde{\mathbf{V}}_2^{(0)} \bar{\mathbf{V}}_2^{(1)}, \dots, \tilde{\mathbf{V}}_K^{(0)} \bar{\mathbf{V}}_K^{(1)} \right]$$

and a spatial equalization matrix

$$\mathbf{R} = \begin{bmatrix} \mathbf{R}_1 & \mathbf{0} & \dots & \mathbf{0} \\ \mathbf{0} & \mathbf{R}_2 & \dots & \mathbf{0} \\ \vdots & \vdots & \ddots & \vdots \\ \mathbf{0} & \mathbf{0} & \dots & \mathbf{R}_K \end{bmatrix}$$

where $\mathbf{R}_k = \bar{\mathbf{U}}_k$, then the channel can be totally diagonalized by the left multiplication factor \mathbf{R}^H and the right multiplication factor \mathbf{T}' as

$$\mathbf{R}^H \mathbf{H} \mathbf{T}' = \begin{bmatrix} \bar{\mathbf{D}}_1 & \mathbf{0} & \dots & \mathbf{0} \\ \mathbf{0} & \bar{\mathbf{D}}_2 & \dots & \mathbf{0} \\ \vdots & \vdots & \ddots & \vdots \\ \mathbf{0} & \mathbf{0} & \dots & \bar{\mathbf{D}}_K \end{bmatrix}.$$

We observe that not only the channels of different users are made parallel but the spatial channels of individual users are made parallel as well. The transmission-reception system model now becomes

$$\mathbf{r} = \mathbf{R}^H \mathbf{y} = \mathbf{R}^H \mathbf{H} \mathbf{T}' \mathbf{P} \mathbf{s} + \mathbf{R}^H \mathbf{n}$$

or equivalently,

$$\mathbf{r}_k = \mathbf{R}_k^H \mathbf{H}_k \left(\sum_{k=1}^K \tilde{\mathbf{V}}_k^{(0)} \bar{\mathbf{V}}_k^{(1)} \mathbf{P}_k \mathbf{s}_k \right) + \mathbf{R}_k^H \mathbf{n}_k.$$

Similarly, \mathbf{r} is defined as

$$\mathbf{r} = \begin{bmatrix} \mathbf{r}_1 \\ \mathbf{r}_2 \\ \vdots \\ \mathbf{r}_K \end{bmatrix}.$$

Note that $\mathbf{R}^H \mathbf{n}$ and $\mathbf{R}_k^H \mathbf{n}_k$ are still white and Gaussian since the blocks \mathbf{R}_k , $1 \leq k \leq K$, are orthonormal and so are the columns of the block diagonal matrix \mathbf{R} with block components \mathbf{R}_k .

Now transmitted power allocation can be done based on the preferred objective; either the error rate or the sum-rate. Equal power allocation can be used when the objective function is difficult to optimize.

2.5 Coordinated Interference-Aware Beamforming

Coordinated communications between transmitters and receivers is a natural generalization of precoding techniques since in many cases the CSI acquired by the transmitter is from the receiver, the assumption that CSI in certain form is available at both transmitter and the receiver sides is valid in many cases. For instance, in cellular networks, access terminals report channel quality indicator periodically to the base station. Coordinated beamforming tunes both communication sides jointly to enhance the beam power and therefore has a potential gain over techniques utilizes CSI at only one sides. Many researchers have focused on this topic [52] in recent years.

We assume a homogeneous network setting [53] in which all spatial channels are allocated the same amount of power, i.e., $P/(KN_r)$ for the spatial multiplexing mode and P/K for the full diversity mode. This is in contrast to SVD-MMSE, BDZF and ZFBF techniques that use their own power allocation schemes.

Suppose user k has L_k independent data streams for transmission, $1 \leq L_k \leq N_r$. Each symbol is first multiplied by the transmit beamforming vector and then added to similar terms from other users, as given in Equation (2.1). The channel matrix \mathbf{H}_k operates on the common transmitted signals to result in the received vector as shown in Equation (2.2). The receiver equalizer combines the channel outputs to produce the estimate of the symbol of interest as given by Equation (2.3). We can interpret the relationship between $s_k^{l_k}$ and $\hat{s}_k^{l_k}$ as a realization of a spatial channel and define $\gamma_k^{l_k}$ as the effective SINR for this channel. In the rest, for the sake of brevity, we consider the case where $N_{r,k} = N_r$ for all k and $N_t \geq N_r$. A simple modification is needed when $N_r \geq N_t$.

2.5.1 Full Diversity Mode

First we consider the case where all users are in full diversity mode, i.e., $L_k = 1$ for all users, i.e., $1 \leq k \leq K$. In this case the symbol index l_k can be eliminated. The

effective SINR can now be expressed as

$$\gamma_k = \frac{\mathbb{E} [\mathbf{w}_k^H \mathbf{H}_k \mathbf{t}_k s_k s_k^H \mathbf{t}_k^H \mathbf{H}_k^H \mathbf{w}_k]}{\mathbb{E} \left[\left\| \mathbf{w}_k^H \left(\mathbf{H}_k \sum_{\substack{i=1 \\ i \neq k}}^K \mathbf{t}_i s_i + \mathbf{n}_k \right) \right\|^2 \right]} \quad (2.10)$$

$$= \frac{\mathbf{w}_k^H \mathbf{H}_k \mathbf{t}_k \mathbf{t}_k^H \mathbf{H}_k^H \mathbf{w}_k}{\mathbf{w}_k^H \Phi_k \mathbf{w}_k} \quad (2.11)$$

where

$$\Phi_k = \mathbf{H}_k \sum_{\substack{i=1 \\ i \neq k}}^K \mathbf{t}_i \mathbf{t}_i^H \mathbf{H}_k^H + \mathbf{I},$$

and the expectation is taken over transmit symbols and the noise. The beamforming and the equalization vectors for user k are denoted as \mathbf{t}_k and \mathbf{w}_k as before but the superscripts are eliminated. The effective SINR is the key parameter to design the beamforming and equalization vectors since the capacity and the bit error rate (BER) can be expressed as proportional functions of it. Maximizing this effective SINR pushes the channel capacity toward its maximum and the BER toward its minimum, as what we expected.

It is also notable that the nominator of Equation (2.11) represents the desired signal power whereas the denominator represents the interference power plus the noise power. Equation (2.11) is in the form of a Rayleigh quotient with respect to vector \mathbf{w}_k . Maximization of a Rayleigh quotient results in a generalized eigenvalue problem. To see this, let us first determine the extreme points of $\gamma_k(\mathbf{w}_k)$, i.e., the points \mathbf{w}_k^* satisfying

$$\nabla \gamma_k(\mathbf{w}_k^*) = 0.$$

The gradient $\nabla \gamma_k(\mathbf{w}_k)$ is calculated as

$$\begin{aligned} \nabla \gamma_k(\mathbf{w}_k) &= \frac{2\mathbf{H}_k \mathbf{t}_k \mathbf{t}_k^H \mathbf{H}_k^H \mathbf{w}_k (\mathbf{w}_k^H \Phi_k \mathbf{w}_k) - 2(\mathbf{w}_k^H \mathbf{H}_k \mathbf{t}_k \mathbf{t}_k^H \mathbf{H}_k^H \mathbf{w}_k) \Phi_k \mathbf{w}_k}{(\mathbf{w}_k^H \Phi_k \mathbf{w}_k)^2} \\ &= \frac{2\mathbf{H}_k \mathbf{t}_k \mathbf{t}_k^H \mathbf{H}_k^H \mathbf{w}_k - 2\gamma_k(\mathbf{w}_k) \Phi_k \mathbf{w}_k}{\mathbf{w}_k^H \Phi_k \mathbf{w}_k}. \end{aligned}$$

Setting $\nabla\gamma_k(\mathbf{w}_k) = 0$ we obtain

$$\mathbf{H}_k \mathbf{t}_k \mathbf{t}_k^H \mathbf{H}_k^H \mathbf{w}_k = \gamma_k(\mathbf{w}_k) \Phi_k \mathbf{w}_k. \quad (2.12)$$

Equation (2.12) shows that the solutions of $\gamma_k(\mathbf{w}_k)$ are extreme (stationary) points. Solving Equation (2.12) is equivalent to solving a generalized eigenvalue problem. Since Φ_k is invertible, we can rewrite Equation (2.12) as

$$\Phi_k^{-1} \mathbf{H}_k \mathbf{t}_k \mathbf{t}_k^H \mathbf{H}_k^H \mathbf{w}_k = \gamma_k(\mathbf{w}_k) \mathbf{w}_k.$$

The eigenvalues of $\Phi_k^{-1} \mathbf{H}_k \mathbf{t}_k \mathbf{t}_k^H \mathbf{H}_k^H \mathbf{w}_k$ are the solutions for $\gamma_k(\mathbf{w})$.

Using Sylvester's rank inequality, we have

$$\text{rank}(\Phi_k^{-1} \mathbf{H}_k \mathbf{t}_k \mathbf{t}_k^H \mathbf{H}_k^H) \leq \min(\text{rank}(\Phi_k^{-1}), \text{rank}(\mathbf{H}_k \mathbf{t}_k \mathbf{t}_k^H \mathbf{H}_k^H)).$$

It is easy to see the matrix $\mathbf{H}_k \mathbf{t}_k \mathbf{t}_k^H \mathbf{H}_k^H$ has rank 1. Therefore, the matrix $\Phi_k^{-1} \mathbf{H}_k \mathbf{t}_k \mathbf{t}_k^H \mathbf{H}_k^H$ has only one non-zero eigenvalue. This eigenvalue is positive since γ_k is positive. This unique eigenvalue can be found to be

$$\gamma_k = \mathbf{t}_k^H \mathbf{H}_k^H \Phi_k^{-1} \mathbf{H}_k \mathbf{t}_k \quad (2.13)$$

and the corresponding eigenvector that maximizes γ_k is given by

$$\mathbf{w}_k^{\text{mmse}} \propto \Phi_k^{-1} \mathbf{H}_k \mathbf{t}_k$$

which is indeed the linear MMSE receiver. Note that although individual channel matrices of other users are unknown to user k , $\Phi_k^{-1} \mathbf{H}_k \mathbf{t}_k$ is the information that user k can obtain by using a training sequence.

From Equation (2.13), we observe that the effective SINR of user k depends not only on its own beamforming vector, but also on the beamforming vectors of all other users. This makes individual optimization of each effective SINR quite difficult. Instead of direct optimization of all SINRs, we derive a lower bound on the effective SINRs.

Lemma 1 For any vector \mathbf{a} and any nonsingular Hermitian positive definite matrix \mathbf{Q} , we have

$$\mathbf{a}^H \mathbf{Q}^{-1} \mathbf{a} \geq \frac{(\mathbf{a}^H \mathbf{a})^2}{\mathbf{a}^H \mathbf{Q} \mathbf{a}}$$

Proof: Since matrix \mathbf{Q} is positive definite, by the Cholesky factorization,

$$\mathbf{Q} = \mathbf{B}^H \mathbf{B} \quad \text{and} \quad \mathbf{Q}^{-1} = \mathbf{B}^{-1} \mathbf{B}^{-H}.$$

Using the Cauchy-Schwartz inequality we obtain

$$\mathbf{a}^H \mathbf{Q}^{-1} \mathbf{a} \cdot \mathbf{a}^H \mathbf{Q} \mathbf{a} \geq (\mathbf{a}^H \mathbf{B}^{-1} \mathbf{B} \mathbf{a})^2 = (\mathbf{a}^H \mathbf{a})^2 \quad \blacksquare$$

By Lemma (1), the effective SINR (2.13) is lower bounded as follows,

$$\gamma_k \geq \frac{(\mathbf{t}_k^H \mathbf{H}_k^H \mathbf{H}_k \mathbf{t}_k)^2}{\mathbf{t}_k^H \mathbf{H}_k^H \left(\mathbf{H}_k \sum_{\substack{i=1 \\ i \neq k}}^K \mathbf{t}_i \mathbf{t}_i^H \mathbf{H}_k^H + \mathbf{I} \right) \mathbf{H}_k \mathbf{t}_k} \quad (2.14)$$

$$= \frac{(\mathbf{t}_k^H \mathbf{H}_k^H \mathbf{H}_k \mathbf{t}_k)^2}{\sum_{\substack{i=1 \\ i \neq k}}^K (\mathbf{t}_k^H \mathbf{H}_k^H \mathbf{H}_k \mathbf{t}_i)^2 + \mathbf{t}_k^H \mathbf{H}_k^H \mathbf{H}_k \mathbf{t}_k} \quad (2.15)$$

$$\geq \frac{\mathbf{t}_k^H \mathbf{H}_k^H \mathbf{H}_k \mathbf{t}_k}{\sum_{\substack{i=1 \\ i \neq k}}^K \mathbf{t}_i^H \mathbf{H}_k^H \mathbf{H}_k \mathbf{t}_i + 1} \quad (2.16)$$

where the inequality in (2.16) follows from the Cauchy-Schwartz inequality

$$(\mathbf{t}_k^H \mathbf{H}_k^H \mathbf{H}_k \mathbf{t}_i)^2 \leq (\mathbf{t}_k^H \mathbf{H}_k^H \mathbf{H}_k \mathbf{t}_k) (\mathbf{t}_i^H \mathbf{H}_k^H \mathbf{H}_k \mathbf{t}_i).$$

The above analysis indicates that with a linear MMSE receiver, the effective SINR is lower bounded by the ratio of the signal power to the sum of the interference power of all other streams leaked to the user k and the noise. This interference power can

be approximated by the sum of the interference power from user k to all other users

$$\sum_{\substack{i=1 \\ i \neq k}}^K \mathbf{t}_i^H \mathbf{H}_k^H \mathbf{H}_k \mathbf{t}_i \approx \sum_{\substack{i=1 \\ i \neq k}}^K \mathbf{t}_k^H \mathbf{H}_i^H \mathbf{H}_i \mathbf{t}_k \quad \forall k \in \{1, \dots, K\}. \quad (2.17)$$

We will discuss this approximation (2.17) in detail in Section 2.5.3.

The approximation of the lower bound of the effective SINR

$$\gamma_k \approx \frac{\mathbf{t}_k^H \mathbf{H}_k^H \mathbf{H}_k \mathbf{t}_k}{\mathbf{t}_k^H \left(\sum_{\substack{i=1 \\ i \neq k}}^K \mathbf{H}_i^H \mathbf{H}_i + \frac{K}{P} \mathbf{I} \right) \mathbf{t}_k} \quad (2.18)$$

involves only the transmit beamforming vector of the corresponding user. Each of the quantities given by Equation (2.18) can be maximized individually. Here again the expression in Equation (2.18) is a Rayleigh quotient. The optimal choice of the beamforming vector of user k that maximizes the quotient is the maximum eigenvector, i.e., the eigenvector corresponding to the largest eigenvalue of the matrix

$$\left(\sum_{\substack{i=1 \\ i \neq k}}^K \mathbf{H}_i^H \mathbf{H}_i + \frac{1}{P_k} \mathbf{I} \right)^{-1} \mathbf{H}_k^H \mathbf{H}_k. \quad (2.19)$$

The resulting transmit beamforming vector \mathbf{t}_k , along with receive beamforming vector \mathbf{w}_k maximize the approximate lower bound of user k 's effective SINR. The solutions for both transmit and receive beamforming are in closed form and can be computed with low computational complexity.

2.5.2 Spatial Multiplexing Mode

As we saw in Section 2.1, a user k working in the spatial multiplexing mode can be considered as L_k full diversity users experiencing the same channel matrix. The effective SINRs of user k are then the diagonal elements of

$$\Psi_k = \mathbf{T}_k \mathbf{H}_k^H \Phi_k^{-1} \mathbf{H}_k \mathbf{T}_k,$$

where

$$\Phi_k = \mathbf{H}_k \sum_{\substack{i=1 \\ i \neq k}}^K \mathbf{T}_i \mathbf{T}_i^H \mathbf{H}_k^H + \mathbf{I}$$

and $\mathbf{T}_k = [\mathbf{t}_k^1, \mathbf{t}_k^2, \dots, \mathbf{t}_k^N]$ is designed such that Ψ_k is a diagonal matrix whose elements are the SINRs of each stream. This mode of operation requires \mathbf{T}_k to be column-wise orthogonal and capable to be used in simultaneous diagonalization, which indicates that the spatial channels of one user are orthogonal and the interference among them is canceled. Similar to Equation (2.16), we can lower bound Ψ_k by

$$\Psi_k \succeq \frac{\mathbf{T}_k^H \mathbf{H}_k^H \mathbf{H}_k \mathbf{T}_k}{\mathbf{T}_k^H \left(\sum_{\substack{i=1 \\ i \neq k}}^K \mathbf{H}_i^H \mathbf{H}_i \right) \mathbf{T}_k + \mathbf{I}} \quad (2.20)$$

where the symbol \succeq is defined to mean that $\mathbf{A} \succeq \mathbf{B}$ is equivalent to $\mathbf{A} - \mathbf{B}$ is a diagonal matrix with all elements on the diagonal non-negative. Constrained by the orthogonal structure of \mathbf{T}_k , the maximization of Equation (2.20) results in the first N maximum eigenvectors of

$$\left(\sum_{\substack{i=1 \\ i \neq k}}^K \mathbf{H}_i^H \mathbf{H}_i + \frac{KN}{P} \mathbf{I} \right)^{-1} \mathbf{H}_k^H \mathbf{H}_k \quad (2.21)$$

2.5.3 Interference Equivalence

Considering the model introduced in Section 2.5.2 as an example, the total interference that user k receives from all other users can be defined as

$$I_k^s = \sum_{\substack{i=1 \\ i \neq k}}^K \sum_{l_i=1}^N \mathbf{t}_{i,l_i}^H \mathbf{H}_k^H \mathbf{H}_k \mathbf{t}_{i,l_i} = \sum_{\substack{i=1 \\ i \neq k}}^K \text{tr} (\mathbf{T}_i^H \mathbf{H}_k^H \mathbf{H}_k \mathbf{T}_i)$$

and similarly, the total interference that user k contributes to all other users is defined as

$$I_k^c = \sum_{l_k=1}^N \sum_{\substack{i=1 \\ i \neq k}}^K \mathbf{t}_{k,l_k}^H \mathbf{H}_i^H \mathbf{H}_i \mathbf{t}_{k,l_k} = \sum_{\substack{i=1 \\ i \neq k}}^K \text{tr}(\mathbf{T}_k^H \mathbf{H}_i^H \mathbf{H}_i \mathbf{T}_k).$$

We refer to the condition under which $I_k^s = I_k^c$ for all k , as Interference Equivalence (IE). Many beamforming techniques that have explicit solutions satisfy the IE condition. For instance, BDZF and ZFBF are among those beamforming techniques since both I_k^s and I_k^c are zero. It is easy to check that SVD-MMSE with power allocation proportional to the channel gain of the Eigen channels also satisfies the IE condition. A sufficient condition for IE to be held is that $\mathbf{T}_k = \mathbf{A} \mathbf{H}_k^H$ for all k , where \mathbf{A} is a symmetric matrix because

$$\text{tr}(\mathbf{H}_i \mathbf{A}^H \mathbf{H}_k^H \mathbf{H}_k \mathbf{A} \mathbf{H}_i^H) = \text{tr}(\mathbf{H}_k \mathbf{A}^H \mathbf{H}_i^H \mathbf{H}_i \mathbf{A} \mathbf{H}_k^H)$$

for all $i \neq k$. Note that \mathbf{A} is the same for all users. For CIB, when the number of users, K , gets large, the matrix inside the inverse in Equation (2.21) becomes independent of the user index and therefore satisfies the IE condition [8].

2.5.4 Optimality Analysis

Given that the transmit beamforming matrix of CIB is capable of performing simultaneous diagonalization, Equation (2.20) indicates the optimality of CIB at extreme cases of SNR. At low SNR values, the identity matrix which is the noise power term dominates the denominator and the interference term vanishes. The transmit beamformer tends to match itself along the maximum eigenvectors of $\mathbf{H}_k^H \mathbf{H}_k$ to enhance the signal power. This behavior makes CIB to converge to SVD-MMSE at low SNR. At high SNR values where interference is dominant, the term representing the interference power, i.e., $\mathbf{T}_k^H (\sum_{i \neq k} \mathbf{H}_i^H \mathbf{H}_i) \mathbf{T}_k$, dominates the denominator of Equation (2.20) and \mathbf{T}_k matches to smallest eigenvectors of $\sum_{i \neq k} \mathbf{H}_i^H \mathbf{H}_i$. In other words, in the setting of BDZF, \mathbf{T}_k of CIB converges to the eigenvectors corresponding to the zero eigenvalues which is exactly the approach used by the BDZF strategy.

2.6 Performance Analysis

We first compare the ergodic sum-rate achieved by the CIB, SVD-MMSE, BDZF and ZFBF without waterfilling. The studied scenario has 10 users where each has 2

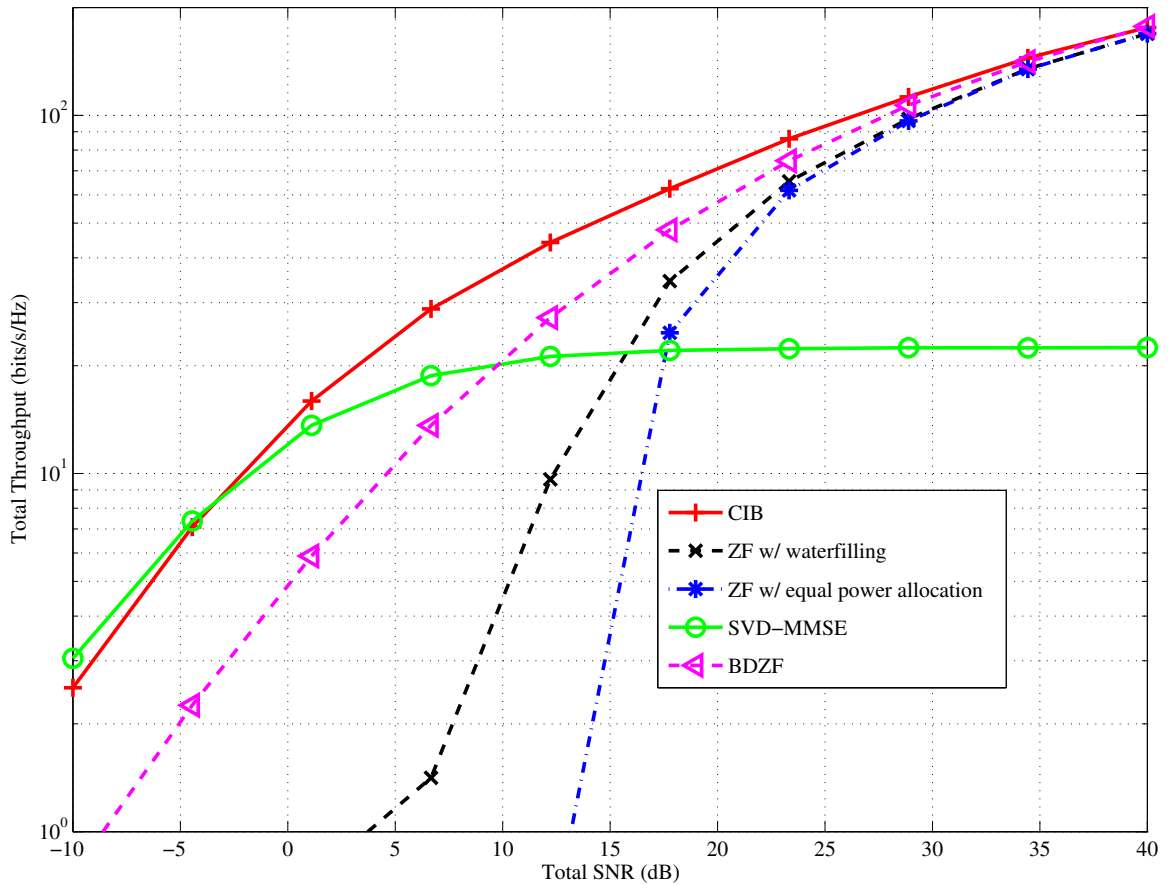


Figure 2.2: Spatial multiplexing mode: 10 users each has 2 receive antennas

receive antennas. The base station has 20 transmit antennas. The total throughput is plotted as a function of the total SNR, shared by 20 spatial channels. As we have seen, SVD-MMSE works good at low SNR values but reaches an upper ceiling at high SNRs where interference dominates the performance. The results of the three ZF techniques are shown in Figure 2.2. These techniques can completely nullify all the inter-user interference at the transmitter side so that the receiver can simply perform an interference-free detection. Although their achievable sum-rate converge together and to the sum-rate of CIB at high SNRs, their performance is poor at low

SNRs where noise has more impact than interference. The proposed CIB roughly connects the peak rate of SVD-MMSE at low SNRs, (with a small offset caused by the approximation error) to the peak rate of ZF at high SNRs. CIB uses equal power allocation which at high SNRs maximizes the sum-rate in a number of different settings [54]. It is also interesting to notice that even though BDZF and ZFBF use waterfilling power allocation schemes to enhance their performance at low SNRs, their performance is inferior to CIB with equal power allocation.

The scaling law of the sum-rate of DPC and linear precoding with respect to the number of users is also of interest [55]. In the plot shown in Figure 2.3 each user

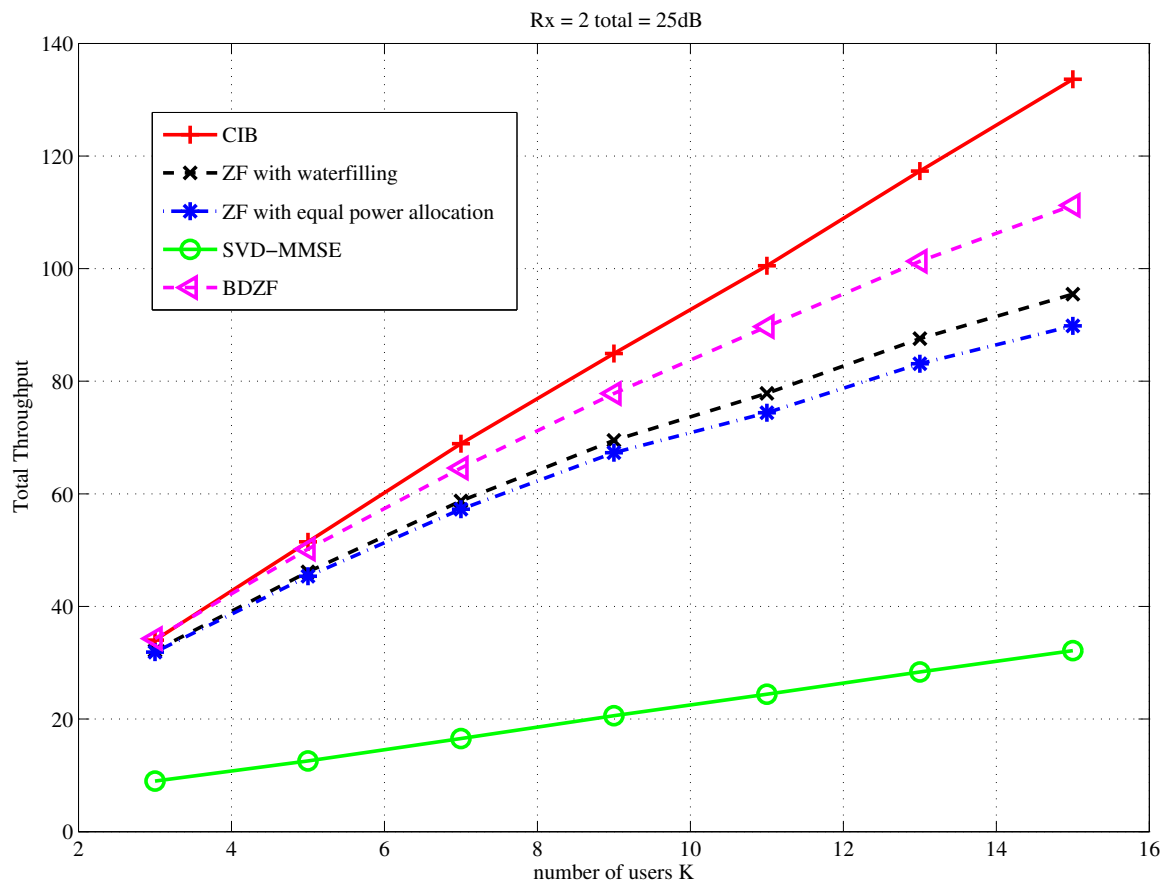


Figure 2.3: Total throughput varies with number of users each has two receive antennas

employs 2 receive antennas and the number of transmit antennas is assumed to be $2K$ in order for BDZF to operate. The total transmit SNR is fixed at 25 dB regardless of

the number of users in the system. As stated in [46], for small number of users, BDZF achieves almost the same throughput as DPC. When the number of users increase, DPC exhibits better performance than BDZF. In Figure 2.3 we can clearly see that the slopes of the ZF techniques are lower than that of CIB and depart more and more from what CIB achieves as the number of users increases. The linear increase of the sum-rate is noticed for the CIB while for BDZF it only increases logarithmically.

2.7 Conclusions

We have introduced the CIB scheme as a coordinated beamforming technique for downlink MIMO BCs which employs both linear transmit precoding and linear receive equalization. This technique is linear, has a closed form solution and requires no iteration in computation, other than the SVDs. Hence, CIB features low complexity. Users in the system can work either in the full diversity mode or the spatial multiplexing mode. The spatial multiplexing order of each user could be any positive integer from one to the minimum of the number of transmit and receive antennas. The selection of the number of transmit and receive antennas is not constrained. The throughput of the CIB is larger than that of the SVD-MMSE and BDZF or ZFBF schemes in many cases of interest including low and high transmit powers, small and large number of users. Consequently, CIB can serve as a base technique for more complicated techniques such as optimal power allocation or user scheduling schemes. The diversity gain and spatial multiplexing gain can be balanced to enhance the performance by providing more flexibility which can be used by upper layer scheduling algorithms.

A similar work is done in [56], where interference of the user of interest to other users is called power leakage. The optimization criteria used there is to maximize signal to leakage and noise power, which results in a solution similar to the CIB.

Chapter 3

A Linear Beamforming Technique for MIMO CDMA

In WCDMA/HSDPA [57], a number of techniques employing MIMO are proposed for FDD and TDD modes as part of the standard [58]. In this chapter, following the discussion of CIB in Chapter 2, a coordinated MIMO beamforming technique for CDMA systems transmitting over frequency selective fading channels is proposed. Factors that affect the performance of CDMA based systems include self-interference due to the delay spread of the channel, multiple access interference from other users, fading due to the small scale multipath propagation, and the additive noise. Frequency selective fading, which models the communication channel in urban areas at high data rates as specified in 3G applications, can cause major problems for system designer. Frequency-selective spatial channel is used in [59] to model such scenarios in the WCDMA channel. MIMO systems are employed in the WCDMA frequency-selective channels, particularly when the number of resolvable taps is so small that the ISI is negligible while ICI is more significant.

In HSDPA FDD mode, one or more High Speed Downlink Shared Channels (HS-DSCH) at spreading factor of 16 are time multiplexed among users, preferably all allocated to a single user at any time to exploit multi-user diversity in order to approach the sum capacity. When the user channels are not ergodic, some users can never get a better channel to select due to the near-far effect. In such cases, simultaneous transmission to multiple users at one time may be required to make transmission

fair to all users. The technique proposed in this chapter, which is similar to Coordinated Interference-aware Beamforming (CIB) for flat-fading channels discussed in Chapter 2 and [60], can provide means to schedule multiple users.

Chip-level receivers are well understood and adequately discussed in [61], [62], and [63]. Effective chip-level equalization tries to restore synchronism and orthogonality amongst active users. The main benefit of chip-level equalization is that the transceiver design becomes independent from the spreading codes resulting in decreased computational complexity especially in MIMO systems. In the proposed CIB technique, chip-level MMSE equalization is coordinated with appropriate transmit precoding to achieve a good balance between performance metrics, i.e., capacity, error rate, and complexity.

3.1 The Single User MIMO-CDMA Channel

A narrowband flat fading channel can be modeled by a single-tap filter, which assumes most of the multipaths arrive during one symbol time. In wideband systems, however, the signal bandwidth is much larger than the channel coherence bandwidth. Therefore, the delay spread is longer than one symbol time meaning that the transmitted signals arrive at the receiver over multiple symbol durations. The discrete baseband equivalent channel can be modeled as

$$y[m] = \sum_{l=0}^{L-1} h_l[m]x[m-l] + w[m], \quad (3.1)$$

where the channel response is assumed to have a finite number of taps L . It is easy to see that there are $L - 1$ replicas of the m th symbol interfering the following symbols. This interfering effect is called inter-symbol interference (ISI).

In wireless communication systems, whether multiple antennas are used or not, there are three common techniques used to combat against the delay effect of the frequency-selective channel. For single carrier systems equalization is normally used to mitigate the ISI by enhancing the current symbol and suppressing the interference symbols. For multiple carrier systems the channel is divided into a number of non-interfering (orthogonal) sub-carriers, hence the wideband channel is transformed into

ISI equalization	MIMO techniques
OFDM	SVD
linear zero-forcing equalizer	decorrelator/interference nulling
linear MMSE equalizer	linear MMSE receiver
decision feedback equalizer	successive interference cancelation (SIC)
ISI precoding	dirty paper coding

Table 3.1: Similarity of ISI and MIMO equalizations

many parallel narrowband channels, thus eliminating the inter-sub-channel interference. In DSSS systems when the processing gain is large enough, we could assume that the maximum delay (the delay of the L th tap) is smaller than one symbol time. In this case the current symbol can at most affect one following symbol. Therefore, the ISI is small and can be neglected, however, the inter-chip interference still exists. When the processing gain is not large enough, the received signal is corrupted by ISI and equalization is needed. In fact, for large processing gains, techniques against multipath are needed to mitigate the inter-chip interference and exploit frequency diversity, which might be considered as equalization for chips. Table 3.1 presents the similarity of ISI equalization techniques and MIMO techniques.

In the system model depicted in Figure (3.1), a single user multiple antenna frequency selective channel is described. Direct sequence spread spectrum is used and the spreading gain is assumed high enough so that the inter-symbol interference is negligible.

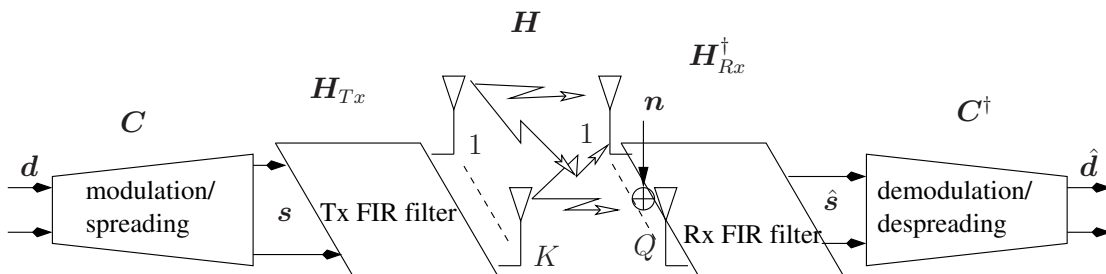


Figure 3.1: CIB-CDMA system model

A sequence of information symbols is organized as a vector \mathbf{d} of length K , which is

The spreading and despreading processes are related by this configuration.

The choice of the transmitter FIR filter \mathbf{H}_{Tx} and the receive FIR filter \mathbf{H}_{Rx} for this MIMO-CDMA frequency-selective channel determines the technique used for the system. Any commonly used linear reception techniques, such as matched filter, decorrelator, and MMSE can be applied to this problem.

3.2.1 The RAKE Receiver

RAKE receiver is the most commonly used reception technique for CDMA systems in frequency-selective channels. Simple extension by employing fingers on each receive antennas allows RAKE receiver to be used in MIMO-CDMA systems. After despreading each tap on each antenna, the receiver uses maximum ratio combining (MRC) to collect the sufficient statistics and forwards them to the detector [65]. In single antenna systems, the RAKE receiver is indeed a spreading sequence matched filter. For MIMO systems, the extended RAKE needs to match not only the spreading sequences but also the matrix channel. Therefore, the extended RAKE can be written as

$$\mathbf{H}_{Rx} = \mathbf{H}\mathbf{H}_{Tx}, \quad (3.3)$$

i.e., the image of the transmit filter experiencing the channel matrix. To see more clearly why this is a matched filter, the received signal \mathbf{r} is written as

$$\mathbf{r} = \mathbf{f}_1 s_1 + \sum_{i \neq 1} \mathbf{f}_i s_i + \mathbf{n},$$

where s_1 and s_i are the entries of the spread signal \mathbf{s} and \mathbf{f}_1 and \mathbf{f}_i are the columns of the matrix $\mathbf{H}\mathbf{H}_{Tx}$. In the above, the first term in the right hand side is the signal term and the other two terms are the interference and noise.

In order to detect the signal s_1 , using matched filter technique, we can design the receiver to be matched to the equivalent channel gain \mathbf{f}_1 so that

$$\hat{s}_1 = \mathbf{f}_1^\dagger \mathbf{r}.$$

This operation maximizes the coefficient of the signal power in the whole received

signal. Meanwhile, the interference and noise are also multiplied by this filter and get enhanced.

3.2.2 Pre-RAKE Transmitter

When the transmitter knows the channel impulse response, such as in TDD CDMA systems, using an idea similar to RAKE, the transmitter can perform pre-matching before transmission so that the hardware and computational complexity is moved from the receiver to the transmitter side. Such pre-matching results in a transmit FIR filter of the form

$$\mathbf{H}_{Tx} = \mathbf{H}^\dagger \mathbf{H}_{Rx}.$$

To compare the performances of these two techniques, we consider two scenarios where in the first we use pre-RAKE transmitter with identity receive FIR matrix and in the second we employ a RAKE receiver with identity transmit FIR matrix, i.e.,

$$\begin{aligned} \text{RAKE: } \hat{\mathbf{s}} &= \mathbf{H}^\dagger \mathbf{H} \mathbf{s} + \mathbf{H}^\dagger \mathbf{n} \\ \text{pre-RAKE: } \hat{\mathbf{s}} &= \mathbf{H} \mathbf{H}^\dagger \mathbf{s} + \mathbf{n}. \end{aligned}$$

Some pre-RAKE diversity receivers for CDMA systems are proposed in [66], [67], [68], [69], in which the performance of the pre-RAKE receiver is proved to be equivalent to the RAKE receiver. Both techniques are computationally simple but not optimal in terms of maximizing the SNR.

3.2.3 Decorrelator and LMMSE Receivers

If the number of antennas is large or the signal power is high, very large interference is observed and receivers, such as RAKE and pre-RAKE, perform very poorly. Zero-forcing nulling is a technique that can completely cancel the multiple access interference (MAI) and has a simple explicit formula for the entire bank of decorrelators, i.e., the Moore-Penrose pseudo-inverse of the channel matrix \mathbf{H}

$$\mathbf{H}_{Rx}^\dagger = (\mathbf{H}^\dagger \mathbf{H})^{-1} \mathbf{H}^\dagger.$$

Although a decorrelator cancels MAI, it still does not maximize the SINR. Actually this receive technique is more significant in analysis than in practical use since when the MAI is canceled, the SINR for each substream is just the SNR and has an explicit form so that the capacity is easy to compute.

The LMMSE receiver is the optimal reception technique that can maximize the received SINR by minimizing the mean square error

$$\min E[(\mathbf{s} - \hat{\mathbf{s}})^2] \Rightarrow \mathbf{H}_{Rx}^\dagger = (\mathbf{H}_{Tx}^\dagger \mathbf{H}^\dagger \mathbf{H} \mathbf{H}_{Tx} + \sigma^2 \mathbf{I})^{-1} \mathbf{H}_{Tx}^\dagger \mathbf{H}^\dagger,$$

where σ^2 is the noise power.

Both these two techniques perform better than RAKE and pre-RAKE especially at high SNR and multi-user cases, however, they require channel inversion operation which is costly for some applications. When CSI is not available at the transmitter, $\mathbf{H}_{Tx} = \mathbf{I}$ is optimal [8]. When CSI is available at the transmitter, there is a potential improvement in the SINR and capacity by making \mathbf{H}_{Tx} a function of \mathbf{H} . Indeed, similar to the pre-RAKE technique which moves the computational complexity of RAKE to the transmitter, decorrelator and LMMSE receive techniques have their equivalents at the transmitter side too.

3.2.4 Eigenprecoder and Selection Combiner

When the receiver can use RAKE and the transmitter has access to the CSI, e.g., in TDD systems, there exists a potential performance gain by optimizing the transmit FIR filter. Applying the chip-level equivalent channel model (3.2) with the RAKE receiver (3.3), we have

$$\hat{\mathbf{s}} = \mathbf{H}_{Tx}^\dagger \mathbf{H}^\dagger \mathbf{H} \mathbf{H}_{Tx} \mathbf{s} + \mathbf{H}_{Tx}^\dagger \mathbf{H}^\dagger \mathbf{n}. \quad (3.4)$$

Assuming the channel matrix \mathbf{H} has a singular value decomposition (SVD) as $\mathbf{H} = \mathbf{U} \mathbf{D} \mathbf{V}^\dagger$ and selecting the transmit FIR filter as $\mathbf{H}_{Tx} = \mathbf{V}$ in (3.4), we obtain

$$\hat{\mathbf{s}} = \mathbf{D}^2 \mathbf{s} + \mathbf{D} \mathbf{U}^\dagger \mathbf{n} = \mathbf{D}^2 \mathbf{s} + \mathbf{D} \mathbf{n},$$

where the second equality follows from the fact that a unitary matrix does not alter the statistics of the Gaussian noise. Since \mathbf{D} and \mathbf{D}^2 are diagonal matrices, the equivalent channel model forms a set of parallel Gaussian subchannels with no inter-channel interference. The SNR of each subchannel is just the corresponding eigenvalue of \mathbf{H} , i.e., the diagonal entries of \mathbf{D} . These subchannels are sometimes called Eigenchannels or Eigenmodes. When waterfilling power allocation scheme is used, such a transceiver achieves capacity.

There are some other techniques that use the idea of eigenvalue decomposition, as discussed in [70], [71], [72].

In practical implementations of RAKE receivers, only a limited number of RAKE fingers may be available due to the complexity and cost constraints. Therefore, a subset of taps are selected to be combined to construct the statistic for detection [73], [74]. [75]. These techniques employ limited hardware resources and can achieve considerable performance gains.

3.3 Multi-User MIMO-CDMA System Model

The system structure in this case is a typical MIMO transceiver with the assumption that perfect CSI is available at both transmitter and receiver sides. A block diagram of the model under study is shown in Figure 3.2.

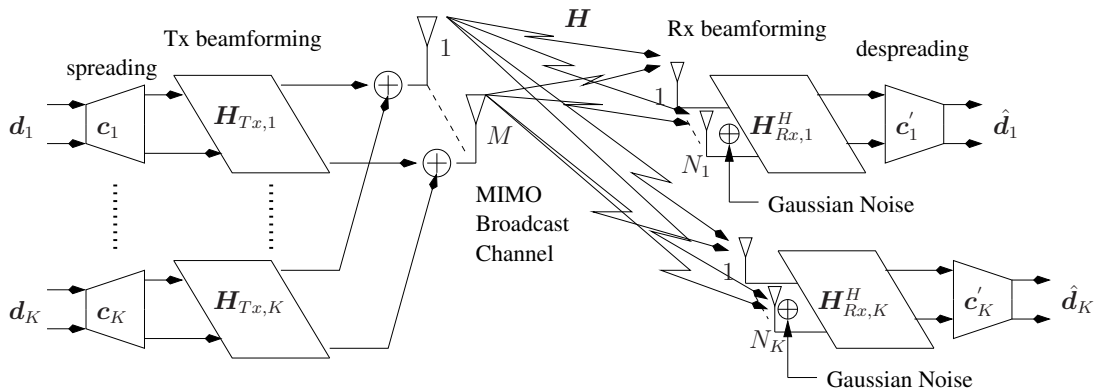


Figure 3.2: Transceiver block diagram and signal flow for a MIMO-CDMA frequency-selective channel with CSI available at both transmitter and receiver

This multi-user system supports K users simultaneously. In practice, the scheduler

can vary resource assignment based on various factors

The number of transmit antennas at the base station, and the number of receive antennas for user k , are denoted by M and N_k , respectively. Independent information bits intended for a specific user k are modulated into symbols \mathbf{d}_k , which is an L_k -dimensional vector with i.i.d. distribution where $L_k = \min(M, N_k)$ denotes the maximum spatial multiplexing order. In typical systems such as WCDMA the number of receive antennas can hardly be larger than the number of transmit antennas at the base station, i.e., $L_k \leq N_k$. For simplicity, we also assume that all users have the same number of receive antennas, i.e., $N_k = N$.

To take advantage of the multiple antenna configuration, each user is assigned one spreading code regardless of its multiplexing order. In multi-code systems data streams spread by one spreading code are treated as if they are intended for one user. Spreading code sequence is denoted by a G -dimensional vector \mathbf{c}_k with spreading gain G and normalized power $|\mathbf{c}_k|^2 = 1$, for all $1 \leq k \leq K$. G can also be the number of samples when over-sampling is applied. Spreading matrix \mathbf{C}_k is a $GN \times N$ block diagonal matrix. The modulated and spread signal of user k is denoted by $\mathbf{s}_k = \mathbf{C}_k \mathbf{d}_k$. At the receiver, \mathbf{C}_k despreads the filtered received signal and constructs the decision variable for the symbol estimate $\hat{\mathbf{d}}_k$.

The channel model considered in this CIB technique is a MIMO frequency-selective Rayleigh fading channel. Due to the frequency selectivity, the transmitted signals experience multipath delay effects that result in channel models with multiple taps. The number of the maximum resolvable taps for all users is denoted by L which is assumed to be much smaller than the length of the spreading sequence. This assumption results in a system in which ISI is small and ICI is the determining factor. For user k , the broadcast channel can be expressed by a block matrix as in Equation (3.5).

$$\mathcal{H}_k = \begin{bmatrix} \mathbf{H}_{1,1,k} & \cdots & \mathbf{H}_{1,M,k} \\ \vdots & \vdots & \vdots \\ \mathbf{H}_{N,1,k} & \cdots & \mathbf{H}_{N,M,k} \end{bmatrix}_{N(G+L-1) \times MG}, \quad (3.5)$$

complex Gaussian noise with power normalized to one,

$$\mathbf{y}_k = [\mathbf{y}_1^T, \dots, \mathbf{y}_N^T]^T = \mathcal{H}_k \mathbf{x} + \mathbf{n}_k.$$

The column vector \mathbf{y}_k has $N(G + L - 1)$ entries where each \mathbf{y}_r^H is a $G + L - 1$ dimensional vector representing the received chips from the n th receive antenna.

The receiver uses multiple RAKE antennas and is assumed to have perfect estimates of the channel \mathcal{H}_k . The knowledge of \mathcal{H}_k allows the receiver performs receive equalization with a $N(G + L - 1) \times NG$ filter $\mathbf{H}_{Rx,k}$, followed by despreading by using \mathbf{C}_k to compute $\hat{\mathbf{d}}_k$ at the receiver given by

$$\hat{\mathbf{d}}_k = \mathbf{C}'_k \mathbf{H}_{Rx,k}^H \mathbf{y}_k = \mathbf{C}'_k \mathbf{H}_{Rx,k}^H \mathbf{H}_k \mathbf{x} + \mathbf{C}'_k \mathbf{H}_{Rx,k}^H \mathbf{n}_k. \quad (3.7)$$

3.4 Coordinated Interference-Aware Beamforming

The detection techniques that are based on Equation (3.7) are referred to as symbol-level detection in which the design of transceivers, i.e., $\mathbf{H}_{Tx,k}$ and $\mathbf{H}_{Rx,k}$, under many design criteria are functions of \mathbf{C}_k . Larger size of the spreading matrix \mathbf{C}_k introduces additional computational complexity. In WCDMA systems the spreading sequence is both user and symbol dependent through the use of scrambling codes, therefore, $\mathbf{H}_{Tx,k}$ and $\mathbf{H}_{Rx,k}$ becomes time dependent and vary from chip to chip. Such time dependency in precoding and equalization in real system is not desired. In particular, when adaptive versions are used, the time varying channel estimation and time varying precoding and equalization will not guarantee the convergence. Moreover, when multiple spreading codes are assigned to one user, the user needs to compute the transmit and receive beamforming filters for each spreading code, which is also costly.

Instead of looking at the detection at the symbol level, we can perform chip-level precoding and equalization in which the successive chips are assumed independent. Under this assumption the transmitter and receiver beamformers are independent of

the spreading matrix, as shown below

$$\hat{\mathbf{s}}_k = (\mathbf{H}_{Rx,k})^H \mathbf{y}_k \quad (3.8)$$

$$= (\mathbf{H}_{Rx,k})^H \mathcal{H}_k \mathbf{H}_{Tx,k} \mathbf{s}_k + (\mathbf{H}_{Rx,k})^H \mathcal{H}_k \sum_{\substack{i=1 \\ i \neq k}}^K \mathbf{H}_{Tx,i} \mathbf{s}_i + (\mathbf{H}_{Rx,k})^H \mathbf{n}_k. \quad (3.9)$$

Although this is a suboptimal solution, the independence of the transceiver for the spreading codes results in a simpler receiver structure and is attractive in certain systems such as HSDPA. The transceiver structure in Figure 3.2 and Equation (3.7) suggest the use of chip-level detection since the spreading and despreading blocks are isolated from the beamforming blocks.

The linear form of Equation (3.8) represents a MIMO broadcast channel within which the parameter SINR plays a key role for computing the capacity and the error probability. In chip-level equalization for the multi-dimensional signal \mathbf{s}_k , the SINR of each entry is of interest. Let us denote by $\mathbf{h}_{Tx,k}^m$ and $\mathbf{h}_{Rx,k}^m$ the m th columns of $\mathbf{H}_{Tx,k}$ and $\mathbf{H}_{Rx,k}$, respectively. Assuming all users use chip-level MMSE equalizers, the SINR of the m th entry can be expressed, similar to Chapter 2, by

$$\gamma_k^m = \frac{\mathbb{E} [(\mathbf{h}_{Rx,k}^m)^H \mathcal{H}_k \mathbf{h}_{Tx,k}^m c_k^m (c_k^m)^H (\mathbf{h}_{Tx,k}^m)^H (\mathcal{H}_k)^H \mathbf{h}_{Rx,k}^m]}{\mathbb{E} \left[\left\| (\mathbf{h}_{Rx,k}^m)^H \left(\mathcal{H}_k \sum_{\substack{(q,j)=(NG,K) \\ (q,j)=(1,1) \\ (q,j) \neq (m,k)}} \mathbf{h}_{Tx,j}^q c_j^q + \mathbf{n}_j \right) \right\|^2 \right]} \quad (3.10)$$

for all $1 \leq m \leq NG$. If we use the simplification assumption discussed previously, i.e., after the use of scrambling codes all chip values c_k^m for $1 \leq k \leq K$ and $1 \leq m \leq NG$ are independent, Equation (3.10) is reduced to

$$\gamma_k^m = \frac{(\mathbf{h}_{Rx,k}^m)^H \mathcal{H}_k \mathbf{h}_{Tx,k}^m (\mathbf{h}_{Tx,k}^m)^H (\mathcal{H}_k)^H \mathbf{h}_{Rx,k}^m}{(\mathbf{h}_{Rx,k}^m)^H \Phi_k^m \mathbf{h}_{Rx,k}^m} \quad (3.11)$$

with

$$\Phi_k^m = \mathcal{H}_k \sum_{\substack{(q,j)=(NG,K) \\ (q,j)=(1,1) \\ (q,j) \neq (m,k)}} [\mathbf{h}_{Tx,j}^q (\mathbf{h}_{Tx,j}^q)^H] \mathcal{H}_k^H + \mathbf{I}.$$

If we consider $\mathbf{h}_{Rx,k}^m$ as a function of $\mathbf{h}_{Rx,j}^q$ and \mathcal{H}_j for all $1 \leq j \leq K$ and $1 \leq q \leq NG$, the Rayleigh quotient in Equation (3.11) can be maximized by solving a generalized eigenvalue problem, as shown in Section 2.5.1. The solution for $\mathbf{h}_{Rx,k}^m$ is

$$\mathbf{h}_{Rx,k}^m \propto (\Phi_k^m)^{-1} \mathcal{H}_k \mathbf{h}_{Tx,k}^m$$

and the resulting maximized γ_k^m is then

$$\gamma_k^m = (\mathbf{h}_{Tx,k}^m)^H \mathcal{H}_k^H (\Phi_k^m)^{-1} \mathcal{H}_k \mathbf{h}_{Tx,k}^m.$$

Global maximization of each γ_k^m over $\mathbf{h}_{Tx,k}^m$ is difficult due to the dependency among $\mathbf{h}_{Tx,k}^m$ s. Using Lemma (1) introduced in the previous chapter and in [76], and Cauchy-Schwartz inequality, we have

$$\begin{aligned} \gamma_k^m &\geq \frac{((\mathbf{h}_{Tx,k}^m)^H \mathcal{H}_k^H \mathcal{H}_k \mathbf{h}_{Tx,k}^m)^2}{(\mathbf{h}_{Tx,k}^m)^H \mathcal{H}_j^H \left(\mathcal{H}_k \sum_{\substack{j=1 \\ j \neq k}}^K \mathbf{h}_{Tx,j}^m (\mathbf{h}_{Tx,j}^m)^H \mathcal{H}_k^H + \frac{NG}{P_k} \mathbf{I} \right) \mathcal{H}_k \mathbf{h}_{Tx,k}^m} \\ &\geq \frac{(\mathbf{h}_{Tx,k}^m)^H \mathcal{H}_k^H \mathcal{H}_k \mathbf{h}_{Tx,k}^m}{\sum_{\substack{j=1 \\ j \neq k}}^K (\mathbf{h}_{Tx,j}^m)^H \mathcal{H}_k^H \mathcal{H}_k \mathbf{h}_{Tx,j}^m + \frac{NG}{P_k}} \end{aligned}$$

where P_k is the power allocated to each spatial channel of each user and is assumed to be $\frac{1}{K}$ of the total power. With the interference equivalence, γ_k^m can be approximately lower bounded by

$$\gamma_k^m \gtrsim \frac{(\mathbf{h}_{Tx,k}^m)^H \mathcal{H}_k^H \mathcal{H}_k \mathbf{h}_{Tx,k}^m}{(\mathbf{h}_{Tx,k}^m)^H \left(\sum_{\substack{j=1 \\ j \neq k}}^K \mathcal{H}_j^H \mathcal{H}_j + \frac{NG}{P_k} \mathbf{I} \right) \mathbf{h}_{Tx,k}^m} \quad (3.12)$$

This lower bound breaks the dependency among the transmit beamforming filters $\mathbf{h}_{Tx,k}^m$ and makes it possible to do the maximization locally. The optimal $\mathbf{h}_{Tx,k}^m$ that maximizes the Rayleigh quotient in the right hand side of Equation (3.12) is the

principle eigenvector of

$$\mathbf{Z}_k = \left(\sum_{\substack{j=1 \\ j \neq k}}^K \mathbf{H}_j^H \mathbf{H}_j + \frac{KNG}{P} \mathbf{I} \right)^{-1} \mathbf{H}_k^H \mathbf{H}_k. \quad (3.13)$$

Because of the spatial multiplexing employed in the system, the transmit beamforming filters $\mathbf{h}_{Tx,k}^m$ for all entries of \mathbf{s}_k , i.e., $m = 1, \dots, NG$, are the NG eigenvectors corresponding to the NG largest eigenvalues of the matrix \mathbf{Z}_k in Equation (3.13).

3.5 Performance Analysis

In this section we compare the average throughput and average symbol error rate achievable by CIB with those of SVD-RAKE and SVD-MMSE transceivers. RAKE receiver and chip-level MMSE receiver are commonly studied in the literature and used in some practical systems.

A RAKE receiver is a filter matched to the channel and the possible transmit beamforming,

$$\mathbf{H}_{Rx,k}^{RAKE} = \mathbf{H}_k \mathbf{H}_{Tx,k}.$$

In single user case the received SNR is maximized by the RAKE receiver. SVD is a transceiver design technique used for derivation of the capacity of MIMO in Gaussian channels [8]. SVD transmission chooses the transmit beamforming filter

$$\mathbf{H}_{Tx,k}^{SVD} = \mathbf{V}_k$$

which is the eigenvector base of the channel matrix from the SVD

$$\mathbf{H}_k = \mathbf{U}_k^H \mathbf{D}_k \mathbf{V}_k.$$

In this thesis we refer to the techniques combining SVD transmission and RAKE reception as SVD-RAKE. The transceiver adopting SVD transmitter and matched filter at the receiver for flat-fading channels is optimal coordinated linear beamforming since all spatial channels are made parallel. In multi-user and frequency-selective

channel scenarios SVD-RAKE performs poorly since the interference which is involved in the design criteria is treated as independent Gaussian noise.

Here we provide the performance of the combination of SVD transmitter and chip-level MMSE receiver as well for comparison purposes.

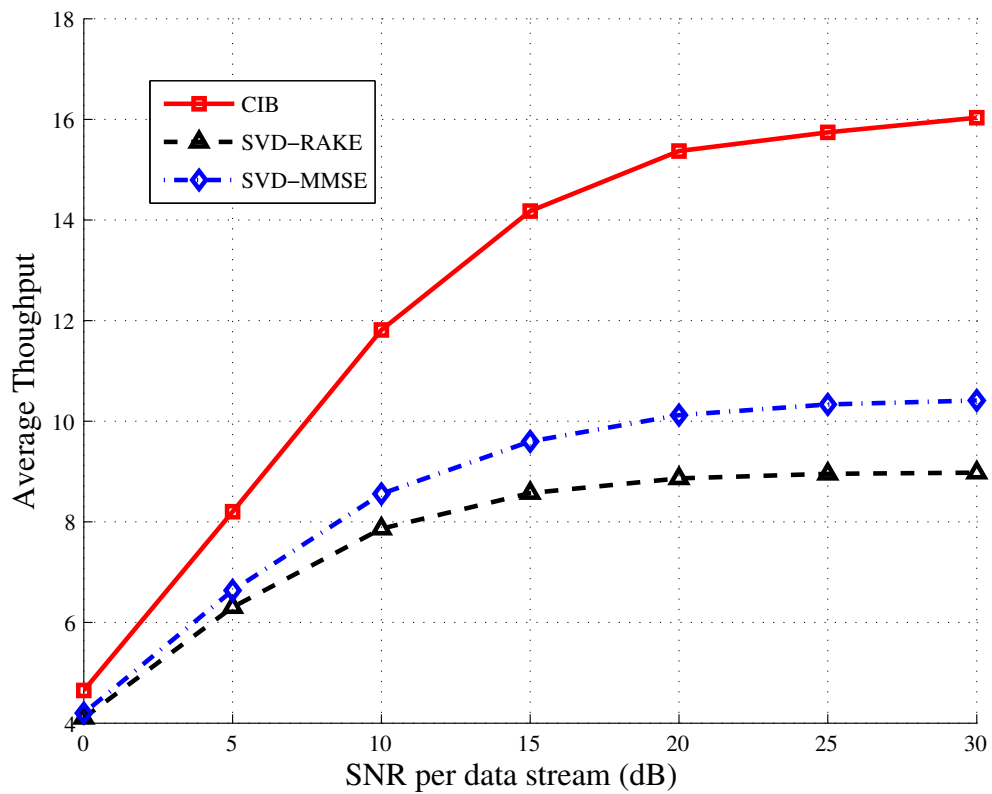


Figure 3.3: Average achievable throughput of CIB, SVD-RAKE, and SVD-MMSE

The average achievable throughput using CIB, SVD-MMSE, and SVD-RAKE are shown and compared in Figure 3.3 for the case where the base station has 6 transmit antennas and there are 3 active users in the system each with 3 receive antennas. A maximum delay spread of $L = 3$ and $G = 16$ chips per symbol are assumed. Antenna-to-antenna channel gains are normalized and the distribution of tap gains are i.i.d. circular complex Gaussian random variables with variance $1/L$. The horizontal axis represents the SNR per spatial channel. The CIB curve has sharper slope and saturate at high SNR values compared to the SVD-MMSE and the SVD-RAKE plots. At SNR

values exceeding 4 dB, CIB achieves much higher average throughput as well. Due to the approximation loss, the simulation results of CIB exhibit worse performance compared to the other two at low SNR values. SVD-MMSE technique always achieves higher capacity compared with SVD-RAKE, as expected.

The performances of these techniques in terms of Symbol Error Rate (SER) are also evaluated with uncoded QPSK modulation and are plotted in Figure 3.4. In

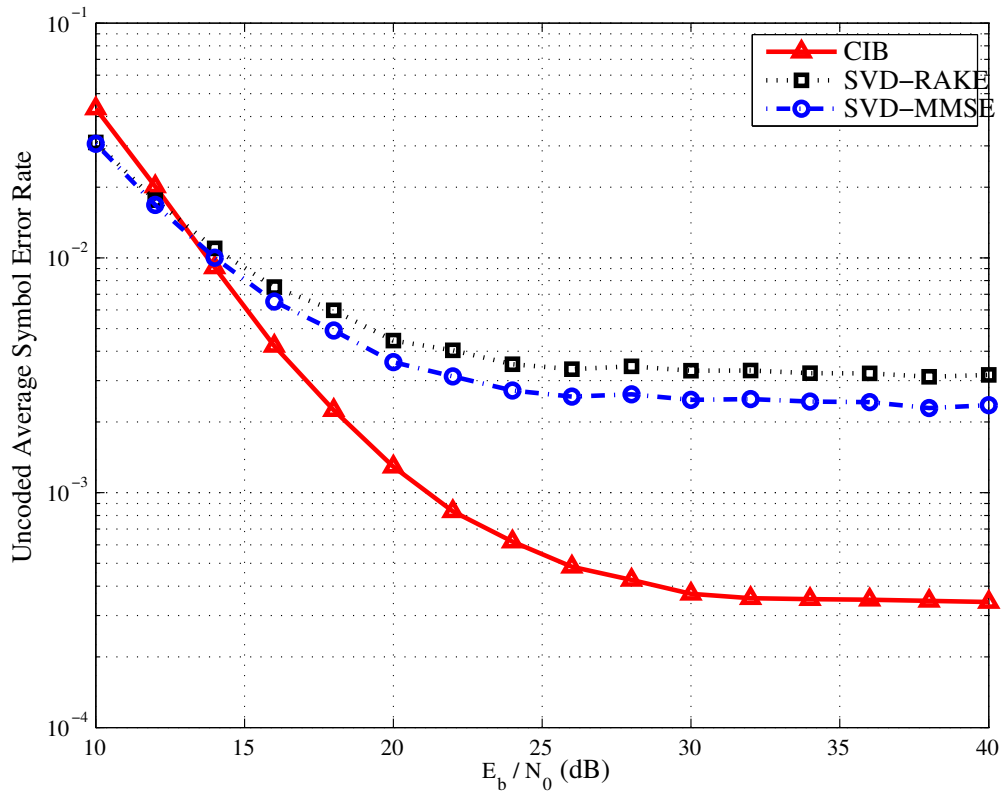


Figure 3.4: Un-coded average symbol error rate of CIB, SVD-RAKE, and SVD-MMSE

this system, the base station has 10 transmit antennas. There are 10 users each with 2 receive antennas. The base station transmits 2 independent data streams to each user simultaneously. As noticed in Figure 3.3, CIB technique outperforms SVD-RAKE and SVD-MMSE at moderate and high SNR values, while at low SNR values, CIB shows inferior performance compared to the other systems due to the inaccuracy of the approximation.

3.6 Conclusions

By suppressing the ICI and multi-user interference and enhancing the signal power, the proposed CIB technique for WCDMA frequency-selective channel provides higher data rate and lower error rate outperforming common techniques, such as SVD-RAKE and SVD-MMSE, in the large interference region. Additionally CIB has low computational complexity since both the transmit and receive beamformers are linear and can be used with all spreading codes so that the beamforming design needs to be performed only once for users having multiple codes. The system also provides flexibility of scheduling.

Chapter 4

Eigenvalue Decomposition Based Lattice Precoding

In this chapter we propose a novel Lattice Precoding scheme based on Eigenvalue Decomposition (EDLP) for single user multiple-input multiple-output (MIMO) systems transmitting over slowly-varying flat-fading channels. This technique uses linear precoding to orthogonalize the channels, thus nullifying the interference. It employs a perturbation vector to reduce the transmitted power. The performance is enhanced by joint optimization of the linear precoder and the perturbation vector. As a result, the EDLP achieves not only full diversity order as we show analytically, but also significant power gain over comparable techniques. Although this structure enables EDLP to perform a global optimization on the closest lattice point search problem, the computational complexity of this nonlinear lattice precoding method is comparable to linear techniques. We also show that when channel estimation error is present, the EDLP technique outperforms other lattice precoding methods.

4.1 Introduction

The diversity order achievable by using linear precoding techniques is limited, and improved performance can be achieved by using nonlinear techniques like the Tomlinson-Harashima precoding (THP) [77]. In order to exploit full diversity order, more advanced techniques like lattice precoding can be used to significantly improve the

performance of the uncoded error probability at moderate to high values of the signal to noise ratio (SNR).

Lattice precoding [78] [79] [80] [51] [81] and lattice detection [17] [20] use lattice reduction (LR) techniques to implement dirty paper coding (DPC) [27] [24]. These techniques can be interpreted as closest lattice point search problems, which can be exactly solved by sphere decoding techniques but with higher computational complexity [82] [83] [84]. LR aided precoding techniques solve the closest lattice point search problem by employing rounding off approximation (using LR only) or nearest plane approximation (using LR plus sorted QR decomposition). However, LR in high dimensions is NP-hard [82] and the proposed suboptimal polynomial-time Lenstra-Lenstra-Lovasz (LLL) LR algorithm in the worst case has unbounded complexity, even for low dimensional cases [17]. This becomes particularly a problem since when implementing the system, the LR algorithm needs to be performed before each frame transmission.

In this chapter, a novel Lattice Precoding technique based on Eigenvalue Decomposition (EDLP) is proposed which not only exploits full diversity order with spatial multiplexing, but provides power gain over the performance of traditional LR precoding as well. The computational complexity of the proposed scheme is similar to the THP with linear precoding. This precoding technique is based on the assumption of the availability of channel state information (CSI) at the transmitter and uses a ZF linear precoding matrix computed from the CSI. The well-known deficiency of using a ZF spatial equalizer at the receiver is the resulting noise enhancement effect. Similarly, the ZF precoding suffers from transmitted power amplification. Despite power amplification at the transmitter caused by ZF precoding, the received signal can be detected by simple per-component quantizers with limited loss when compared with maximum likelihood (ML) detection performance. In order to reduce the transmitted power, the proposed technique employs a vector perturbation technique, through extension of the signal constellation at the transmitter, and solving a closest lattice point search problem. In addition, coordinated spatial rotations at both transmitter and receiver sides are introduced to reduce the transmitted power without affecting the statistics of the noise.

In Section 4.2, we present the structure of the transceiver with nonlinear processing

at the transmitter and linear processing at the receiver. Based on the proposed structure, the optimization metric that minimizes transmitted power is proposed. This optimization problem is addressed and solved in Section 4.3. We study the error rate performance of the system using analytical and simulation approaches in Section 4.4. In the same section we analyze the computational complexity of the proposed scheme and its robustness against channel estimation errors. Finally, Section 4.5 concludes this chapter with some remarks.

4.2 System Model

Common techniques for linear coherent reception when CSI is available at the receiver include canceling interference (ZF), maximizing SNR (matched filtering), or minimizing the mean square error. Nonlinear techniques can be regarded as additional blocks that use decision feedback to suppress the interference (successive interference cancellation), or transform the problem into an equivalent domain where the signals on different dimensions become approximately orthogonal (lattice reduction). When CSI is available at the transmitter as well, precoding techniques can be utilized. In this case the computational burden to perform the tasks outlined above can be put at the transmitter side, resulting in a simpler receiver which is of outmost significance in high throughput networks.

Precoding techniques shape the transmitted signal to manage its power, thus preventing noise enhancement and spatial interference at the receiver. This operation usually enhances the power and hence some linear and nonlinear processing at the transmitter is necessary to reduce the transmitted power.

We consider a slowly-varying, flat-fading, N_t -input and N_r -output channel, which means the complex channel matrix is assumed to remain constant during one transmission frame and changes independently from one frame to another. The SVD of the complex channel matrix is denoted by $\mathbf{H} = \mathbf{U}\mathbf{\Lambda}\mathbf{V}^H$. The complex channel matrix \mathbf{H} is assumed to be known at the transmitter and receiver sides. The baseband transmitted signal of the proposed EDLP is constructed in three steps.

- We first denote the number of independent data streams that are transmitted over the spatial channels by L . This parameter L is bounded physically by

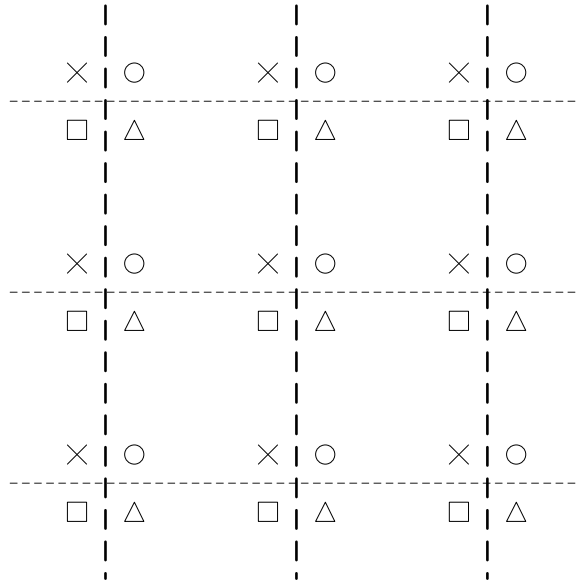


Figure 4.1: Example of periodically extended signal constellation by the two dimensional real lattice

$1 \leq L \leq \min(N_t, N_r)$ [8]. The transmit symbol vector \mathbf{s} is formed by the information bits to an L -dimensional vector whose elements take value in an M -QAM signal constellation. The symbol vector \mathbf{s} is added to a perturbation vector \mathbf{p} that belongs to a lattice structure, resulting in a periodically extended signal constellation. As seen in Figure 4.1, a QPSK constellation is periodically extended by a two dimensional real lattice.

- Secondly, the sum of the symbol vector \mathbf{s} and the perturbation vector \mathbf{p} is shaped by a square matrix which depends on the given channel matrix \mathbf{H} .
- Thirdly, a scalar multiplier τ is used to scale the transmitted power.
- Finally, the transmitted signal is given by

$$\mathbf{x} = \tau \mathbf{H}^{-1} \mathbf{U} \mathbf{B} (\mathbf{s} + \mathbf{p}) = \tau \mathbf{V} \mathbf{\Lambda}^{-1} \mathbf{B} (\mathbf{s} + \mathbf{p}) \quad (4.1)$$

where \mathbf{B} is a unitary matrix. In order to reduce the transmitted power, the choice of \mathbf{B} , along with the perturbation vector \mathbf{p} , depends on the realization of the channel, \mathbf{H} , and symbol vector \mathbf{s} .

The received signal, $\mathbf{y} = \mathbf{H}\mathbf{x} + \mathbf{n}$, is linearly equalized in spatial domain by $\mathbf{R} = \mathbf{U}\mathbf{B}$, as

$$\begin{aligned} \mathbf{r} &= \mathbf{R}^H \mathbf{y} = \mathbf{R}^H \mathbf{H}\mathbf{x} + \mathbf{R}^H \mathbf{n} \\ &= \tau \mathbf{B}^H \mathbf{U}^H \mathbf{H} \mathbf{V} \mathbf{\Lambda}^{-1} \mathbf{B}(\mathbf{s} + \mathbf{p}) + \mathbf{B}^H \mathbf{U}^H \mathbf{n} \\ &= \tau(\mathbf{s} + \mathbf{p}) + \mathbf{n}' \end{aligned}$$

where $\mathbf{n} \sim \mathcal{CN}(\mathbf{0}, \sigma_n^2 \mathbf{I})$. Since \mathbf{R} is unitary, the noise after linear equalization, i.e., \mathbf{n}' , has the same statistics as the original channel noise \mathbf{n} . The receiver also uses a modulo operator to subtract the perturbation vector \mathbf{p} , which was deliberately added at the transmitter to reduce the transmitted power. This simple modulo operator, denoted by $\mathbb{Q}_{\alpha\mathbb{G}^L}$, performs modulo operations on the real and imaginary parts of every component of the vector separately. Here α is the divisor of the modulo operation and \mathbb{G} is the set of the Gaussian integers. This constraint indicates that the lattice \mathbf{p} belongs to the scaled Gaussian integer lattice. The symbol decision statistic $\hat{\mathbf{s}}$ is the output of the per-component complex modulo and stays inside the Voronoi region,

$$\hat{\mathbf{s}} = \mathbb{Q}_{\alpha\mathbb{G}^L} \left(\frac{\mathbf{r}}{\tau} \right) = \mathbf{s} + \mathbb{Q}_{\alpha\mathbb{G}^L}(\mathbf{n}'').$$

In this way, the estimated signal is free of interference and corrupted only by a quantized Gaussian noise $\mathbf{n}'' \sim \mathcal{CN}(\mathbf{0}, \sigma_n^2/\tau^2 \mathbf{I})$.

The power in the transmit signal, $\|\mathbf{x}\|^2$ is given by

$$\|\mathbf{x}\|^2 = \|\tau \mathbf{\Lambda}^{-1} \mathbf{B}(\mathbf{s} + \mathbf{p})\|^2,$$

which is a function of the linear precoding matrix \mathbf{B} , the perturbation vector \mathbf{p} , and the channel. As noted earlier, our design goal is to select the unitary matrix \mathbf{B} and \mathbf{p} to minimize the average transmitted power. This optimization is taken over the choices of \mathbf{B} and \mathbf{p} ,

$$\min_{\substack{\mathbf{B} \in U(L) \\ \mathbf{p} \in \alpha\mathbb{G}^L}} \mathbb{E}[\|\tau \mathbf{\Lambda}^{-1} \mathbf{B}(\mathbf{s} + \mathbf{p})\|^2 | \mathbf{H}]$$

where in (4.2) the expectation is over equiprobable symbol vectors. Here $U(L)$ denotes the set of unitary matrices with dimension L . The linear part of the precoding

operation, i.e., the unitary matrix \mathbf{B} depends only on the channel and once is determined, will remain the same for the entire transmission frame. The perturbation vector \mathbf{p} is a point in the scaled L dimensional Gaussian integer lattice. The scaling scalar α is selected such that the Voronoi regions of the signal constellation, which is periodically extended by the lattice through $\mathbf{s} + \mathbf{p}$, do not overlap.

4.3 An Eigenvalue Decomposition Based Lattice Precoding (EDLP)

To be specific, we consider a system using an M -QAM constellation in each independent data stream and spatial multiplexing order of L . Define the signal space as $\tilde{\mathbf{S}} = [\tilde{\mathbf{s}}_1 \dots \tilde{\mathbf{s}}_N]$ and $\tilde{\mathbf{s}}_i = \mathbf{s}_i + \mathbf{p}_i$, $1 \leq i \leq N$ with cardinality $N = M^L$. The set $\{\mathbf{s}_i\}_{i=1}^N$ is the set of all uniquely ordered combinations of L M -QAM signals. We can rewrite Equation (4.2) as

$$\begin{aligned} \mathbb{E}[\|\mathbf{x}\|^2 | \mathbf{H}] &= \mathbb{E}[\tau^2 \tilde{\mathbf{s}}^H \mathbf{B}^H \mathbf{\Lambda}^{-2} \mathbf{B} \tilde{\mathbf{s}} | \mathbf{H}] \\ &= \frac{\tau^2}{N} \sum_{i=1}^N \tilde{\mathbf{s}}_i^H \left(\sum_{j=1}^L \gamma_j^2 \mathbf{b}_j \mathbf{b}_j^H \right) \tilde{\mathbf{s}}_i \\ &= \frac{\tau^2}{N} \sum_{j=1}^L \gamma_j^2 \mathbf{b}_j^H \mathbf{R}_a \mathbf{b}_j \end{aligned} \quad (4.2)$$

where γ_j is the j th singular value on the diagonal of $\mathbf{\Lambda}^{-1}$, \mathbf{b}_j is the j th column of \mathbf{B}^H , and $\mathbf{R}_a = \tilde{\mathbf{S}} \tilde{\mathbf{S}}^H$. For $L = 2$, Equation (4.2) can be written in the following form,

$$\mathbb{E}[\|\mathbf{x}\|^2 | \mathbf{H}] = \frac{\tau^2}{N} \mathbf{b}_1^H \mathbf{\Phi} \mathbf{b}_1 \quad (4.3)$$

where

$$\mathbf{\Phi} = \gamma_1^2 \mathbf{R}_a + \gamma_2^2 \det(\mathbf{R}_a) \mathbf{R}_a^{-1}.$$

We provide here a simple proof of this relation. Define a unitary matrix as

$$\mathbf{B}^H = [\mathbf{b}_1, \mathbf{b}_2] = \begin{bmatrix} x & z \\ y & w \end{bmatrix}.$$

Let us define $z = -\bar{y}\rho$. Based on the condition $-\bar{x}z + \bar{y}w = 0$, we simply have $w = \bar{x}\rho$ and

$$\mathbf{B}^H = \begin{bmatrix} x & -\bar{y}\rho \\ y & \bar{x}\rho \end{bmatrix}$$

Since $|x|^2 + |y|^2 = 1$ and $|x|^2 + |-\bar{y}\rho|^2 = 1$, the magnitude of ρ is $|\rho|^2 = 1$. Now define an operator Υ as

$$\Upsilon = \begin{bmatrix} 0 & -1 \\ 1 & 0 \end{bmatrix}$$

and write $\mathbf{b}_2 = \rho\Upsilon\bar{\mathbf{b}}_1$. For the Hermitian matrix \mathbf{R}_a ,

$$\mathbf{b}_2^H \mathbf{R}_a \mathbf{b}_2 = |\rho|^2 \bar{\mathbf{b}}_1^H \Upsilon^H \mathbf{R}_a \Upsilon \bar{\mathbf{b}}_1.$$

Since the cross terms of a quadratic form of a binomial are conjugate, we have

$$\mathbf{b}_2^H \mathbf{R}_a \mathbf{b}_2 = \mathbf{b}_1^H \Upsilon^H \mathbf{R}_a \Upsilon \mathbf{b}_1.$$

Applying the operator Υ to both sides results in

$$\Upsilon^H \mathbf{R}_a \Upsilon = \begin{bmatrix} \mathbf{R}_a(2, 2) & -\mathbf{R}_a(2, 1) \\ -\mathbf{R}_a(1, 2) & \mathbf{R}_a(1, 1) \end{bmatrix} = \det(\mathbf{R}_a) \mathbf{R}_a^{-1}$$

where $\mathbf{R}_a(i, j)$ is the element on the i th row and j th column of \mathbf{R}_a . This results in Equation (4.3).

Therefore, the optimization problem in (4.2) reduces to the minimization of the quadratic form given in Equation (4.3), which is minimized when:

1. The minimum eigenvalue of the Hermitian matrix Φ , denoted by η_{\min} , is minimized.
2. When \mathbf{b}_1 is selected to be the eigenvector corresponding to η_{\min} .

Since Φ is Hermitian, using the eigenvalue decomposition $\mathbf{R}_a = \mathbf{U}_a \mathbf{D}_a \mathbf{U}_a^H$, we have

$$\begin{aligned}\Phi &= \ln \left(\mathbf{U}_a e^{\gamma_1^2 \mathbf{D}_a} \mathbf{U}_a^H \mathbf{U}_a e^{\gamma_2^2 \det(\mathbf{R}_a) \mathbf{D}_a^{-1}} \mathbf{U}_a^H \right) \\ &= \mathbf{U}_a (\gamma_1^2 \mathbf{D}_a + \gamma_2^2 \det(\mathbf{R}_a) \mathbf{D}_a^{-1}) \mathbf{U}_a^H.\end{aligned}$$

It is easy to see that the eigenvalues of Φ , denoted by η_1 and η_2 , equal to the eigenvalues of the matrix $\gamma_1^2 \mathbf{D}_a + \gamma_2^2 \det(\mathbf{R}_a) \mathbf{D}_a^{-1}$ and

$$\gamma_1^2 \mathbf{D}_a + \gamma_2^2 \det(\mathbf{R}_a) \mathbf{D}_a^{-1} = \gamma_1^2 \begin{bmatrix} a_1 & 0 \\ 0 & a_2 \end{bmatrix} + \gamma_2^2 a_1 a_2 \begin{bmatrix} \frac{1}{a_1} & 0 \\ 0 & \frac{1}{a_2} \end{bmatrix}.$$

Therefore,

$$\begin{aligned}\eta_1 &= \gamma_1^2 a_1 + \gamma_2^2 a_2 \\ \eta_2 &= \gamma_1^2 a_2 + \gamma_2^2 a_1\end{aligned}$$

where a_1 and a_2 are the eigenvalues of \mathbf{R}_a . Therefore, the minimum eigenvalue of Φ is given by

$$\eta_{\min} = \gamma_{\max}^2 a_{\min} + \gamma_{\min}^2 a_{\max} \quad (4.4)$$

where $\gamma_{\min} = \min(\gamma_1, \gamma_2)$ and $\gamma_{\max} = \max(\gamma_1, \gamma_2)$. From the definition of \mathbf{R}_a , we have

$$\mathbf{R}_a = \frac{N}{2} \mathbf{I} + \sum_{j=1}^N (\mathbf{p}_j \mathbf{s}_j^H + \mathbf{s}_j \mathbf{p}_j^H + \mathbf{p}_j \mathbf{p}_j^H).$$

Hence, $\mathbf{R}_a - \frac{N}{2} \mathbf{I}_2$ is positive semi-definite and

$$\det(\mathbf{R}_a) = a_{\min} a_{\max} \geq \frac{N^2}{4} \quad (4.5)$$

where equality holds when $\mathbf{p}_j = \mathbf{0}, \forall 1 \leq j \leq N$, and $\mathbf{R}_a = N\mathbf{I}/2$. This result can be

used to bound the minimum transmitted power through (4.4),

$$\mathbb{E}[\|\mathbf{x}\|^2|\mathbf{H}] \geq \frac{2\tau^2}{N} \gamma_{\max} \gamma_{\min} \sqrt{a_{\min} a_{\max}} = \frac{2\tau^2 |\det(\mathbf{\Lambda}^{-1})|}{N} \sqrt{\det(\mathbf{R}_a)} \geq \tau^2 |\det(\mathbf{\Lambda}^{-1})|, \quad (4.6)$$

where first equality holds for $\gamma_{\max}^2 a_{\min} = \gamma_{\min}^2 a_{\max}$.

One approach to find the optimizing set, $\{\mathbf{p}_i\}_{i=1}^N$, for a given channel is to consider a graphical representation of Equation (4.4) as shown in Figure 4.2. In this figure

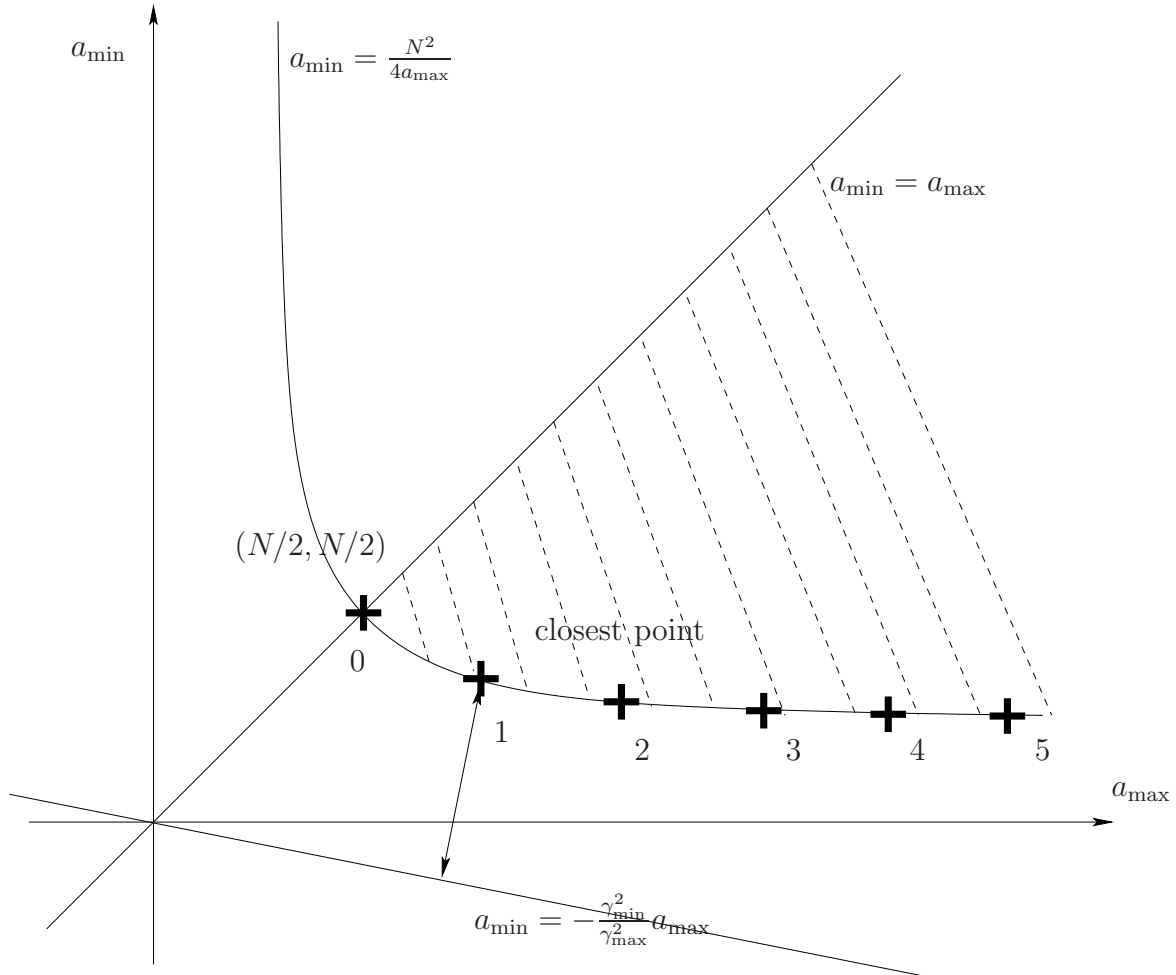


Figure 4.2: Sketch for finding solutions of minimizing transmitted power

the eigenvalues of \mathbf{R}_a , i.e., a_{\max} and a_{\min}), are represented as points in the plane, where each point is determined by the choice of $\{\mathbf{p}_i\}_{i=1}^N$. Since \mathbf{R}_a is Hermitian, these

discrete points are all in the first quadrant and are left and lower bounded by the hyperbola given by Equation (4.5) and shown in Figure 4.2 as the shaded area. The channel determines the slope of the straight line

$$a_{\min} = -\frac{\gamma_{\min}^2}{\gamma_{\max}^2} a_{\max} \quad (4.7)$$

passing through the origin. One of the discrete points on the lower bound hyperbola that is at minimum distance to this straight line represents the set of perturbation vectors that minimize the transmitted power. We denote the minimum distance between them by η_{\min} .

The points on the boundary hyperbola can be computed in a systematic way. As an example, we consider a system using a 4-QAM scheme, i.e., $M = 4$. Elements of \mathbf{s}_i take values of $\pm 1/2 \pm j/2$ and therefore $\alpha = 2$. The value of the signal on the constellation \mathbf{s}_i is defined in the following way: convert decimal integer $(i-1)_d$ into binary $(i-1)_b$; then map $+1 \rightarrow 1/2$ and $0 \rightarrow -1/2$ to construct the sequence $c_i = c_i^1 c_i^2 c_i^3 c_i^4$ where c_i^4 is the most significant bit; finally define $\mathbf{s}_i = [c_i^1 + j c_i^3, c_i^2 + j c_i^4]^T$. A series of points on the lower part of the hyperbola in the first quadrant are constructed below. These points are indexed by n , $0 \leq n \leq \infty$ in increasing order, as shown in Figure 4.2. Let us use superscript n to denote the index and define two $2 \times N$ matrices

$$\mathbf{P}_{b1} = \begin{bmatrix} 0 & -1 & 0 & 0 & 0 & -1 & -i & -i & i & i & 1 & 0 & 0 & 0 & 1 & 0 \\ 0 & 0 & 0 & 0 & 0 & 0 & 0 & 0 & 0 & 0 & 0 & 0 & 0 & 0 & 0 & 0 \end{bmatrix}$$

$$\mathbf{P}_{b2} = \begin{bmatrix} -1 & 0 & -i & -i & -1 & 0 & 0 & 0 & 0 & 0 & 0 & 1 & i & i & 0 & 1 \\ 0 & 0 & 0 & 0 & 0 & 0 & 0 & 0 & 0 & 0 & 0 & 0 & 0 & 0 & 0 & 0 \end{bmatrix}.$$

If n is an even number, \mathbf{p}_i^n is the i th column of the matrix $\alpha n(\mathbf{P}_{b1} + \mathbf{P}_{b2})$. If n is odd \mathbf{p}_i^n is the i th column of the matrix $\alpha(n+1)\mathbf{P}_{b1} + \alpha(n-1)\mathbf{P}_{b2}$. It can be easily verified that all points have $\det(\mathbf{R}_a^n) = N^2/4$, indicating that all points lie on the hyperbola. Every corresponding \mathbf{R}_a^n satisfies $\text{tr}(\mathbf{R}_a^n) = N(n^2 + 1)$, therefore, the coordinates of point n can be found as

$$\gamma_1, \gamma_2 = N \left(n^2 + 1 \pm \sqrt{(n^2 + 1)^2 - 1} \right).$$

However, this algorithm is not guaranteed to generate all possible points defined by pairs of eigenvalues.

If we denote the norm-2 condition number of matrix \mathbf{H} by $\kappa_2(\mathbf{H})$ with $\kappa_2(\mathbf{H}) = \kappa_2(\mathbf{H}^{-1}) = \gamma_{\max}/\gamma_{\min}$, Equation (4.7) can be rewritten as $a_{\min} = -\kappa_2^{-2}(\mathbf{H})a_{\max}$. Also denote the slope of the line segment connecting two consecutive points with index $n - 1$ and n on the lower boundary as δ_n and define $\delta_0 = -1$, the sequence $-\delta_n^{-1}$ for $0 \leq n < \infty$ partitions the range $[1, \infty)$ and we denote the resulting partition by \mathcal{D} . It is obvious that the index of the set in the partition that $\kappa_2^2(\mathbf{H})$ falls in is the index of the closest point on the lower hyperbola to the line in Equation (4.7), as shown in Figure 4.2, and the corresponding set of $\{\mathbf{p}_i\}_{i=1}^N$ is the optimum perturbation vector set. The channel characteristics, which are known at the transmitter, determine $\kappa_2(\mathbf{H})$. Using this value, the transmitter looks for the corresponding partition and uses the corresponding set of $\{\mathbf{p}_i\}_{i=1}^N$ for precoding. The selected perturbation vector \mathbf{p} is then used in Equation (4.3) to compute the linear precoding matrix \mathbf{B} .

The precoding process is depicted in Figure 4.3. Knowing the CSI, the transmitter first computes the eigenvalues of the channel inverse, which are used to find the perturbation vector obtained from the partition set \mathcal{D} , and then the forward rotation matrix \mathbf{R} . Once the encoder maps the coded bits into a symbol vector, the symbol vector is summed with the associated perturbation vector and then the linear precoding matrix is determined to construct the transmitter baseband signal. At the receiver, the received signal is passed through a linear backward rotation equalizer and quantized by a per-component complex scalar quantizer. The result is the transmit symbol vector estimate and is ready to be sent to the decoder.

4.4 Performance and Complexity Analysis

In Section 4.3 a transceiver structure for single user MIMO system is proposed and shown in Figure 4.3. The parameters in the system are designed to optimize the performance as given by Equation (4.2). In the following, we discuss the error probability performance and the computational complexity of the system.

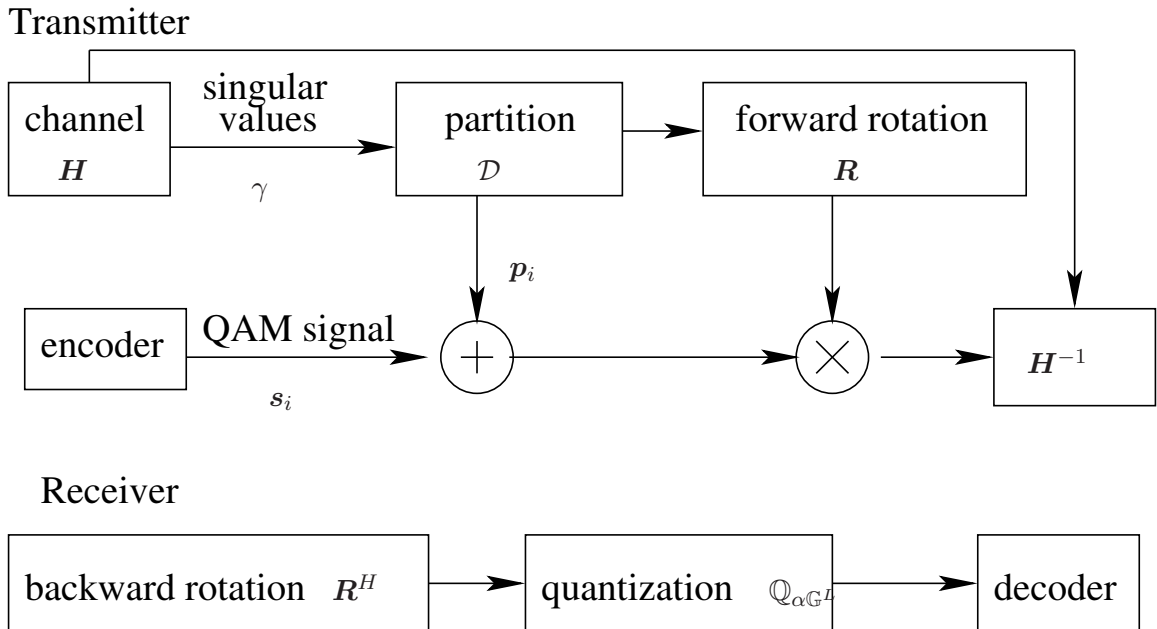


Figure 4.3: The block diagram for the EDLP transceiver

4.4.1 Simulation Results

From Equation (4.6), we see that the transmitted power used by the EDLP is lower bounded by $|\det(\mathbf{\Lambda}^{-1})|$. The bit error rate (BER) of a genie aided system, whose transmitted power equals to the lower bound, can be computed and used to evaluate the performance of the algorithm proposed in Section 4.3 for computing the perturbation vector. In other words, in order to meet the target BER, EDLP algorithm results an average transmitted power, $\mathbb{E}[\|\mathbf{x}\|^2|\mathbf{H}]$, no less than this lower bound in Equation 4.6. Since the noise components on every N_r receive antenna and every real/imaginary dimension are assumed to be independent, the marginal distribution of the noise presents in bit detection n_b is Gaussian with zero mean and variance

$$\sigma_b^2 = \frac{N_r |\det(\mathbf{\Lambda}^{-1})|}{2L \text{ SNR}} \quad (4.8)$$

where SNR is defined as the ratio of total transmitted power to noise power per receive antenna. As a result of using the per-component quantizer, signal is corrupted by the quantized Gaussian noise centered at the transmitted signal. Figure 4.4 depicts the

case of $M = 4$ and the cross marks are the extended transmitted signal constellation. An error event happens when the received signal on that dimension falls in the shaded bins. The BER averaged over all channel realizations is

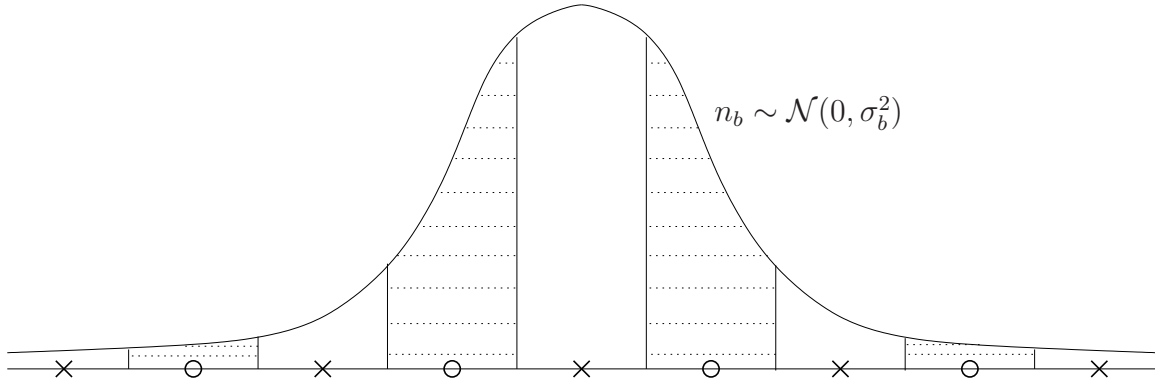


Figure 4.4: BER calculation with extended constellation

$$P_{error} = 2\mathbb{E} \sum_{n=0}^{\infty} \left[Q\left(\frac{2n + \frac{1}{2}}{\sigma_b}\right) - Q\left(\frac{2n + \frac{3}{2}}{\sigma_b}\right) \right]. \quad (4.9)$$

. As shown in Figure 4.5, the gap between the real system performance and the genie aided system performance is negligible. From [49], the average of the transmitted power taken over all realizations of the channels can be computed as $\mathbb{E}[\tau^2 |\det(\mathbf{\Lambda}^{-1})|] = \tau^2 \Gamma(3/2)\Gamma(1/2)/2 = \pi\tau^2/4$ [21] where we have used the fact that $\mathbf{H}\mathbf{H}^H \sim \mathcal{W}_t(r, \mathbf{I})$ is a central complex Wishart matrix with $t = \min(N_t, N_r)$ and $r = \max(N_t, N_r)$.

In this section we also compare the performance and complexity of the proposed EDLP scheme with a number of other recently proposed techniques. In [85] a new technique for MIMO broadcast channels is proposed. The single antenna receivers use per-component complex scalar quantizers to determine symbol estimates. At the transmitter, the enhanced transmitted power due to using the ZF linear precoding is reduced by introducing a perturbation vector. This power reduction is carried out by performing a closest lattice point search, the exact solution of which is NP-hard [84]. Nearest plane and rounding off approximation techniques are used to solve this problem and find the perturbation vector. The EDLP transceiver structure introduced above differs from [85] in the additional coordinated linear precoding and

equalization represented by the orthonormal transformation matrix \mathbf{R} . By doing this, the transmit signal can be shaped to match the channel through a unitary transformation in order to achieve a larger channel gain. Furthermore, the original lattice basis, for example in Equation (5) in [85], are not optimized for LR with receive antenna joint processing. Different original lattice basis, when fed into the LR algorithm, require different numbers of iterations in the lattice reduction process and result in different reduced lattice basis. The transmitter rotation matrix \mathbf{B} is introduced to provide the LR process an additional degree of freedom such that the resulting reduced basis is shorter and more orthogonal.

A single user LR aided precoding and reception technique is proposed in [78] and is referred to as LRAPR. This technique uses a ZF linear precoding matrix whose bases are reduced by LR from the channel inverse precoding matrix. Hence, the condition number of the precoding matrix becomes smaller and the transmitted power is reduced. However, at the receiver the unimodular lattice transformation matrix needs to be computed from the channel, or be sent by the transmitter to transform back the original transmit constellation.

In Figure 4.5, BER performance of EDLP is evaluated through simulation and is compared with the techniques described above. It can be seen that all these techniques achieve full diversity order, thanks to the nonlinear perturbation. However, EDLP displays a clear power gain over all other precoding techniques. Comparing to the nearest plane and rounding off approximation techniques, the receive antenna collaboration and the coordination between the transmitter and the receiver in the EDLP provides a significant 2.5 dB power gain. Although the single user LR aided precoding also provides a power gain over the two broadcast channel techniques mentioned above through the receive antenna collaboration, it still cannot outperform the EDLP in the normal operating BER-SNR range since the linear precoding part of it is not optimized for LR. Notice that in order to reduce the complexity at the receiver, the EDLP uses linear equalization and per-component quantizers, therefore, there remains a gap between its performance and the performance of ML detection.

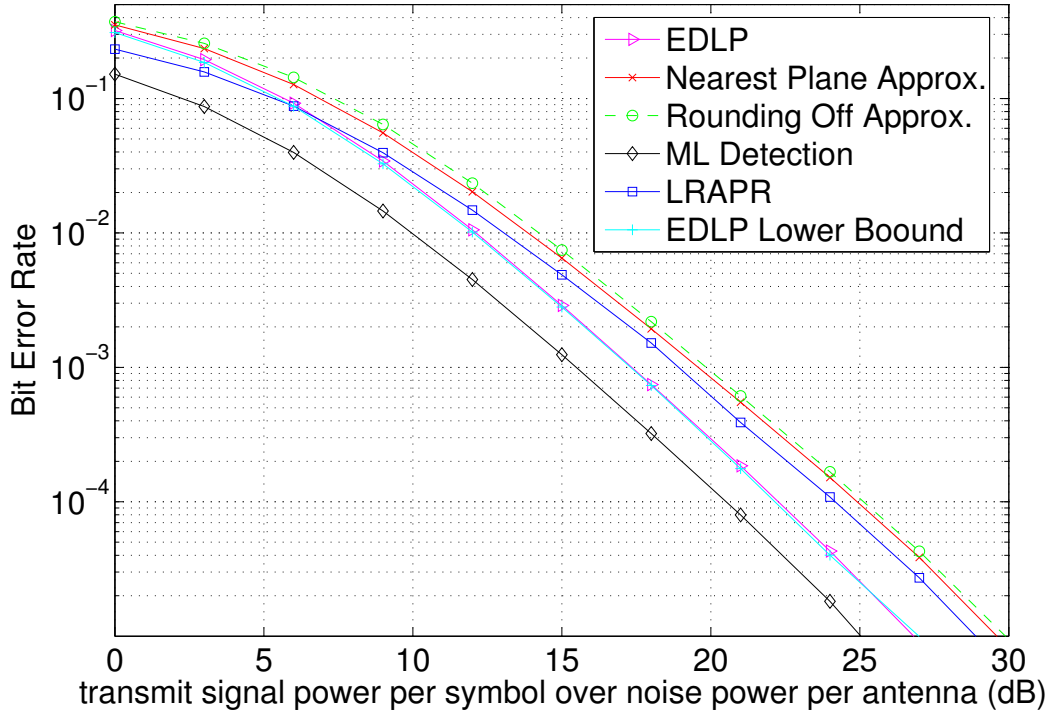


Figure 4.5: Error rate performance comparison of different techniques

4.4.2 Complexity

We use the required number of operations to evaluate the overall complexity of different transmission and reception techniques. The computational operations required for ML, LRAP, LRAPR, and EDLP are listed in Table 4.1, where the operations are categorized based on location and stage of the computation. The stage in which the transceiver processes the CSI to prepare for the succeeding operations at the transmitter (Tx) and the receiver (Rx) is referred to as the “frame overhead” at Tx and Rx. The operations needed for transmission and reception of each symbol are referred to as “per channel use”. It is also insightful to compare the computational complexity by quantifying the total operations of every technique in terms of the number of floating-point operations (flops). Here a system with $N_t = N_r = L = 2$ and 4-QAM modulation is studied. We assume the costs of rounding and quantization operations are negligible when compared to floating-point addition and multiplication. It is also

Table 4.1: Types of computations needed for the EDLP and comparable techniques

	frame overhead		per channel use	
	Tx	Rx	Tx	Rx
MLD	none	compute the constellation at the receiver side	none	compute and compare distances to receive constellation points
LRAP	matrix inverse, pre-ordered LR, ordered QRD	none	linear precoding and THP	per-component quantization
LRAPR	matrix inverse and LR	matrix inverse and LR	matrix multiplication	matrix multiplications and detection
EDLP	SVD, EVD and partition searching	SVD, EVD and partition searching	lattice point attachment and linear precoding	linear equalization and per-component quantization

assumed that complex addition requires 2 flops and complex multiplication requires 6 flops. In the case of real numbers, both addition and multiplication require 1 flop. For EDLP, since it is assumed that the receiver has the capability to estimate the channel matrix, the backward rotation matrix \mathbf{R} can be determined with no extra hardware expense. Since channel estimation algorithm varies significantly with the system requirement and implementation, and is common for all these coherent techniques, it is not included in our complexity analysis. Note that the computational complexities of the LR algorithm in LRAP and LRAPR approaches are already reduced using the results from [86].

For coherent ML detection, after the CSI is acquired, the receiver generates the receiver side signal constellation which takes $NN_r(6L + 2(L - 1))$ flops. Upon receiving each symbol, the constellation point that has the closest distance to the received signal is selected as the ML transmitted symbol which requires $N(6L - 1)$ flops for

computing distance, and N flops for searching the minimum. For ML detection no significant operation is needed at the transmitter side. For the LRAP, more computation is needed at the transmitter; this includes two matrix inversions, two matrices multiplications, one QR decomposition, and pre-ordered complex LLL algorithm which requires 2×48 , $2N_r^2(8L-2) + N_r$, 173, and 156 flops, respectively[86]. At each symbol transmission, there are three matrix-vector multiplications and L iterative feedback operations adding up to $3N_r(8L-2) + 16L - 4$ number of flops. Although the LRAPR performs better than the LRAP, it is costly at the receiver since complex LLL LR algorithm should be conducted at both sides which requires 145 flops. In addition, at the transmitter, matrix inversion requires another 48 flops for the $N_r = 2$ case using adjugate matrix. For each channel use, matrix-vector multiplication is implemented at both sides. The EDLP is the most efficient technique, where the computationally complex LR algorithms are replaced by the partition searching and lattice point matching at the first and second detection stages, respectively. The major computational burden in this algorithm is to solve two Hermitian matrix eigen problems and some matrix multiplications, which take totally $16L^3/3 + 2N_rM^L$ flops [87] [88]. The total numbers of required flops for different techniques are listed in Table 4.2. We can

Table 4.2: Estimated numbers of flops

	frame overhead		per channel use	
	Tx	Rx	Tx	Rx
MLD	0	448	0	192
LRAP	539	0	112	0
LRAPR	193	145	28	28
EDLP	107	0	28	28

see that the ML detection is costly at the receiver side and the LRAP is costly at the transmitter side. The LRAPR reduces the complexity of LRAP at the transmitter by more than half, however it requires more computation at the receiver side. The EDLP requires the least number of computations in the “frame overhead” stage and same number of flops for each transmitted symbol.

We have provided an efficient algorithm for computation of the partition set \mathcal{D} and the associated lattice point set $\{\mathbf{p}_j\}_{j=1}^N$ in Section 4.3. However, the number of sets

in partition \mathcal{D} is indeed infinite. In practice we may further simplify the precoding computation by constraining the number of sets in partition \mathcal{D} into a finite number since this partition depends only on the singular values of the channel matrix and is invariant to the unitary transformations at left and right sides of the channel matrix.

For random matrices distributed as \mathbf{H} , the tail of the distribution of the condition number has been explored and loosely upper bounded in [89] by,

$$\mathbb{P} \left[\frac{\kappa_2(\mathbf{H})}{N_r/(|N_r - N_t| + 1)} > \theta \right] < \frac{1}{2\pi} \left(\frac{6.298}{\theta} \right)^{2(|N_r - N_t| + 1)}. \quad (4.10)$$

For instance, for a channel with $N_r = N_t = 2$, the first 30 points on the hyperbola can partition $\kappa_2(\mathbf{H})$ from 1 to 1626. From above, the probability that the condition number is larger than 1626, i.e., $\kappa_2(\mathbf{H}) > 1626$, can be calculated. From Equation 4.10, $\kappa_2(\mathbf{H}) > 1626$ yields $\theta = 813$. Plugging $\theta = 813$ in RHS results in roughly 10^{-5} . This shows that if a EDLP algorithm stores 30 points, the probability that this algorithm cannot result in the optimal solution for any realization of the channel is less than 10^{-5} .

A more precise upper bound is discussed below. The joint probability density function of the ordered strictly positive eigenvalues of the Wishart matrix $\mathcal{W}_t(r, \mathbf{I})$, denoted by $\omega_1 \geq \dots \geq \omega_t > 0$ is given in [49] by

$$f(\omega_1, \dots, \omega_t) = e^{-\sum_{i=1}^t \omega_i} \prod_{i=1}^t \frac{\omega_i^{r-t}}{(t-i)!(r-i)!} \prod_{i < j}^t (\omega_i - \omega_j)^2.$$

In our case since $N_r = N_t = 2$, with $\omega_1 \geq \omega_2 \geq 0$, we have

$$f(\omega_1, \omega_2) = e^{-\omega_1 - \omega_2} (\omega_1 - \omega_2)^2 \quad (4.11)$$

Numerical integration of $f(\omega_1, \omega_2)$ over the region $\omega_1 \geq \omega_2 \geq 0$ and $\omega_1/\omega_2 \geq \kappa_2(\mathbf{H})$ shows that for an outage probability of 10^{-5} only the first 15 points are needed. Therefore, a finite partition set can be used with only an inconspicuous impact on the performance. However, for most LR based systems it is not possible to apply a similar simplification.

4.4.3 Channel Estimation Error

Channel estimation error is an important factor that affects system performance. If the CSI at the transmitter needs to be obtained from the receiver, then the CSI is a quantized version of the CSI estimated at the receiver. For MMSE MIMO channel estimation, the estimated channel matrix can be expressed as [90] [91] [92]

$$\hat{\mathbf{H}} = \mathbf{H} \mathbf{s}_p \mathbf{s}_p^H (\sigma_n^2 \mathbf{I}_{N_t} + \mathbf{s}_p \mathbf{s}_p^H)^{-1} + \mathbf{n} \mathbf{s}_p^H (\sigma_n^2 \mathbf{I}_{N_t} + \mathbf{s}_p \mathbf{s}_p^H)^{-1} \quad (4.12)$$

where \mathbf{s}_p is an N_t -by- N_p pilot symbols matrix with average energy E_p . It is shown in [90] that the optimal \mathbf{s}_p for LMMSE estimation converge to the optimal solution for ML estimation, which is any \mathbf{s}_p that satisfies

$$\mathbf{s}_p \mathbf{s}_p^H = N_p E_p \mathbf{I}_{N_t}.$$

Equation (4.12) now becomes

$$\hat{\mathbf{H}} = \frac{N_p E_p}{\sigma_n^2 + N_p E_p} \mathbf{H} + \frac{1}{\sigma_n^2 + N_p E_p} \mathbf{n}_p \mathbf{s}_p^H,$$

where \mathbf{n}_p is an AWGN matrix whose elements are zero mean circular complex Gaussian random variable with variance σ_n^2 . In order to construct our channel matrix estimate such that each element has unit variance, $\hat{\mathbf{H}}$ is further normalized as

$$\tilde{\mathbf{H}} = \sqrt{\frac{\sigma_n^2 + N_p E_p}{N_p E_p}} \hat{\mathbf{H}} = \sqrt{\frac{N_p E_p}{\sigma_n^2 + N_p E_p}} \mathbf{H} + \Delta \mathbf{H}$$

where $\Delta \mathbf{H} = \mathbf{n}_p \mathbf{s}_p^H / \sqrt{N_p E_p (\sigma_n^2 + N_p E_p)}$ is the estimation error matrix, which is a zero-mean i.i.d. circular complex Gaussian random variable, uncorrelated with $\hat{\mathbf{H}}$. It can be easily verified that

$$\mathbb{E}[\tilde{\mathbf{H}}^H \tilde{\mathbf{H}}] = N_r \mathbf{I}_{N_t}.$$

The system uses $\tilde{\mathbf{H}}$ to compute both precoding and equalization. We define the channel estimation error rate σ_e^2 as

$$\sigma_e^2 = \frac{\mathbb{E}[\Delta \mathbf{H}^H \Delta \mathbf{H}]}{\mathbb{E}[\tilde{\mathbf{H}}^H \tilde{\mathbf{H}}]} = \frac{\sigma_n^2}{N_p E_p}.$$

Figure 4.6 shows the BER performances of three precoding techniques when the channel estimation error is $\sigma_e^2 = 0.01$. As SNR increases, we observe an increasing

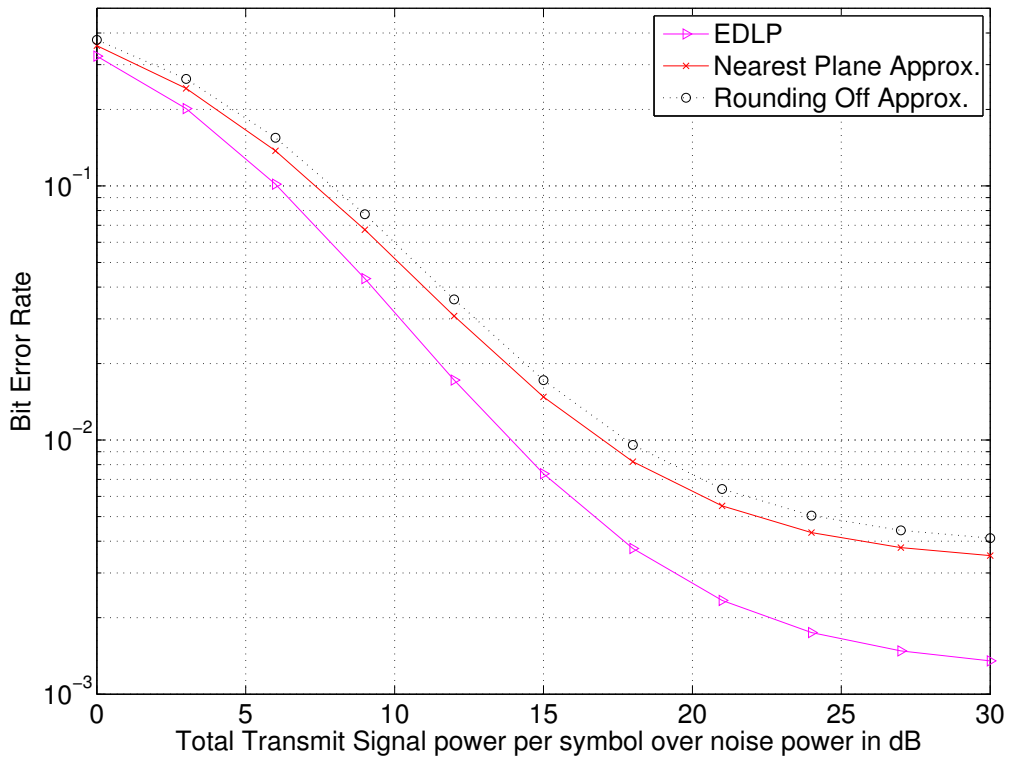


Figure 4.6: A performance comparison of different techniques with 1% channel estimation error variance

gap and a better error floor for EDLP compared to the other two lattice precoding techniques. This indicates that when small channel estimation errors are present EDLP provides a more robust performance.

4.4.4 Diversity Order When More Antennas Are Available

For large SNR, using the approximation $Q(x) \leq 1/2e^{-x^2/2}$ [21], Equation (4.9) can be approximated by

$$P_{error} \approx \mathbb{E} \sum_{n=0}^{\infty} \left[e^{(2n+\frac{1}{2})^2 \frac{-L \text{SNR}}{|\det(\mathbf{\Lambda}^{-1})|N_r}} - e^{(2n+\frac{3}{2})^2 \frac{-L \text{SNR}}{|\det(\mathbf{\Lambda}^{-1})|N_r}} \right]. \quad (4.13)$$

Introducing $\xi = L\text{SNR}/(4N_r)$, we observe that when the SNR increases, for any value of $\det(\mathbf{\Lambda})$ we have

$$e^{-\xi|\det(\mathbf{\Lambda})|} \gg -e^{-\xi|\det(\mathbf{\Lambda})|} + \sum_{n=1}^{\infty} \left[e^{(2n+\frac{1}{2})^2 \frac{-L \text{SNR}}{|\det(\mathbf{\Lambda}^{-1})|N_r}} - e^{(2n+\frac{3}{2})^2 \frac{-L \text{SNR}}{|\det(\mathbf{\Lambda}^{-1})|N_r}} \right]$$

which allows us to further simplify Equation 4.13 to

$$P_{error} \approx \mathbb{E}[e^{-\xi|\det(\mathbf{\Lambda})|}].$$

The joint probability density function of the unordered eigenvalues of the complex Wishart matrix $\mathcal{W}_t(r, \mathbf{I})$, with $t = 2$ and $\omega_1, \omega_2 > 0$ is given in [49] as

$$\begin{aligned} f_{\omega_1, \omega_2} &= \frac{1}{2} e^{-\omega_1 - \omega_2} \prod_{i=1}^2 \frac{\omega_i^{r-2}}{(2-i)!(r-i)!} (\omega_1 - \omega_2)^2 \\ &= \frac{1}{2} [(r-1)!(r-2)!]^{-1} e^{-\omega_1 - \omega_2} \omega_1^{r-2} \omega_2^{r-2} (\omega_1 - \omega_2)^2. \end{aligned}$$

Consequently,

$$[2(r-1)!(r-2)!]P_{error} \approx \iint_{\mathbb{R}_+^2} e^{-\xi\sqrt{\omega_1\omega_2} - \omega_1 - \omega_2} \omega_1^{r-2} \omega_2^{r-2} (\omega_1 - \omega_2)^2 d\omega_1 d\omega_2. \quad (4.14)$$

By introducing the change of variables $a = \frac{1}{4}(2-\xi)(\sqrt{\omega_1} - \sqrt{\omega_2})^2$ and $b = \frac{1}{4}(2+\xi)(\sqrt{\omega_1} + \sqrt{\omega_2})^2$, we have the determinant of Jacobian matrix $\det(J)$ as

$$\det(J) = \frac{2}{4-\xi^2} \left(\sqrt{\frac{a(\xi+2)}{b(\xi-2)}} - \sqrt{\frac{b(\xi-2)}{a(\xi+2)}} \right)$$

and Equation (4.14) becomes

$$[2(r-1)!(r-2)!]P_{error} \approx \iint \det(J) \frac{16ab(4-\xi^2)^3}{[(\xi-2)b - (\xi+2)a]^4} \left(\frac{b}{\xi+2} + \frac{a}{\xi-2} \right)^r e^{-a-b} da db, \quad (4.15)$$

For $\xi \gg 2$, Equation (4.15) can be simplified as

$$[2(r-1)!(r-2)!]P_{error} \approx \iint \frac{2}{\xi^2} \left(\sqrt{\frac{a}{b}} - \sqrt{\frac{b}{a}} \right) \frac{16ab\xi^6}{(b-a)^4\xi^4} (a+b)^r \xi^{-r} e^{-a-b} da db.$$

Therefore, $P_{error} = K\xi^{-r}$ where K is a constant scalar. From this we conclude that EDLP achieves full diversity order. In Figure 4.7, simulated BER of EDLP for different values of the numbers of transmit and receive antennas are shown. In both

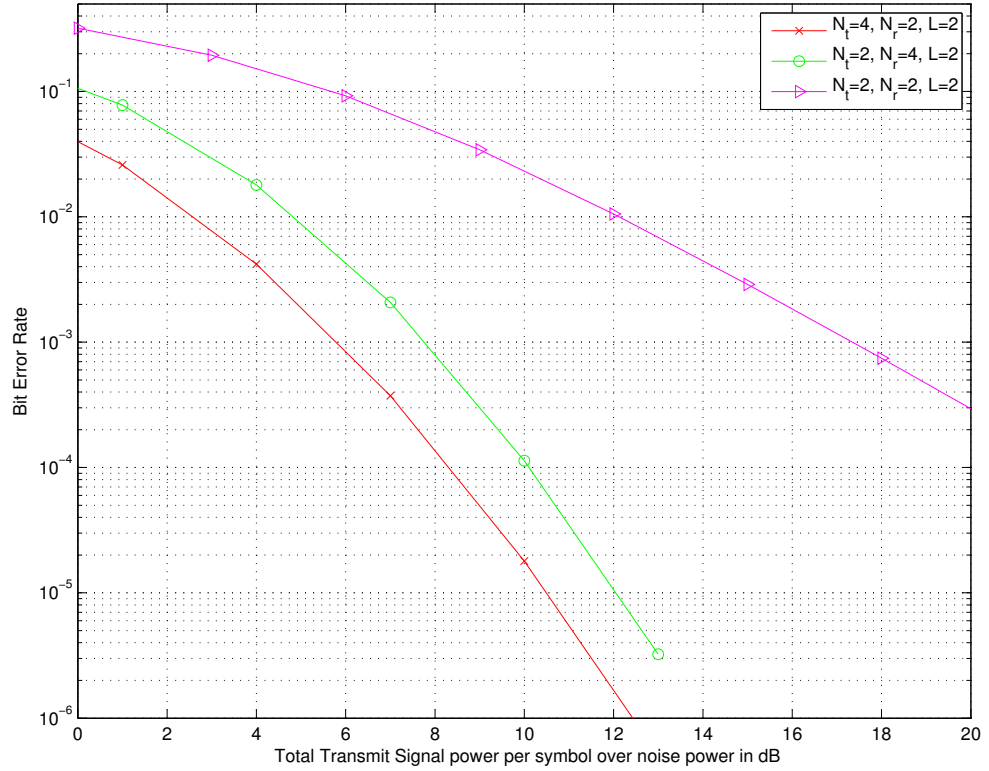


Figure 4.7: EDLP with different antenna settings

$N_r = 4, N_t = 2$ and $N_r = 2, N_t = 4$ cases, the BER curves show diversity order of 4 and in $N_r = 2, N_t = 2$ case, the diversity order is shown to be 2.

4.5 Conclusions

In this chapter an eigenvalue-decomposition based lattice-precoding technique, EDLP, is proposed for use in MIMO flat-fading channels. This technique requires CSI at both transmitter and receiver sides. For this system, the required computation at the receiver side is limited to linear processing and simple per-component modulo operations. We derived a very tight lower performance bound for EDLP for the entire range of SNR's. This bound is used to prove that this system achieves full diversity gain. The performance of EDLP in terms of BER-SNR also shows a clear power gain compared with other techniques. Although a nonlinear precoding scheme is used at the transmitter side, but unlike other lattice precoding techniques, this system does not require to use a LR algorithm. When channel estimation errors are present, EDLP exhibits a more robust performance than other schemes at moderate to high SNR values.

Chapter 5

Lattice Precoding for MIMO Broadcast Channels

In multi-user systems, interuser interference is a major impairment introduced by the channel and user signals. Linear precoding schemes can combat the interuser interference to a certain extent, however, nonlinear precoding schemes are better suited to cancel the interuser interference. In multiple antenna broadcast channels, the nonlinear DPC [24] scheme, which is optimum for interference channels, is proved to achieve both the sum capacity and the overall capacity region [29]. Hence, practical DPC schemes, such as Tomlinson-Harashima Precoding (THP) [22] [23] and vector perturbation [51] have received a great deal of attention. Some of these schemes exhibit excellent performances, particularly achieving the full diversity order, with moderate complexity.

The practical DPC schemes used for multiple antenna broadcast channels are closely related to lattice representation of the symbol constellation. Based on this point of view, Lattice-Reduction (LR) techniques are used to enhance the performance of single user MIMO detectors. Lattice reduction in high dimensions is known to be an NP-hard problem. In [17], a polynomial-time, sub-optimal LR algorithm, called the LLL algorithm, is used to find the shortest lattice bases. There are some other LR techniques employed in certain systems, such as complex LLL [86] and Seysen's LR [93] [94]. The complexity of these iterative polynomial-time LR techniques is determined by the number of iterations required for lattice reduction, however, the

worst-case complexity remains unbounded.

Lattice searching techniques can be used with linear equalization techniques such as ZF, MMSE, extended MMSE, BLAST, and hybrids of them [17] [20]. It has been shown that the performance of LR aided MMSE SIC detector nearly reaches the performance of ML detection [86].

Precoding methods for single user MIMO systems using LR have also been developed to move the complexity of LR from the receiver side to the transmitter side without sacrificing performance [95]. For broadcast channels, LR aided ZF [85] and BDZF [81] based precoding schemes have been proposed. These techniques use linear precoding to separate user signals and use LR to reduce the transmit power. The resulting performance achieves full diversity order.

In this chapter, we first introduce a general system structure that allows us to apply the lattice reduction algorithm. Following this general structure, we discuss a solution for a multi-user system with multiple transmit antennas and a single receive antenna per each user. This solution, referred to as the WFH scheme, is also useful to provide insight for more complicated channels. When each receiver has multiple antennas, similar to ZF, it is possible to orthogonalize each user's block channels and make the multi-user channel free of interuser interference. In order to do so, block-diagonal ZF linear precoding is introduced. A block-diagonal ZF and EDLP based algorithm, referred to as BDZF-EDLP, is proposed afterwards. This algorithm features low complexity and coordinated structure for multi-user multiple antenna system that have multiple receive antennas per user. BDZF-EDLP is also capable for large scale extension due to the linearity of BDZF and the linearly scalable EDLP algorithm made possible through BDZF. For the same channel, a previously proposed algorithm that also offers the support for spatial multiplexing for each user is then discussed. Unlike the WFH scheme and BDZF-EDLP, this algorithm simply stacks BDZF and a simple implementation of the LR algorithm [96]. Finally we discuss and compare the error probability and computational complexity of these techniques.

5.1 General System Structure

The transmit antennas transmit \mathbf{x} , which is the sum of signal vectors from different users, i.e.,

$$\mathbf{x} = \sum_{k=1}^K \mathbf{T}_{p,k} \tilde{\mathbf{s}}_k = \sum_{k=1}^K \mathbf{T}_{p,k} (\mathbf{s}_k + \mathbf{p}_k), \quad (5.1)$$

where $\mathbf{T}_{p,k}$ is the $M \times L_k$ precoding matrix used to precode the L_k dimensional signal vector of user k onto M transmit antennas for $1 \leq k \leq K$. Here $L_k \leq \min(M, N_k)$ where N_k denotes the number of receiver antennas of user k . An integer-component vector \mathbf{p}_k is added to \mathbf{s}_k to get a periodic extension of the signal constellation. Similar to EDLP, the goal is to reduce the transmitted power. To avoid overlap of the detection regions of the signal constellation points, elements of \mathbf{p}_k have to be discrete numbers, i.e., $\mathbf{p}_k \in A\mathbb{G}^{L_k}$ where \mathbb{G} denotes the set of Gaussian integers. For example, if system uses 4-QAM modulation, the elements in \mathbf{s}_k take values from $\pm 1/2 \pm j/2$, then $A = 2$. In other words, \mathbf{p}_k lies in a L_k dimensional complex lattice defined by $A\mathbb{G}^{L_k}$. The 4-QAM signal points \mathbf{s}_k are located within the Voronoi region of the associated lattice point \mathbf{p}_k .

We denote the signal that is to be precoded by $\tilde{\mathbf{s}}_k$, where $\tilde{\mathbf{s}}_k = \mathbf{s}_k + \mathbf{p}_k$. Then, Equation (5.1) can be expressed by $\mathbf{x} = \mathbf{T}_p \tilde{\mathbf{s}}$ where $\mathbf{T}_p = [\mathbf{T}_{p,1}, \mathbf{T}_{p,2}, \dots, \mathbf{T}_{p,K}]$ and $\tilde{\mathbf{s}} = [\tilde{\mathbf{s}}_1^T, \tilde{\mathbf{s}}_2^T, \dots, \tilde{\mathbf{s}}_K^T]^T$. The received signal \mathbf{y} , which is expressed by the column concatenation of the signals on the antennas of different users in natural order, is written as

$$\mathbf{y} = [\mathbf{y}_1^T, \mathbf{y}_2^T, \dots, \mathbf{y}_K^T]^T = \mathbf{H}\mathbf{x} + \mathbf{n} = \mathbf{H}\mathbf{T}_p \tilde{\mathbf{s}} + \mathbf{n}. \quad (5.2)$$

The receiver first linearly equalizes the received signal by

$$\mathbf{r} = \mathbf{R}^H \mathbf{y} = \mathbf{R}^H \mathbf{H}\mathbf{T}_p \tilde{\mathbf{s}} + \mathbf{R}^H \mathbf{n} \quad (5.3)$$

where \mathbf{R} is the linear equalization matrix multiplier. Since in broadcast channels users are decentralized and are unable to collaborate with each other, \mathbf{R} is a block-diagonal

matrix of the form

$$\mathbf{R} = \begin{bmatrix} \mathbf{R}_1 & \mathbf{0} & \dots & \mathbf{0} \\ \mathbf{0} & \mathbf{R}_2 & \dots & \mathbf{0} \\ \vdots & \vdots & \ddots & \vdots \\ \mathbf{0} & \mathbf{0} & \dots & \mathbf{R}_K \end{bmatrix} \quad (5.4)$$

where each \mathbf{R}_k is an $N_k \times L_k$ dimensional unitary matrix. The decision variable $\hat{\mathbf{s}}$ is then acquired by element-wise quantization of \mathbf{r} , i.e.,

$$\hat{\mathbf{s}} = \mathbb{Q}_{\text{AG}}(\mathbf{r}) = \mathbb{Q}_{\text{AG}}(\mathbf{R}^H \mathbf{H} \mathbf{T}_p \tilde{\mathbf{s}}) + \mathbb{Q}_{\text{AG}}(\mathbf{R}^H \mathbf{n}).$$

The modulo function $\mathbb{Q}_{\text{AG}}(x)$ for a complex scalar is defined as

$$\mathbb{Q}_{\text{AG}}(x) = \Re(x) - A \left\lfloor \frac{\Re(x) + A/2}{A} \right\rfloor + j \left(\Im(x) - A \left\lfloor \frac{\Im(x) + A/2}{A} \right\rfloor \right),$$

where $\Re(\cdot)$ and $\Im(\cdot)$ denote the real and imaginary parts, respectively. The value $\left\lfloor \frac{\Re(x) + A/2}{A} \right\rfloor$ is the unique integer such that $\mathbb{Q}_{\text{AG}}(\Re(x)) \in [-A/2, A/2)$. The objective of including THP in precoding and a modulo operation in equalization is to reduce the transmit power by forcing the transmit signal to be in the Voronoi region. Then, the average transmit power becomes solely related to the volume of the Voronoi region, which equals to the reciprocal of the lattice density, or the determinant of the lattice generator matrix [18]. The design criteria for the optimal \mathbf{p}_{opt} is

$$\mathbf{p}_{\text{opt}} = \underset{\mathbf{p}' \in \text{AG}^M}{\text{argmin}} \|\mathbf{x}\|^2 = \underset{\mathbf{p}' \in \text{AG}^M}{\text{argmin}} \|\mathbf{T}_p(\mathbf{s} + \mathbf{p}')\|^2. \quad (5.5)$$

At the receiver, the modulo operation uses slice partitioning to find and eliminate the perturbation \mathbf{p} , which was added deliberately at the transmitter. Such partitioning is not optimal but its implementation is particularly simple because it only involves several one dimensional modulo operations [26]. Moreover, the performance loss is small, even though we use multiple identical one dimensional modulo operations to replace a single multi-dimensional modulo operation, if the lattice reduction algorithm finds the closest lattice point and forces the received signal constellation to stay inside the Voronoi region. The Gaussian noise after modulo operation is approximately

uniform over $[-A/2, A/2)$ as described in Section 4.4 and in [97] [98].

The above setup shows a general transceiver model for the lattice reduction algorithm based systems. As an example, suppose we have a multi-user system, in which the precoding matrix \mathbf{T}_p consists of a ZF channel precoding matrix \mathbf{H}^{-1} and a block-diagonal matrix \mathbf{W} with each block a unitary precoding matrix for one user's signal vector. The receiver equalizer is configured to be the same as \mathbf{W} ,

$$\mathbf{T}_p = \mathbf{H}^{-1}\mathbf{W} \quad \text{and} \quad \mathbf{R} = \mathbf{W}.$$

Plugging into Equation (5.3), we have

$$\mathbf{r} = \mathbf{W}^H \mathbf{H} \mathbf{H}^{-1} \mathbf{W} (\mathbf{s} + \mathbf{p}) + \mathbf{W}^H \mathbf{n} = \mathbf{s} + \mathbf{p} + \mathbf{n}'. \quad (5.6)$$

Since the receiver equalization is unitary for each user and each antenna, the channel noise remains i.i.d., in contrary to ZF equalization which causes noise enhancement. In other words, $\mathbf{n}' = \mathbf{W}^H \mathbf{n}$ has the same statistics as the original channel noise \mathbf{n} . The received signal after equalization becomes

$$\hat{\mathbf{s}} = \mathbb{Q}_{\text{AG}}(\mathbf{r}) = \mathbf{s} + \mathbb{Q}_{\text{AG}}(\mathbf{n}').$$

In this way the signal estimate for all signals contains the transmitted signal without the deliberately added perturbation vector \mathbf{p} but with the quantization effect on the channel noise.

5.2 MISO Broadcast Channel and the WFH Scheme

In this section we study lattice precoding for multiple input single output (MISO) channels. MISO channels are defined as channels where the transmitter has multiple antennas but each receiver has a single antenna. In this case, for each user $N_k = 1$ and since there is no collaboration possible among users, $\mathbf{W} = \mathbf{I}$.

In [85], Windpassinger, Fischer, and Huber proposed a lattice-reduction based precoding for MISO BC that we refer to it as the WFH scheme. The linear precoding technique used in the WFH scheme is ZF, i.e., $\mathbf{T}_p = \mathbf{H}^{-1}$ with the assumptions that

the number of transmit antennas equals to the number of users in the system, i.e., $M = K$, and that the channel matrix is invertible. The transmitter sends M symbols, each for one user, simultaneously over the M transmit antennas. The system model can be shown as a special case of Equation (5.6) as

$$\hat{\mathbf{s}} = \mathbb{Q}_{\text{AG}}(\mathbf{H}\mathbf{x}) + \mathbb{Q}_{\text{AG}}(\mathbf{n})$$

where

$$\mathbf{x} = \mathbf{H}^{-1}(\mathbf{s} + \mathbf{p}).$$

The transmitted signal is designed such that the transmitted power for each symbol vector is minimized through optimal selection of \mathbf{p}

$$\mathbf{p} = \underset{\mathbf{p}' \in \text{AG}^M}{\text{argmin}} \|\mathbf{H}^{-1}(\mathbf{s} + \mathbf{p}')\|^2. \quad (5.7)$$

Note that, instead of minimizing the average transmitted power, the metric that we commonly use, here we are actually minimizing the transmitted power for each symbol vector combination, resulting in the minimization of the average transmitted power.

In the WFH scheme, shown in Figure 5.1, a lattice-reduction aided algorithm is employed. The optimization problem in Equation (5.7) is equivalent to finding a lattice point \mathbf{p} on the lattice $A\mathbf{H}^{-1}\mathbb{G}^M$ closest to $-\mathbf{H}^{-1}\mathbf{s}$. This is the nearest lattice point search problem and is well-addressed in [99] [83]. The exact solution for this problem is known to be NP-hard. Sphere decoding technique can be used to solve this problem but its complexity is still high for high dimensional cases. Instead, two approximate solutions can be used, both closely related to LR.

Lattice reduction factorizes the precoding lattice basis into a reduced lattice basis \mathbf{W} and a unimodular matrix \mathbf{T}

$$\mathbf{H}^{-1} = \mathbf{W}\mathbf{T}.$$

A lattice can be expressed in terms of many different basis. A unimodular matrix transforms a lattice basis to another without changing the lattice itself. The reduced lattice basis is composed of the shortest basis vectors.

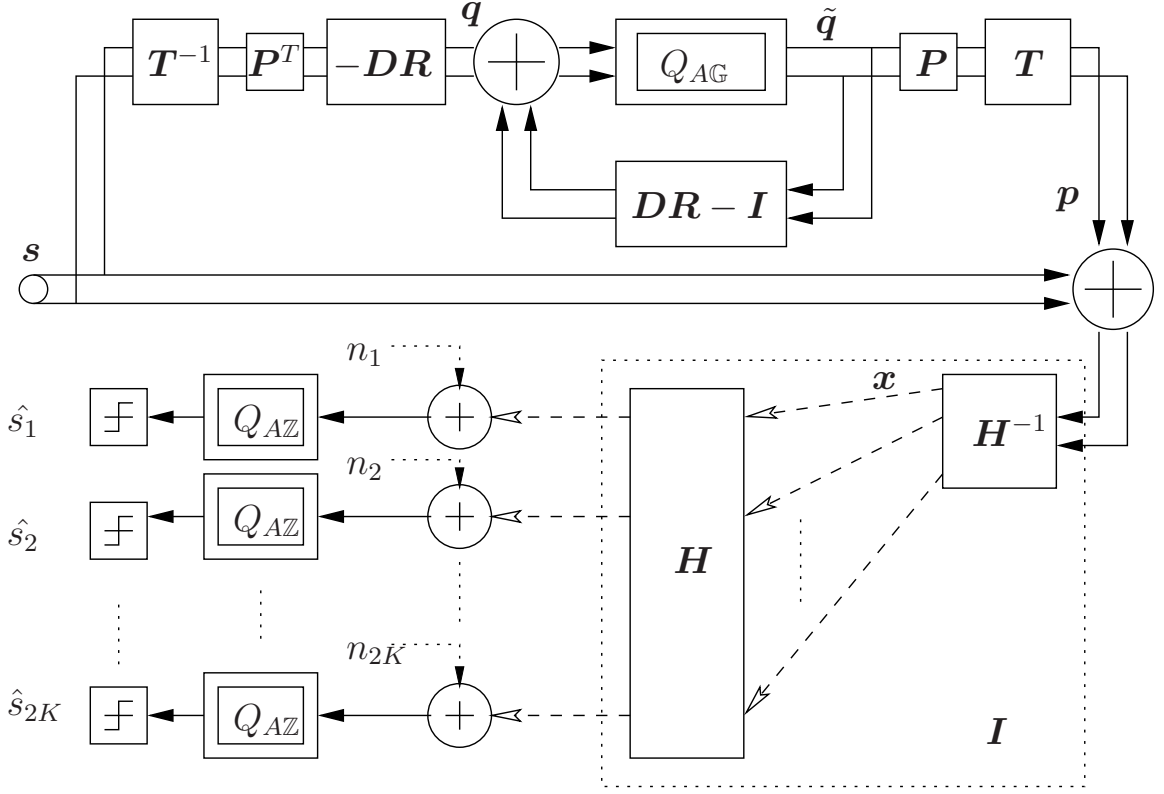


Figure 5.1: The WFH scheme

One approximate solution for the nearest lattice point problem is by rounding off approximation. With the help of the LR algorithm, the problem to find the closest lattice point on the lattice $A\mathbf{H}^{-1}\mathbb{G}^M$ to the point $-\mathbf{H}^{-1}\mathbf{s}$ is transformed to the problem of finding the closest lattice point $\mathbf{W}\mathbf{p}_t$ on the lattice $\mathbf{W}\mathbf{A}\mathbb{G}^M$ to the point $-\mathbf{H}^{-1}\mathbf{s}$. Recall that \mathbf{p}_t is on the same lattice $\mathbf{A}\mathbb{G}^M$ as \mathbf{p} . Now if \mathbf{W} is a scaled orthonormal matrix which rotates and then scales the axis, then taking out it does not change the solution, meaning that finding the point $\mathbf{W}\mathbf{p}_t$ that is closest to $-\mathbf{H}^{-1}\mathbf{s}$ is equivalent to finding the point \mathbf{p}_t on the even Gaussian lattice $\mathbf{A}\mathbb{G}^M$ that is closest to $-\mathbf{T}\mathbf{s}$. This problem can be solved by simply quantizing $-\mathbf{T}\mathbf{s}$ to the closest even Gaussian numbers. However, the reduced lattice basis \mathbf{W} in general is not scaled orthonormal but an approximation of it since \mathbf{W} is the basis of the shortest basis

vector. This approximate solution is shown as

$$\mathbf{p}_{\text{rounding}} = \mathbf{T} \mathbb{Q}_{\text{AG}}(-\mathbf{T}^{-1} \mathbf{s}).$$

Upon finding \mathbf{p}_t by approximation and quantization, it is transformed back to the original lattice point \mathbf{p} .

In order to improve the approximation accuracy and constrain the complexity, nearest plane approximation can be used. To implement this approximation, \mathbf{W} is decomposed using QR decomposition with optimum ordering [100] [20],

$$\mathbf{W}\mathbf{P} = \mathbf{Q}\mathbf{R}$$

where \mathbf{P} is the ordering permutation matrix that exchanges indices of columns in \mathbf{W} . Then the problem becomes of finding the closest lattice point $\mathbf{DRP}^{-1}\mathbf{p}_t$ to the point $-\mathbf{DRP}^{-1}\mathbf{T}^{-1}\mathbf{s}$ where \mathbf{D} is the diagonal matrix whose diagonal elements are reciprocals of the diagonal elements of \mathbf{R} . The reduced lattice basis \mathbf{W} can be regarded as the lattice basis closest to orthogonal basis \mathbf{Q} with an approximation error matrix \mathbf{R} . The approximation error matrix \mathbf{R} is selected to be an upper triangular matrix with positive diagonal elements in increasing order from top to bottom. The block diagram of this algorithm is shown in Figure 5.1. The quantization process starts from the bottom row of \mathbf{R} . The dimensions with longer basis vectors are processed before the dimensions with smaller basis vectors since longer basis vector results in larger correlations to other basis vectors, which are the off-diagonal elements of \mathbf{R} . The small off-diagonal elements result in a better approximation. If these elements are zero, then the reduced lattice basis \mathbf{W} becomes a pure orthonormal basis. This algorithm in principle and in implementation is very similar to SIC and DFE.

The nearest plane approximation is derived explicitly as

$$\begin{aligned} \mathbf{H}^{-1}\mathbf{p} &\mapsto -\mathbf{H}^{-1}\mathbf{s} \\ \Rightarrow \mathbf{W}\mathbf{T}^{-1}\mathbf{p} &\mapsto -\mathbf{W}\mathbf{T}^{-1}\mathbf{s} \\ \Rightarrow \mathbf{W}\mathbf{P}\mathbf{P}^{-1}\mathbf{T}^{-1}\mathbf{p} &\mapsto -\mathbf{W}\mathbf{P}\mathbf{P}^{-1}\mathbf{T}^{-1}\mathbf{s} \end{aligned}$$

where \Rightarrow denotes *is equivalent to* and \mapsto denotes *is closest to*. Substituting $\mathbf{QR} = \mathbf{WP}$,

$$\mathbf{QRP}^{-1}\mathbf{T}^{-1}\mathbf{p} \mapsto -\mathbf{QRP}^{-1}\mathbf{T}^{-1}\mathbf{s}. \quad (5.8)$$

Since we have defined $\mathbf{D} = \text{diag}(\mathbf{R})^{-1}$, by multiplying both sides of Equation 5.8 by \mathbf{DQ}^T we have

$$\mathbf{DRP}^{-1}\mathbf{T}^{-1}\mathbf{p} \mapsto -\mathbf{DRP}^{-1}\mathbf{T}^{-1}\mathbf{s},$$

from which the block diagram in Figure (5.1) is constructed.

5.3 Block-Diagonal ZF and EDLP

In Section 4.3 we discussed a rewarding lattice precoding technique for multiple input single output broadcast channels, i.e., the multi-user channels in which each user uses one single receive antenna and carries a single and independent data stream. In scenarios where users have multiple antennas, we are naturally interested in techniques that can benefit from the availability of extra antennas.

One straightforward method is to simply apply the techniques introduced in Section 4.3 or [80] by treating each antenna as an independent user. In this way the receiver only needs to have multiple paths from single antenna RF radio to baseband processing DSP to decode each data stream from each antenna. Clearly this treatment ignores the fact that the multiple receivers, belonging to a single user, are able to cooperate with each other. By utilizing the potential coordination among multiple receivers we may improve the robustness and/or data throughput, similar to the gain obtained by using MIMO channels. However, techniques applying lattice-reduction based precoding for this kind of multi-user multiple antenna broadcast channels are still under development. The difficulty lies in the required mathematical tools to deal with this channel into lattice domain and the high complexity of the resulting techniques [18].

In this section, instead of minimizing the transmitted power versus error rate with spatial multiplexing, we focus on developing a low-complexity and scalable lattice precoding scheme that supports full spatial multiplexing and full receiver diversity order

for every user with a reasonable complexity-performance tradeoff. This scheme utilizes EDLP, discussed in Chapter 4, as an inner precoding method and block-diagonal zero-forcing (BDZF) technique, discussed in Section 2.4 as an outer precoding method to orthogonalize each users' channels. Therefore, this method can also be viewed as a multi-user extension of EDLP precoding or a non-linear modification of BDZF precoding. It is known that the BDZF has advantages over channel inversion techniques in that it makes less noise feeding into the receivers [51]. This is because the noise enhancement effect in BDZF only exists within each block. On the downside, this method requires either global CSI at the transmitter and all the receivers, or an additional training phase for estimating their equivalent channels. As we already know, the EDLP algorithm requires CSI at the receiver, hence, the combination of BDZF and EDLP adds no additional complexity at the receiver since a training is needed anyway. Furthermore, by using EDLP, the receive equalization is unitary, which does not enhance the channel noise. Detailed presentation of this method is discussed below.

Similar to the notation we used in previous chapters, we have N_t transmit antennas shared by K active users. The number of receive antennas for each active user is denoted by $N_{r,k}$. The channel matrix for user k is denoted by the $N_{r,k} \times N_t$ matrix \mathbf{H}_k . The multi-user channel matrix can be expressed by

$$\mathbf{H} = \begin{bmatrix} \mathbf{H}_1 \\ \mathbf{H}_2 \\ \vdots \\ \mathbf{H}_K \end{bmatrix}$$

which is a $N_r \times N_t$ matrix where

$$N_r = \sum_{k=1}^K N_{r,k}.$$

Using BDZF, we are able to orthogonalize the multi-user channel with a penalty

of increased transmitted power. In order to do so, we define the null channel $\tilde{\mathbf{H}}_k$ by

$$\bar{\mathbf{H}}_k = \begin{bmatrix} \mathbf{H}_1 \\ \vdots \\ \mathbf{H}_{k-1} \\ \mathbf{H}_{k+1} \\ \vdots \\ \mathbf{H}_K \end{bmatrix}.$$

For $1 \leq k \leq K$, the null channel $\bar{\mathbf{H}}_k$ is decomposed by SVD into $\bar{\mathbf{H}}_k = \bar{\mathbf{U}}_k \bar{\mathbf{D}}_k \bar{\mathbf{V}}_k^\dagger$. Since $\bar{\mathbf{H}}_k$ is an $(N_r - N_{r,k}) \times N_t$ matrix, the matrix $\bar{\mathbf{D}}_k$ is an $(N_r - N_{r,k}) \times N_t$ diagonal matrix with positive singular values on the diagonal in descending order. Matrix $\bar{\mathbf{V}}_k$ is an N_t dimensional square matrix the rightmost $N_{r,k}$ column vectors of which define the null space of $\bar{\mathbf{H}}_k$, i.e., the null space of all other user channels $\mathbf{H}_1, \dots, \mathbf{H}_{k-1}, \mathbf{H}_{k+1}, \mathbf{H}_K$. Therefore, BDZF uses the null space vectors to nullify the interuser interference. Let $\mathbf{T}_{k,null}$ be the rightmost $N_{r,k}$ column vectors of $\bar{\mathbf{V}}_k$ that has dimension $N_t \times N_{r,k}$. BDZF precodes the multi-user channel \mathbf{H} using \mathbf{T}_{null} , defined by

$$\mathbf{T}_{null} = [\mathbf{T}_{1,null}, \mathbf{T}_{2,null}, \dots, \mathbf{T}_{K,null}].$$

The result of precoding by \mathbf{T}_{null} is

$$\begin{aligned} \tilde{\mathbf{H}} = \mathbf{H}\mathbf{T}_{null} &= \begin{bmatrix} \mathbf{H}_1 \\ \mathbf{H}_2 \\ \vdots \\ \mathbf{H}_K \end{bmatrix} [\mathbf{T}_{1,null}, \mathbf{T}_{2,null}, \dots, \mathbf{T}_{K,null}] \\ &= \begin{bmatrix} \mathbf{H}_1 \mathbf{T}_{1,null} & \mathbf{0} & \dots & \mathbf{0} \\ \mathbf{0} & \mathbf{H}_2 \mathbf{T}_{2,null} & \dots & \mathbf{0} \\ \vdots & \vdots & \ddots & \vdots \\ \mathbf{0} & \mathbf{0} & \dots & \mathbf{H}_K \mathbf{T}_{K,null} \end{bmatrix}. \end{aligned}$$

Now if we define $\tilde{\mathbf{H}}_k = \mathbf{H}_k \mathbf{T}_{k,null}$ as the effective transmission channel of user k , we observe that user k is free of multi-user interference under the effective channel since

the interference is nullified by $\mathbf{T}_{k,null}$. This is true for all users.

After the multi-user MIMO broadcast channel is successfully made block-wise parallel through previously defined effective channels, we are able to apply EDLP as an inner precoding scheme. In order to do so, instead of the real channel of user k , expressed by

$$\mathbf{y}_k = \mathbf{H}_k \mathbf{T}_k \mathbf{x}_k + \mathbf{H}_k \left(\sum_{i \neq k} \mathbf{T}_i \mathbf{x}_i \right) + \mathbf{n}_k,$$

we consider the effective channel and eliminate the multi-user interference when BDZF is used,

$$\mathbf{y}_k = \mathbf{H}_k \mathbf{T}_k \mathbf{x}_k + \mathbf{n}_k = \tilde{\mathbf{H}}_k \mathbf{x}_k + \mathbf{n}_k. \quad (5.9)$$

We employ the SVD of the effective channel $\tilde{\mathbf{H}}_k = \tilde{\mathbf{U}}_k \tilde{\mathbf{D}}_k \tilde{\mathbf{V}}_k^\dagger$ and let

$$\mathbf{x}_k = \tau_k \tilde{\mathbf{H}}_k^{-1} \tilde{\mathbf{U}}_k \mathbf{B}_k (\mathbf{s}_k + \mathbf{p}_k), \quad (5.10)$$

where τ_k is the power scale of user k , and $\tilde{\mathbf{H}}_k^{-1}$ is the inverse or pseudo-inverse of the channel matrix. We also define the equalization matrix at the receiver side of user k as $\mathbf{R}_k = \tilde{\mathbf{U}}_k \mathbf{B}_k$ and the effective channel model with transmit precoding and receive equalization as

$$\begin{aligned} \mathbf{r}_k &= \mathbf{R}_k^\dagger \mathbf{y}_k \\ &= \mathbf{B}_k^\dagger \tilde{\mathbf{U}}_k^\dagger \tilde{\mathbf{H}}_k \mathbf{x}_k + \mathbf{B}_k^\dagger \tilde{\mathbf{U}}_k^\dagger \mathbf{n}_k \\ &= \tau_k (\mathbf{s}_k + \mathbf{p}_k) + \mathbf{n}'_k \end{aligned}$$

where \mathbf{n}'_k is the unitary transformed noise that has the same statistical characters as the original channel noise. In another words, the transformed noise is still circular-symmetric white Gaussian noise. We can write a unified equation to express this multi-user channel as

$$\mathbf{r} = \mathbf{R}^\dagger \mathbf{H} \mathbf{x} + \mathbf{n}'$$

where \mathbf{R} is defined by Equation (5.4),

$$\mathbf{x} = \begin{bmatrix} \mathbf{x}_1 \\ \vdots \\ \mathbf{x}_K \end{bmatrix},$$

and

$$\mathbf{n}' = \begin{bmatrix} \mathbf{n}'_1 \\ \vdots \\ \mathbf{n}'_K \end{bmatrix}.$$

The symbol decision statistic $\hat{\mathbf{s}}_k$ is the output of the per-component complex modulo and stays inside the Voronoi decision region,

$$\hat{\mathbf{s}}_k = \mathbb{Q}_{AG^L} \left(\frac{\mathbf{r}_k}{\tau_k} \right) = \mathbf{s}_k + \mathbb{Q}_{AG^L}(\mathbf{n}''_k)$$

where L_k is the spatial multiplexing order of user k . In order to apply EDLP technique with the provided algorithm to calculate the perturbation vector introduced in previous chapter, we limit the number of simultaneous data stream of every user to be $L_k = L = 2$, for all $1 \leq k \leq K$ and a common modulation scheme to be 4-QAM. Therefore, the number of transmit and receive antennas can be any number larger than 2.

The noise part that the symbol estimate experiences, as discussed before, is circular symmetric complex Gaussian before the modulo operation. If the interval A in the one-dimensional modulo operation is fixed, it can be easily seen that if the per dimension power $\sigma^2/2N_k$ of the circular symmetric complex Gaussian noise \mathbf{n} is much smaller, i.e.,

$$\frac{\sigma^2}{2N_k} \ll A,$$

the effect of this one-dimensional modulo operation is negligible. Meaning that the noise distribution remains approximately Gaussian. In other words, since the signal power is proportional to the area of the Voronoi region, which is characterized by A , when signal power goes to infinity, the noise that the symbol estimate sees, $\mathbb{Q}_{AG^L}(\mathbf{n}''_k)$, remains circular symmetric complex Gaussian distribution.

5.4 Block-Diagonalization ZF and LR

After studying BDZF for multi-user broadcast channels with multiple transmit and multiple receive antennas and lattice-reduction based single user MIMO channels, it is natural to explore the possibility of combining these two techniques. The technique proposed in [96] is one of them that simply uses BDZF to orthogonalize the user channels in blocks, as the same as BDZF-EDLP, and uses lattice-reduction based algorithms to reduce the transmitted signal power. It also combines the advantages and the disadvantages of both techniques combined.

The channel block-diagonalization part is exactly the same as BDZF-EDLP, i.e., as in Equation 5.9. Each user has an effective channel parallel with the channels of all other users. The inner precoding uses lattice-reduction, as proposed in [17] and [85], i.e.,

$$\mathbf{x}_k = \tau_k \tilde{\mathbf{H}}_k^{-1}(\mathbf{s}_k + \mathbf{p}_k), \quad (5.11)$$

where

$$\mathbf{p}_k = \operatorname{argmin}_{\mathbf{p}'_k \in AG^M} \|\tilde{\mathbf{H}}_k^{-1}(\mathbf{s}_k + \mathbf{p}'_k)\|^2.$$

If we compare Equation 5.11 with Equation 5.10, we can see that they differ in the unitary precoding $\mathbf{U}_k \mathbf{B}_k$ part. This part gives EDLP a power gain in the single user case and requires a coordination of the receiver and the transmitter, which indicates that besides the initial phase of channel estimation, the receiver needs to run estimation again to acquire the transmitter's precoded channel information. The lattice-reduction based precoding algorithm, however, does not have this latency. Note that since the initial channel estimation is always needed, the hardware cost is still the same for the two techniques.

5.5 Comparative Analysis

The three techniques we have introduced in previous sections, the WFH zero-forcing scheme for MISO channels, block-diagonalization zero-forcing with eigenvalue decomposition based lattice precoding (BDZF-EDLP), and block-diagonalization zero-forcing with lattice-reduction based precoding (BDZF-LR) differ in many aspects.

The WFH scheme is designed for multi-user multiple antenna MISO channels but can be employed in multi-user multiple antenna MIMO broadcast channels. BDZF-EDLP and BDZF-LR are both designed for multi-user multiple antenna MIMO broadcast channels. All these precoding-equalization algorithms need channel side information at the transmitter (CSIT). If no reverse pilot channels are assumed, the transmitter requires CSI feedbacks from the receivers. So all receivers have to estimate the channel in this case. In addition, at every receiver there is a modulo operation to compensate for the lattice precoding at the transmitter.

In terms of transmitter precoding complexity, the WFH scheme uses channel inversion while BDZF-EDLP and BDZF-LR use SVD as the front-end. Numerical computations of channel inversion and channel SVD require $\mathcal{O}(n^3)$ for an n -dimensional square matrix [88]. The WFH scheme uses nearest-plane approximation, also known as the LLL lattice reduction algorithm, to compute the perturbation vector jointly for all data streams, which allows this scheme to approach near optimal diversity performance. BDZF-EDLP and BDZF-LR compute the perturbation vectors for each individual user's block channel. Thus, these computations can be performed in parallel. If we denote the ratio of the largest norm to the smallest norm in the channel matrix (column vectors) by R_{norm} , i.e., the ratio of the norm of the longest vector to that of the shortest vector, the complexity of computing the LLL lattice reduction is $\mathcal{O}(n^4 \log R_{norm})$ [86]. This R_{norm} depends on channel realizations and distributions. Since $R_{norm} \geq 1$, the lattice reduction part dominates the overall complexity.

In order to have a more intuitive sense about the complexity of lattice reduction algorithms of these three schemes, let us assume a system with $N_t = 8$ transmit antennas and $K = 4$ users each has $N_{r,k} = 2$, for $1 \leq k \leq 4$ receive antennas, as an example. This broadcast channel has an 8-dimensional complex square channel matrix. Following the assumption in Section 4.4, i.e., 2 flops per complex addition and 6 flops per complex multiplication, the average complexity for the real and complex LLL lattice reduction algorithms in terms of flops are 34823.71 and 19201.68, respectively [86]. It is also important to notice that in the WFH scheme the same number of operations are needed for each symbol vector that is fed into the precoder. However, only 428 flops on the average are necessary for BDZF-EDLP precoding in 'frame overhead' phase and exactly 112 flops are necessary 'per channel use' phase.

Table 5.1: Average flops of lattice precoding for MIMO broadcast channels

	frame overhead		per channel use	
	Tx (K=6)	Rx (K=6)	Tx (K=6)	Rx (K=6)
WFH	0	0	62544	0
BDZF-EDLP	642	0	168	168
BDZF-LR	0	0	1806	0
	Tx (K=8)	Rx (K=8)	Tx (K=8)	Rx (K=8)
WFH	0	0	142524	0
BDZF-EDLP	856	0	224	224
BDZF-LR	0	0	2408	0

Therefore, using BDZF-EDLP saves 98% flops in numerical computation in ‘frame overhead’ phase and 99.4% in ‘per channel use’ phase in this example, if the complex LLL algorithm is used for this comparison. A brief list of number of flops required for precoding computation with different channel dimensions is depicted in Table 5.1. Since the effort of the modulo operations can be neglected compared to the number of flops, it is not included in in this table. Another part of the computation process that is not included is the linear precoding part, for example the channel inversion in the WFH scheme and SVD in BDZF-EDLP and BDZF-LR. We observe that the WFH scheme features a heavy average computational load for each channel use in terms of flops. Such load increases exponentially with the dimension of the channel precoding matrix. Instead, the complexities of BDZF based techniques in lattice reduction part grow linearly. Other than the average computational complexity, the number of flops for the methods using lattice reduction algorithms, i.e., the WFH scheme and BDZF-LR, vary with different realizations of the channel matrices. This gives the symbol vector scheduler much uncertainty and causes extra latency.

Furthermore, we notice that the lattice precoding parts in BDZF-EDLP and BDZF-LR consist of a group of independent computations, each of which is the same function supplied with different inputs. For example, in the BDZF-LR algorithm we have K different effective channel matrices passed into the same lattice reduction algorithm. Therefore, for systems that can handle parallel computing, using

BDZF-EDLP or BDZF-LR reduces the latency by a factor of $1/K$.

The bit error rate versus transmitted power performance is also critical for system evaluation. The WFH scheme performs a joint optimization over signals of all users, therefore it achieves close to maximum diversity gain, i.e., diversity order equals to N_t . The diversity orders that BDZF based algorithms can achieve are limited by the BDZF linear precoding. Therefore, they can only achieve the maximum diversity gains of each effective block channel. Similar to the EDLP versus LR, BDZF-EDLP has an additional power gain over BDZF-LR due to the coordinated transmission. The performance comparison of these three algorithms is depicted in Figure 5.2. This figure show the uncoded BER as a function of transmitted power in a system

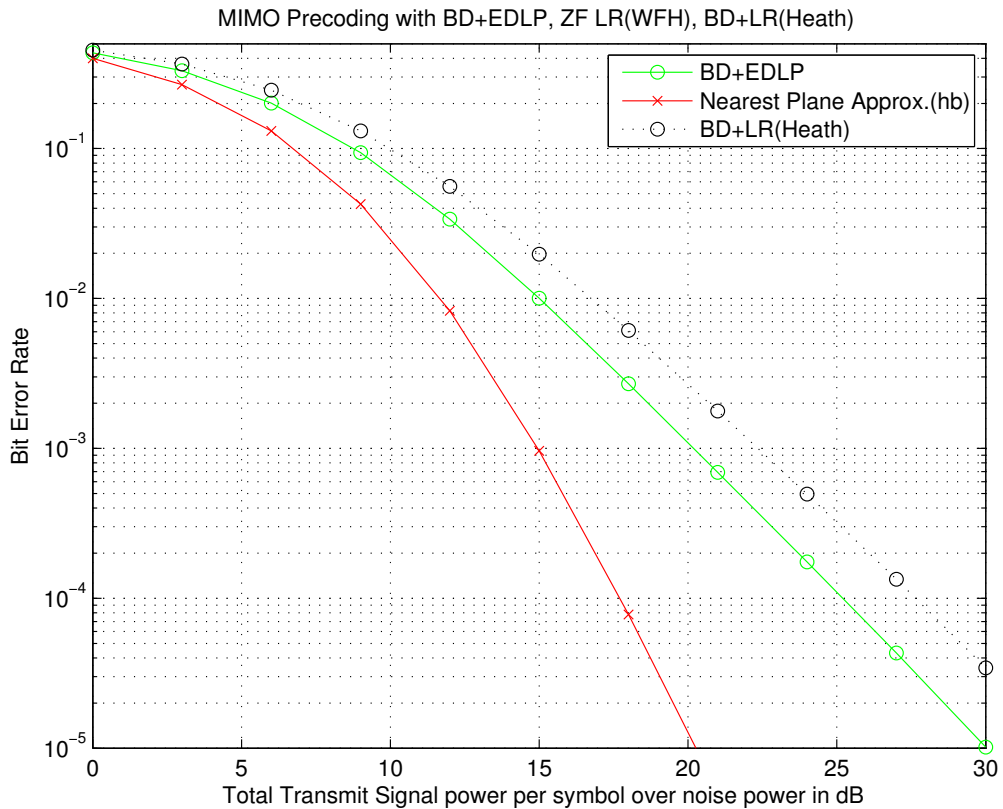


Figure 5.2: BER vs Tx-power performance comparison of the WFH Scheme, BDZF-EDLP and BDZF-LR

with 4 transmit antennas, 2 users each has 2 receive antennas that employs 4-QAM

modulation. From this figure the WFH scheme approaches full diversity gain of order 4. BDZF-EDLP and BDZF-LR achieve a diversity order of 2 but with much lower complexity. A power gain of BDZF-EDLP over BDZF-LR is also shown in the figure which is due to coordinated precoding and quantization in BDZF-EDLP.

5.6 Conclusions

In this chapter, we discussed nonlinear lattice based precoding/equalization techniques for MIMO broadcast channels that support multiple stream transmissions, i.e., the WFH scheme and BDZF-LR from the literature and our proposed BDZF-EDLP technique. All these three techniques have a linear precoding front end and a nonlinear lattice based precoding as a back end. They all require CSIT, in addition, BDZF-EDLP needs another training phase at the receivers to estimate the effective channels that the transmitter precoded.

The WFH scheme employs the LLL lattice reduction algorithm on the channel inverse directly and computes the perturbation vector based on each symbol vector input and the channel matrices. Computing the perturbation vector is basically solving the search for the closest lattice point problem. In implementation, the WFH scheme uses a nearest plane approximation method to solve this problem sub-optimally. This precoding method jointly compute the perturbation vector for all user signals. Therefore, a close to full diversity order performance is expected and is achieved.

BDZF-EDLP and BDZF-LR, however, use linear BDZF precoding to completely nullify the interuser interference. This suboptimal linear precoding results in a lower than optimal diversity order.

Since the WFH scheme needs to compute the precoding based on each symbol vector input and channel matrix realization, the complexity and latency overhead is massive and has large variation and therefore may not be possible for certain implementations. In BDZF-EDLP and BDZF-LR, the creation of effective user channels allows successive algorithms to do precoding for each user independently. By doing so, complexity and latency can be contained. Different level of quality of service (QoS) differentiating users can be possible, for example, giving higher power scale to users requesting higher QoS. In addition, the proposed BDZF-EDLP technique has

a fixed number of operations in the lattice precoding part, which saves latency furthermore against the WFH scheme and the BDZF-LR. Also, due to the coordinated precoding/equalization, BDZF-EDLP shows a power gain advantage over BDZF-LR. Similar to the EDLP, BDZF-EDLP does not really need the lattice reduction algorithm to compute the perturbation vector. Therefore, there is a complexity advantage of BDZF-EDLP over BDZF-LR too.

These three techniques each have a particular complexity and performance trade-off. In different applications and scenarios, the choice on the techniques should be based on these tradeoffs.

Chapter 6

Advanced Equalization Techniques for CDMA Receivers

In this chapter, we will first review the theoretical basis and discuss some implementation issues of advanced equalization techniques for spread spectrum systems in frequency-selective fading channels. Generalized RAKE (G-RAKE) and Linear Minimum Mean Square Error (LMMSE) are two widely used techniques which are employed in Wideband Code Division Multiple Access (WCDMA) / High-Speed Downlink Packet Access (HSDPA) systems. These techniques, when used in multiple antenna systems, can serve as the front end, followed by spatial equalization, in the baseband receiver structure [101], [102]. We will show the equivalence between G-RAKE and LMMSE Chip-level Equalization (CE) under various system implementation constraints. Finger placement algorithm is a key factor in implementation and greatly affects the performance of G-RAKE. Optimal solution for finger placement is prohibitively complex even for small number of fingers since the symbol Signal to Interference and Noise Ratio (SINR) is not a convex function of the finger delays. We will propose a novel and computationally efficient finger placement algorithm that significantly reduces the complexity of the optimal solution with a reasonable performance loss. We call this algorithm the maximum weight placement (MWP) algorithm for reasons that will become clear later. We then compare the performance and complexity trade off of this algorithm with other algorithms through analysis and by providing simulation results.

6.1 Introduction

In WCDMA systems each downlink physical channel characterizes a spreading code that is composed of an OVSF (Orthogonal Variable Spreading Factor) code and a long scrambling code after channel encoding and symbol modulation [103]. OVSF codes are assigned by base station controllers and are designed to differentiate other synchronous channels within the same cell based on the orthogonality of the OVSF codes. The OVSF code of each channel remains the same from symbol to symbol. The scrambling codes are assigned by the base station controller and are designed to differentiate neighboring cells. Therefore, these codes are the same to all downlink physical channels within one cell when secondary scrambling code is not used. The period of the scrambling code is a very large multiple of the symbol time hence the scrambling code varies from symbol to symbol pseudo-randomly. Therefore, in flat-fading channels the intra-cell interference is eliminated by the OVSF codes and the inter-cell interference is reduced by the scrambling code.

In frequency-selective fading channels RAKE receivers with Maximal Ratio Combining (MRC) are commonly used to combat multipath effects of the channel. The receiver takes advantage of the frequency-selectivity of the channel, coherently combines the outputs of the fingers (correlators) to exploit the multipath diversity gain. In this way, the signal power attenuation problem caused by fading effects is mitigated. The multipath effects of the frequency-selective channel also breaks the orthogonality of the downlink physical channels, thus resulting in Multiple Access Interference (MAI). Meanwhile, the correlations among consecutive symbols of one physical channel result in Inter-Symbol Interference (ISI). RAKE receivers are not, however, designed to suppress these types of interferences, i.e., MAI and ISI.

HSDPA is a protocol in 3GPP that promises high speed data transmission in downlink channels, in the order of megabit per second. The spreading factor defined in HSDPA channels ($SF = 16$) is much smaller than many other WCDMA channels, i.e., 128 or 256. In this case, using a small spreading factor results in the MAI and ISI to cause more performance degradation, especially when the wireless channel has large delay spread.

G-RAKE [104] and LMMSE-CE [61] are two major equalization techniques that

are proposed for HSDPA receivers. G-RAKE is similar to RAKE in structure but is derived based on the Maximum Likelihood (ML) criteria so that the interferences can be mitigated. G-RAKE differs from RAKE mainly in the number of fingers, locations of the fingers, and the computation of the combining weight. G-RAKE requires larger number of fingers to better probe the channel and computes the combining weights by a method other than MRC to suppress the interference. G-RAKE employs the ML principle and can also be interpreted as a pre-whitening matched filter. An analysis of G-RAKE is presented extensively in Section 6.2 with focuses on equalization properties, noise whitening effects and the resulting output symbol SINR. It is shown that under certain simplifying assumptions together with a linear transversal Finite Impulse Response (FIR) structure, LMMSE-CE, which is based on the LMMSE criteria is equivalent to G-RAKE [105] in terms of combining weights, assuming that both systems employ the same finger placement strategy. We develop this equivalence in this chapter while relaxing the constraints gradually. Our analysis in Section 6.5 reveals that this equivalence holds in a wider scope. With limited number of fingers, the performance of a G-RAKE receiver varies significantly by selection of finger delays. Optimal solutions to this problem can be obtained through exhaustive search where the dimension of the search space is equal to the number of fingers and for each dimension the search window spans more than one symbol. This method is hard to implement due to its high complexity. We propose a low complexity alternative by modifying this multi-dimensional exhaustive search problem into multiple one-dimensional search problems. Another practical algorithm which merely utilizes the channel path delays is also introduced. Both these algorithms have reduced complexity at the price of some performance loss.

Later we derive a novel efficient finger placement algorithm called the Maximum Weight Placement (MWP) algorithm and show that it provides a good balance between performance and complexity. Supporting simulation results are also presented.

6.2 The Generalized RAKE Receiver

In WCDMA the pulse-shaping filter, denoted by $p(t)$, is a root-raised cosine (RRC) filter with a roll-off factor of $\alpha = 0.22$

$$p(t) = \frac{\sin(\pi t/T_c(1 - \alpha)) + 4\alpha t/T_c \cos(\pi t/T_c(1 + \alpha))}{\pi t/T_c(1 - (4\alpha t/T_c)^2)}$$

where $T_c = 1/\text{ChipRate}$ with fixed chip rate 3.84 Mcps. The autocorrelation function (ACF) of the chip pulse-shaping filter is a raised cosine function given by

$$R_p(t) = \int_{-\infty}^{\infty} p(t + \tau)p(\tau)d\tau = \frac{\sin(\pi t/T_c) \cos(\pi \alpha t/T_c)}{\pi t/T_c(1 - 4\alpha^2 t^2/T_c^2)}. \quad (6.1)$$

We assume that the spreading factor is N , with $N = 16$ in HSDPA and the total number of active users in the cell is K . The user-symbol-dependent complex spreading sequence is $\{c_{k,i}(j)\}_{j=0}^{N-1}$ for user k 's symbol i , which is the element-wise multiplication of the user's OVSF code and the scrambling code of the cell. The elements of this sequence take values of $(\pm 1 \pm j)/2$. The OVSF codes are mutually orthogonal and scrambling codes are pseudo-random. The spreading waveform is denoted by

$$a_{k,i}(t) = \frac{1}{\sqrt{N}} \sum_{j=0}^{N-1} c_{k,i}(j)p(t - jT_c).$$

The energy of each spreading waveform per symbol is normalized to unity

$$\int_{-\infty}^{\infty} |a_{k,i}(t)|^2 dt = 1, \quad 0 \leq k \leq K - 1 \text{ and } i \in \mathbb{Z}.$$

The symbol energy for user k is PSK modulation and denoted by E_k . Each user's complex data symbol is denoted by $s_k(i)$, whose amplitude is normalized to be one. The symbol period is given by $T_s = NT_c$. The transmitted signal for user k can be

expressed as

$$\begin{aligned} x_k(t) &= \sqrt{E_k} \sum_{i=-\infty}^{\infty} s_k(i) a_{k,i}(t - iT_s) \\ &= \sqrt{E_k} \sum_{i=-\infty}^{\infty} s_k(i) \frac{1}{\sqrt{N}} \sum_{j=0}^{N-1} c_{k,i}(j) p(t - jT_c - iT_s). \end{aligned}$$

The baseband equivalent transmitted signal $x(t)$ is the sum of the signals for all users $x(t) = \sum_{k=0}^{K-1} x_k(t)$.

The baseband equivalent impulse response of the multipath channel is modeled as

$$g(\tau) = \sum_{l=0}^{L-1} g_l \delta(\tau - \tau_l),$$

where L is the number of significant paths, g_l is the complex path gain and τ_l is the path delay for the l th path.

The noise process $n(t)$ models the inter-cell interference plus thermal noise. Such noise process is assumed to be Gaussian with one-sided power spectral density N_0 .

We consider the 0th symbol of user 0. The received signal at the receiver of user 0 is

$$\begin{aligned} r(t) &= \sum_{k=0}^{K-1} \sum_{l=0}^{L-1} g_l x_k(t - \tau_l) + n(t) \\ &= \sum_{k=0}^{K-1} \sqrt{E_k} \sum_{l=0}^{L-1} g_l \sum_{i=-\infty}^{\infty} s_k(i) a_{k,i}(t - \tau_l - iT_s) + n(t). \end{aligned}$$

Similar to a RAKE receiver, G-RAKE samples the received signal at different times at the output of the matched filter. For the 0th symbol of user 0, the output at time t can be expressed as

$$\begin{aligned} y(t) &= \int_{-\infty}^{\infty} r(\tau) a_{0,0}^*(\tau - t) d\tau \\ &= \sum_{k=0}^{K-1} \sum_{l=0}^{L-1} \sum_{i=-\infty}^{\infty} \sqrt{E_k} g_l s_k(i) R_{k,i}(t - iT_s - \tau_l) + \tilde{n}(t), \end{aligned}$$

where

$$\begin{aligned} R_{k,i}(t) &= \int_{-\infty}^{\infty} a_{k,i}(t+\tau)a_{0,0}^*(\tau)d\tau \\ &= \int_{-\infty}^{\infty} \frac{1}{N} \sum_{l=0}^{N-1} c_{k,i}(l)p(t+\tau-lT_c) \sum_{m=0}^{N-1} c_{0,0}^*(m)p^*(\tau-mT_c)d\tau \end{aligned}$$

is the cross-correlation function (CCF) of the spreading waveforms of the k th user's i th symbol and 0th user's 0th symbol. Defining $\tau' = \tau - mT_c$ and $q = m - l$,

$$R_{k,i}(t) = \frac{1}{N} \sum_{l=0}^{N-1} \sum_{l+q=0}^{N-1} c_{k,i}(l)c_{0,0}^*(l+q)R_p(t+qT_c) \quad (6.2)$$

$$= \sum_{q=0}^{N-1} \sum_{l=0}^{N-1-q} c_{k,i}(l)c_{0,0}^*(l+q)R_p(t+qT_c) \quad (6.3)$$

$$+ \sum_{q=1-N}^{-1} \sum_{l=0}^{N-1+q} c_{k,i}(l-q)c_{0,0}^*(l)R_p(t+qT_c). \quad (6.4)$$

The sampling output is the product of a number of discrete-time signals and a single continuous-time correlation function, i.e., the ACF of RRC. Such RRC ACF function can be computed by the analytical form given in Equation (6.1). To further simplify the CCF between the spreading waveforms, we express it as [104]

$$C_{k,i}(m) \triangleq \begin{cases} \sum_{n=0}^{N-1-m} c_{k,i}(n)c_{0,0}^*(n+m), & 0 \leq m \leq N-1 \\ \sum_{n=0}^{N-1+m} c_{k,i}(n-m)c_{0,0}^*(n), & 1-N \leq m < 0 \end{cases}$$

The spreading sequence CCF allows us to capture the cross-correlation of two spreading sequences with time shifts and to simplify Equation (6.4) to

$$R_{k,i}(t) = \frac{1}{N} \sum_{m=1-N}^{N-1} C_{k,i}(m)R_p(t+mT_c).$$

Based on the assumptions that the scrambling codes are random and the channelization codes are orthogonal, we have [104]

$$C_{k,0}(0) = 0, k \neq 0 \quad (6.5)$$

$$C_{0,0}(0) = N \quad (6.6)$$

$$\mathbb{E}[C_{k,i}(m)C_{k,i}^*(n)] = 0, m \neq n \quad (6.7)$$

$$\mathbb{E}[|C_{k,i}(m)|^2] = \begin{cases} 0, & i = m = 0, k \neq 0 \\ N^2, & i = m = k = 0 \\ N - |m|, & \text{otherwise} \end{cases} \quad (6.8)$$

The noise process is assumed to be Gaussian and independent of the signal and the intra-cell interference. The noise at the matched filter output is

$$\tilde{n}(t) = \int_{-\infty}^{\infty} n(\tau) a_{0,0}^*(\tau - t) d\tau.$$

The ACF of this noise can be expressed as

$$\begin{aligned} R_{\tilde{n}}(t_1 - t_2) &= \mathbb{E}[\tilde{n}(t_1)\tilde{n}^*(t_2)] \\ &= \mathbb{E} \left[\int_{-\infty}^{\infty} n(\tau_1) a_{0,0}^*(\tau_1 - t_1) d\tau_1 \int_{-\infty}^{\infty} n^*(\tau_2) a_{0,0}(\tau_2 - t_2) d\tau_2 \right]. \end{aligned}$$

Noise is assumed to be independent of the spreading sequences. We define the normalized noise $n'(t) = N_0^{-1/2}\tilde{n}(t)$, then the ACF of $n'(t)$ is

$$R_{n'}(t_1 - t_2) = \frac{1}{N} \sum_{m=1-N}^{N-1} C_{0,0}(m) R_p(t_1 - t_2 + mT_c). \quad (6.9)$$

This ACF depends on the spreading waveform. This is not preferred since the number

of spreading waveforms is large. Therefore, we approximate it by

$$\begin{aligned} R_{n'}(t_1 - t_2) &= \frac{1}{N} \sum_{m=1-N}^{N-1} \mathbb{E}[C_{0,0}(m)R_p(t_1 - t_2 + mT_c)] \\ &= \frac{1}{N} \sum_{m=1-N}^{N-1} N\delta(m)R_p(t_1 - t_2 + mT_c) \\ &= R_p(t_1 - t_2) \end{aligned}$$

where the expectation is with respect to the realizations of the spreading sequences.

The symbol energy of user k and the total base station energy per symbol are denoted by E_k and E_s , respectively. The sampled signal is expressed as

$$y(t) = \sqrt{E_0}y_d(t)s_0(0) + \sqrt{E_s}y_{II}(t) + \sqrt{N_0}n'(t)$$

where the signal part is expressed as

$$y_d(t) = \sum_{l=0}^{L-1} g_l R_p(t - \tau_l).$$

The intra-cell interference term, which is the sum of the inter-path interference, the inter-symbol interference and the inter-user interference, is denoted by $y_{II}(t)$.

With J matched filter fingers configured in the receiver with decimation performed at different delays $\{d_0, d_1, \dots, d_{J-1}\}$, the J output signals are expressed in a vector form by $\mathbf{y} = [y(d_0), y(d_1), \dots, y(d_{J-1})]^T$, then

$$\mathbf{y} = \sqrt{E_0}\mathbf{y}_d s_0(0) + \sqrt{E_s}\mathbf{y}_{II} + \sqrt{N_0}\mathbf{n}' \quad (6.10)$$

where \mathbf{y}_d , \mathbf{y}_{II} and \mathbf{n}' are defined similarly. For the sake of conciseness, the functional dependence on t is eliminated.

A linear detector can be expressed as $z = \mathbf{w}^H \mathbf{y}$, where z is the decision statistic and \mathbf{w} is the weight vector characterizing the receive filter. The finger output vector can be written as $\mathbf{y} = \mathbf{h}s_0(0) + \mathbf{u}$, where $\mathbf{h} = \sqrt{E_0}\mathbf{y}_d$ and $\mathbf{u} = \sqrt{E_s}\mathbf{y}_{II} + \sqrt{N_0}\mathbf{n}'$ which are assumed to be jointly Gaussian, then the maximum likelihood detector

for $s_0(0)$ given the observation \mathbf{y} depends only on the statistic z with weight vector $\mathbf{w} = \mathbf{R}_u^{-1}\mathbf{h}$. Here \mathbf{R}_u is the ACF of the intra-cell interference plus noise. Thus, the decision statistic becomes

$$z = \mathbf{w}^H \mathbf{y} = \mathbf{h}^H \mathbf{R}_u^{-1} (\mathbf{h}s_0(0) + \mathbf{u}). \quad (6.11)$$

The fact that GRAKE is an optimal maximum-likelihood detector is explicitly shown below. The conditional mean of the received signal random variable is

$$\mathbb{E}[\mathbf{y}|s_0(0)] = \mathbf{h}s_0(0)$$

and its conditional covariance matrix is

$$\mathbb{E}[(\mathbf{y} - \mathbb{E}[\mathbf{y}])^H (\mathbf{y} - \mathbb{E}[\mathbf{y}]) | s_0(0)] = \mathbb{E}[(\mathbf{y} - \mathbf{h}s_0(0))^H (\mathbf{y} - \mathbf{h}s_0(0))] = \mathbb{E}[\mathbf{u}^H \mathbf{u}] = \mathbf{R}_u$$

Therefore, the likelihood function of the received sample can be written as

$$\mathcal{L}_{s_0(0)}(\mathbf{y}) = \frac{1}{(2\pi)^{N/2} |\mathbf{R}_u|^{1/2}} e^{-\frac{1}{2}(\mathbf{y} - \mathbf{h}s_0(0))^H \mathbf{R}_u^{-1} (\mathbf{y} - \mathbf{h}s_0(0))}.$$

The ML detector maximizes the log-likelihood function

$$\begin{aligned} \hat{s}_0(0) &= \operatorname{argmax}_{s_0(0)} \mathcal{L}^*(\mathbf{y}) \\ &= -\frac{N}{2} \log 2\pi - \frac{1}{2} \log |\mathbf{R}_u| - \frac{1}{2} (\mathbf{y} - \mathbf{h}s_0(0))^H \mathbf{R}_u^{-1} (\mathbf{y} - \mathbf{h}s_0(0)) \\ &\Leftrightarrow \operatorname{argmin}_{s_0(0)} (\mathbf{y} - \mathbf{h}s_0(0))^H \mathbf{R}_u^{-1} (\mathbf{y} - \mathbf{h}s_0(0)). \end{aligned}$$

Since it can be shown that the quadratic function of $s_0(0)$ is concave, by putting

the derivative on the objective function with respect to $s_0(0)$ equal to zero, we have

$$\begin{aligned}
& \frac{d}{ds_0(0)} (\mathbf{y} - \mathbf{h}s_0(0))^H \mathbf{R}_u^{-1} (\mathbf{y} - \mathbf{h}s_0(0)) = 0 \\
& \Leftrightarrow \frac{d}{ds_0(0)} [\mathbf{y}^H \mathbf{R}_u^{-1} \mathbf{y} - 2\text{Re}(\mathbf{y}^H \mathbf{R}_u^{-1} \mathbf{h}s_0(0)) + \mathbf{h}^h \mathbf{R}_u^{-1} \mathbf{h}s_0^*(0)s_0(0)] = 0 \\
& \Leftrightarrow 2\mathbf{h}^h \mathbf{R}_u^{-1} \mathbf{h}\hat{s}_0(0) = 2\mathbf{h}^H \mathbf{R}_u^{-1} \mathbf{y} \\
& \Leftrightarrow \hat{s}_0(0) \propto \mathbf{h}^H \mathbf{R}_u^{-1} \mathbf{y}.
\end{aligned}$$

The last equation is exactly Equation 6.11.

Since the signal, interference, and noise are all uncorrelated,

$$\mathbf{R}_u = E_s \mathbf{R}_{II} + N_0 \mathbf{R}_{n'}.$$

From Equation (6.10), the ACF of the matched filter output is

$$\begin{aligned}
R_y(d_1, d_2) &= \mathbb{E}[y(d_1)y^*(d_2)] \\
&= \mathbb{E} \left[\sum_{k_1=0}^{K-1} \sum_{l_1=0}^{L-1} \sum_{i_1=-\infty}^{\infty} \sqrt{E_{k_1}} s_{k_1}(i_1) g_{l_1} R_{k_1, i_1}(d_1 - i_1 T_s - \tau_{l_1}) \right. \\
&\quad \left. \times \sum_{k_2=0}^{K-1} \sum_{l_2=0}^{L-1} \sum_{i_2=-\infty}^{\infty} \sqrt{E_{k_2}} s_{k_2}^*(i_2) g_{l_2}^* R_{k_2, i_2}^*(d_2 - i_2 T_s - \tau_{l_2}) \right] \\
&\quad + N_0 R_{n'}(d_1, d_2)
\end{aligned}$$

Assuming that all symbols are independent and have unit amplitude, and using the properties in Equations (6.7) and (6.8), the first term which is the sum of the signal

ACF and the intra-cell ACF can be expressed as

$$\begin{aligned}
R_{nn}(d_1, d_2) &= \mathbb{E} \left[\sum_{k=0}^{K-1} \sum_{l_1=0}^{L-1} \sum_{l_2=0}^{L-1} \sum_{i=-\infty}^{\infty} E_k g_{l_1} g_{l_2}^* R_{k,i}(d_1 - iT_s - \tau_{l_1}) R_{k,i}^*(d_2 - iT_s - \tau_{l_2}) \right] \\
&= \sum_{k=0}^{K-1} E_k \sum_{l_1=0}^{L-1} \sum_{l_2=0}^{L-1} \sum_{i=-\infty}^{\infty} g_{l_1} g_{l_2}^* \mathbb{E} \left[\frac{1}{N^2} \sum_{m_1=1-N}^{N-1} C_{k,i}(m_1) R_p(d_1 + m_1 T_c - iT_s - \tau_{l_1}) \right. \\
&\quad \left. \times \sum_{m_2=1-N}^{N-1} C_{k,i}^*(m_2) R_p^*(d_2 + m_2 T_c - iT_s - \tau_{l_2}) \right] \\
&= \sum_{k=0}^{K-1} E_k \sum_{l_1=0}^{L-1} \sum_{l_2=0}^{L-1} \sum_{i=-\infty}^{\infty} g_{l_1} g_{l_2}^* \frac{1}{N^2} \sum_{m_1=1-N}^{N-1} \sum_{m_2=1-N}^{N-1} \mathbb{E} [C_{k,i}(m_1) C_{k,i}^*(m_2)] \\
&\quad \times R_p(d_1 + m_1 T_c - iT_s - \tau_{l_1}) R_p^*(d_2 + m_2 T_c - iT_s - \tau_{l_2})
\end{aligned}$$

According to the third property of the aperiodic spreading sequence cross-correlation function, i.e., Equation (6.7),

$$\begin{aligned}
R_{nn}(d_1, d_2) &= \sum_{k=0}^{K-1} E_k \sum_{l_1=0}^{L-1} \sum_{l_2=0}^{L-1} \sum_{i=-\infty}^{\infty} g_{l_1} g_{l_2}^* \frac{1}{N^2} \sum_{m=1-N}^{N-1} \mathbb{E} [|C_{k,i}(m)|^2] \\
&\quad \times R_p(d_1 + m T_c - iT_s - \tau_{l_1}) R_p^*(d_2 + m T_c - iT_s - \tau_{l_2})
\end{aligned}$$

Plugging in the fourth property of the aperiodic spreading sequence cross-correlation

function, i.e., Equation (6.8), we obtain

$$\begin{aligned}
R_{nn}(d_1, d_2) &= E_0 \sum_{l_1=0}^{L-1} \sum_{l_2=0}^{L-1} g_{l_1} g_{l_2}^* R_p(d_1 - \tau_{l_1}) R_p^*(d_2 - \tau_{l_2}) \\
&\quad \text{(CASE: } i = k = m = 0\text{)} \\
&+ \frac{E_0}{N^2} \sum_{l_1=0}^{L-1} \sum_{l_2=0}^{L-1} g_{l_1} g_{l_2}^* \sum_{\substack{i=-\infty \\ m \neq 0}}^{\infty} \sum_{m=1-N}^{N-1} (N - |m|) \\
&\quad \times R_p(d_1 + mT_c - iT_s - \tau_{l_1}) R_p^*(d_2 + mT_c - iT_s - \tau_{l_2}) \\
&\quad \text{(CASE: } k = 0, m \neq 0\text{)} \\
&+ \frac{E_0}{N} \sum_{l_1=0}^{L-1} \sum_{l_2=0}^{L-1} g_{l_1} g_{l_2}^* \sum_{\substack{i=-\infty \\ i \neq 0}}^{\infty} R_p(d_1 - iT_s - \tau_{l_1}) R_p^*(d_2 - iT_s - \tau_{l_2}) \\
&\quad \text{(CASE: } k = m = 0\text{)} \\
&+ \frac{1}{N^2} \sum_{k=1}^{K-1} E_k \sum_{l_1=0}^{L-1} \sum_{l_2=0}^{L-1} g_{l_1} g_{l_2}^* \sum_{\substack{i=-\infty \\ m \neq 0}}^{\infty} \sum_{m=1-N}^{N-1} (N - |m|) \\
&\quad \times R_p(d_1 + mT_c - iT_s - \tau_{l_1}) R_p^*(d_2 + mT_c - iT_s - \tau_{l_2}) \\
&\quad \text{(CASE: } k \neq 0, m \neq 0\text{)} \\
&+ \frac{1}{N} \sum_{k=1}^{K-1} E_k \sum_{l_1=0}^{L-1} \sum_{l_2=0}^{L-1} g_{l_1} g_{l_2}^* \sum_{\substack{i=-\infty \\ i \neq 0}}^{\infty} R_p(d_1 - iT_s - \tau_{l_1}) R_p^*(d_2 - iT_s - \tau_{l_2}) \\
&\quad \text{(CASE: } k \neq 0, i \neq 0, m = 0\text{)}
\end{aligned}$$

It is easy to see that the first term is the autocorrelation function of the signal and that the remaining terms can be combined into

$$\begin{aligned}
E_s R_{II}(d_1, d_2) &= \frac{E_s}{N^2} \sum_{l_1=0}^{L-1} \sum_{l_2=0}^{L-1} g_{l_1} g_{l_2}^* \sum_{\substack{i=-\infty \\ m \neq 0}}^{\infty} \sum_{m=1-N}^{N-1} (N - |m|) \\
&\quad \times R_p(d_1 + mT_c - iT_s - \tau_{l_1}) R_p^*(d_2 + mT_c - iT_s - \tau_{l_2}) \\
&+ \frac{E_s}{N} \sum_{k=1}^{K-1} E_k \sum_{l_1=0}^{L-1} \sum_{l_2=0}^{L-1} g_{l_1} g_{l_2}^* \sum_{\substack{i=-\infty \\ i \neq 0}}^{\infty} R_p(d_1 - iT_s - \tau_{l_1}) R_p^*(d_2 - iT_s - \tau_{l_2})
\end{aligned}$$

Consider the second term at the case when $m = 0$,

$$\begin{aligned}
E_s R_{II}(d_1, d_2) &= \frac{E_s}{N^2} \sum_{l_1=0}^{L-1} \sum_{l_2=0}^{L-1} g_{l_1} g_{l_2}^* \sum_{\substack{i=-\infty, m=1-N \\ (i,m) \neq (0,0)}}^{i=\infty, m=N-1} (N - |m|) \\
&\quad \times R_p(d_1 + mT_c - iT_s - \tau_{l_1}) R_p^*(d_2 + mT_c - iT_s - \tau_{l_2}) \\
&= \frac{E_s}{N} \sum_{l_1=0}^{L-1} \sum_{l_2=0}^{L-1} g_{l_1} g_{l_2}^* \sum_{\substack{j=-\infty \\ j \neq 0}}^{\infty} R_p(d_1 + jT_c - \tau_{l_1}) R_p^*(d_2 + jT_c - \tau_{l_2})
\end{aligned}$$

where E_c is the base station energy per chip,

$$E_c = E_s/N$$

and

$$R_I(d_1, d_2) = \sum_{l_1=0}^{L-1} \sum_{l_2=0}^{L-1} g_{l_1} g_{l_2}^* \sum_{\substack{j=-\infty \\ j \neq 0}}^{\infty} R_p(d_1 + jT_c - \tau_{l_1}) R_p^*(d_2 + jT_c - \tau_{l_2})$$

This expression of the G-RAKE weight vector is slightly different from the one presented in [104] but coincide with the expression in [106] and [105].

Since the impairment matrix \mathbf{R}_u is positive semi-definite, Cholesky factorization $\mathbf{R}_u = \mathbf{L}\mathbf{L}^H$ can help to interpret G-RAKE as a noise whitening matched filter [107]. Following Equation (6.11) we have

$$z = \mathbf{h}^H (\mathbf{L}^{-1})^H \mathbf{L}^{-1} \mathbf{h}_{s_0}(0) + \mathbf{h}^H (\mathbf{L}^{-1})^H \mathbf{L}^{-1} \mathbf{u}$$

Let $\tilde{\mathbf{u}} = \mathbf{L}^{-1} \mathbf{u}$ and $\tilde{\mathbf{h}} = \mathbf{L}^{-1} \mathbf{h}$, then the decision statistic becomes

$$z = \tilde{\mathbf{h}}^H \tilde{\mathbf{h}}_{s_0}(0) + \tilde{\mathbf{h}}^H \tilde{\mathbf{u}}$$

The ACF of $\tilde{\mathbf{u}}$ is an identity matrix, meaning that the overall impairment term is whitened. The equivalent weight vector is indeed a matched filter.

The symbol SINR of the G-RAKE receiver can be computed as

$$\text{SINR}_{\text{GRAKE}} = \frac{\mathbf{w}^H \mathbf{h} \mathbf{h}^H \mathbf{w}}{\mathbf{w}^H \mathbf{R}_u \mathbf{w}} = \mathbf{h}^H \mathbf{R}_u^{-1} \mathbf{h}$$

The symbol SINR for the RAKE receiver is

$$\text{SINR}_{\text{RAKE}} = \frac{(\mathbf{h}^H \mathbf{h})^2}{\mathbf{h}^H \mathbf{R}_u \mathbf{h}}$$

From Lemma (1) in [76], combining Cholesky factorization and Cauchy-Schwartz inequality we obtain

$$\frac{\text{SINR}_{\text{GRAKE}}}{\text{SINR}_{\text{RAKE}}} = \frac{\mathbf{h}^H \mathbf{R}_u \mathbf{h} \mathbf{h}^H \mathbf{R}_u^{-1} \mathbf{h}}{(\mathbf{h}^H \mathbf{h})^2} \geq 1$$

with equality if and only if $\mathbf{R}_u^{-1} = \mathbf{R}_u$ and the selected weight vector for G-RAKE maximizes the symbol SINR.

6.3 GRAKE Parameter Estimation

In previous sections the elements of the impairment cross-correlation matrix have been derived, assuming perfect estimation of the channel characteristics, such as path gains and path delays. However, in real circumstances estimation errors can not be avoided. For legacy purposes the GRAKE receiver uses similar approach as the RAKE receiver to estimate the channel characteristics through pilot channels. Methods to compute the impairment cross-correlation matrix through pilot channels for WCDMA system are discussed in this section [106].

In a GRAKE receiver that is aligned with a pilot channel, the finger output vector for the k th symbol is

$$\mathbf{y}_p(k) = \mathbf{h}_p s_p(k) + \mathbf{u}.$$

Assuming, as in the RAKE receiver, that \mathbf{h}_p is estimated as $\hat{\mathbf{h}}_p$, a short-term sample covariance estimate, or so called sample window based estimate, can be obtained from the pilot channel based on

$$\mathbf{R}_u^{ST} \triangleq \frac{1}{W} \sum_{w=1}^W (s_p^*(w) \mathbf{y}_p(w) - \hat{\mathbf{h}}_p) (s_p^*(w) \mathbf{y}_p(w) - \hat{\mathbf{h}}_p)^H, \quad (6.12)$$

where W is the window length in terms of symbols. Equation 6.12 can also be written

as

$$\mathbf{R}_u^{ST} = \alpha \mathbf{R}_I^{ST} + \beta \mathbf{R}_{n'}^{ST},$$

or in an equivalent vector-matrix form as

$$\begin{bmatrix} r_{u,1}^{ST} \\ \vdots \\ r_{u,J^2}^{ST} \end{bmatrix} = \begin{bmatrix} r_{I,1}^{ST} & r_{n,1}^{ST} \\ \vdots & \vdots \\ r_{I,J^2}^{ST} & r_{n,J^2}^{ST} \end{bmatrix} \begin{bmatrix} \alpha \\ \beta \end{bmatrix} \quad (6.13)$$

where $r_{u,i}^{ST}$, $r_{I,i}^{ST}$, and $r_{n,i}^{ST}$ for $1 \leq i \leq J^2$ are reshaped elements of \mathbf{R}_u^{ST} , \mathbf{R}_I^{ST} , and $\mathbf{R}_{n'}^{ST}$, respectively.

More accurate estimate can be acquired by larger sample window size and convergence of the estimate can be reached when the training sequence is long enough. However, a careful observation may potentially reduces the number of symbols in training phase in order to make the matrix estimate converge. The elements involved in Equation (6.13) have different properties. Parameters α , β , and $\mathbf{R}_{n'}^{ST}$ change much slower than \mathbf{R}_I^{ST} . A possible approach to improve the estimate with the same size of the sample window is to employ this prior information to tune and constrain the changing speed of the parameters. Using the least square method gives

$$\begin{bmatrix} \alpha \\ \beta \end{bmatrix} = \begin{bmatrix} r_{I,1}^{ST} & r_{n,1}^{ST} \\ \vdots & \vdots \\ r_{I,J^2}^{ST} & r_{n,J^2}^{ST} \end{bmatrix}^{-1} \begin{bmatrix} r_{u,1}^{ST} \\ \vdots \\ r_{u,J^2}^{ST} \end{bmatrix}.$$

Now based on this observation, the slow varying feature of α and β can be utilized by a smoothing filter, such as a one-order exponential filter

$$\begin{aligned} \alpha(j) &= \lambda \alpha(j-1) + (1-\lambda) \alpha(j) \\ \beta(j) &= \lambda \beta(j-1) + (1-\lambda) \beta(j). \end{aligned}$$

The value of the parameter λ reflects the changing speed of α and β and can be found through empirical approaches.

6.4 Other Types of Linear Equalizations

We begin by defining $\mathcal{C}(\mathbf{g})$ as the convolution matrix

$$\mathcal{C}(\mathbf{g}) = \begin{bmatrix} g_0 & 0 & \cdots & \vdots \\ g_1 & g_0 & \cdots & \vdots \\ \vdots & g_1 & \cdots & 0 \\ g_{L-1} & \vdots & \cdots & g_0 \\ 0 & g_{L-1} & \cdots & g_1 \\ \vdots & 0 & \cdots & \vdots \\ \vdots & \vdots & \cdots & g_{L-1} \end{bmatrix}.$$

Then,

$$\begin{aligned} z_{lc} &= \mathbf{a}_{0,0}^H \mathbf{W}_{lc}^H \mathbf{r} \\ &= \mathbf{a}_{0,0}^H \mathbf{W}_{lc}^H \mathcal{C}(\mathbf{g}) \sum_{k=0}^{K-1} \mathbf{a}_{k,0} s_k + \mathbf{a}_{0,0}^H \mathbf{W}_{lc}^H \mathbf{n} \end{aligned}$$

The LMMSE chip level equalizer in matrix form can be obtained by optimization [108]

$$\mathbf{W}_{lc} = \underset{\mathbf{W}}{\operatorname{argmin}} \mathbb{E}[\|\mathbf{W}^H \mathbf{r} - \sum_{k=0}^{K-1} \mathbf{a}_{k,0} s_k(0) E_k\|^2].$$

whose solution can be given as

$$\mathbf{W}_{lc} = \left(\mathcal{C}(\mathbf{g}) \left(\sum_{k=0}^{K-1} E_k \mathbf{a}_{k,0} \mathbf{a}_{k,0}^H \right) \mathcal{C}^H(\mathbf{g}) + N_0 \mathbf{I} \right)^{-1} \mathcal{C}(\mathbf{g}) \quad (6.14)$$

Notice that the despreading operation is placed after the chip level equalizer. This indicates that the task of the equalizer is to restore the orthogonality of the channel codes.

If the LMMSE criteria is directly applied on the symbol value estimation, we have

$$\mathbf{W}_{ls} = \underset{\mathbf{W}}{\operatorname{argmin}} \mathbb{E}[\|\mathbf{W}^H \mathbf{r} - s_0(0)\|^2],$$

which yeilds

$$\mathbf{w}_{l_s} = E_0 \left(\mathcal{C}(\mathbf{g}) \left(\sum_{k=0}^K E_k \mathbf{a}_{k,0} \mathbf{a}_{k,0}^H \right) \mathcal{C}^H(\mathbf{g}) + N_0 \mathbf{I} \right)^{-1} \mathcal{C}(\mathbf{g}) \mathbf{a}_{0,0}. \quad (6.15)$$

We observe that within a window of length equal to one symbol, the symbol level LMMSE estimate and chip level LMMSE are the same, up to a positive scaling factor.

It can be observed from Equation (6.14) that the spreading sequences of each user and symbol are included inside the expression of the equalizer. This follows from the dependency between consecutive chips and as a result of it the equalizer becomes time varying. This is not desirable due to implementation constraints. In order to prevent such non-stationary estimation, we introduce a simplifying assumption. We assume that the chip values are random and i.i.d., thus approximating the autocorrelation matrix of the chip sequence spreading a single symbol by an identity matrix which is independent with spreading sequences. This is necessary in order to make a stationary equalizer albeit the scrambling codes and spreading codes are deterministic [61].

In chip-level equalization, the multipath channel is equalized at the chip level, which is prior to despreading. Thus the equalizer restores to some extent the orthogonality of channelization codes and suppresses MAI. We can also write the chip level channel model as

$$\mathbf{r} = \mathbf{h}c_x + \mathbf{c}_I + \mathbf{n}$$

where \mathbf{c}_I characterizes the summation of all the interferences and \mathbf{n} denotes the white noise powers at chip level. Linear chip level estimate of the chip value has the vector form of

$$\hat{c}_x = \mathbf{w}_l^H \mathbf{r}.$$

The LMMSE criteria at chip level can be shown to be

$$\mathbf{w}_{lc} = \underset{\mathbf{w}}{\operatorname{argmin}} \mathbb{E}[\|\hat{c}_x - c_x\|^2], \quad (6.16)$$

and the LMMSE chip level estimator is obtained by solving Equation (6.16) as

$$\mathbf{w}_{lc} = (\mathbb{E}[\mathbf{r}\mathbf{r}^H])^{-1}\mathbf{h} = (E_c\mathcal{C}(\mathbf{g})\mathcal{C}^H(\mathbf{g}) + N_0\mathbf{I})^{-1}\mathbf{h}. \quad (6.17)$$

With the simplification introduced earlier, we can call the value computed by de-spreading the LMMSE equalized chip sequence as the estimate of the symbol value.

Similarly, the linear chip level equalizer based on the zero-forcing criteria can be derived as

$$\mathbf{W}_{zc} = \mathcal{C}(\mathbf{g}) (\mathcal{C}^H(\mathbf{g})\mathcal{C}(\mathbf{g}))^{-1}$$

and the matched filter solution (the RAKE receiver) is simply

$$\mathbf{W}_{rake} = \mathcal{C}(\mathbf{g}).$$

6.5 GRAKE and LMMSE-CE Equivalence

The GRAKE and LMMSE-CE equivalence is shown partly in [105]. This section gives a complete and rigid derivation. Linear chip level equalizers and GRAKE receiver can have either a block form or a vector form to be implemented in FIR (linear transversal, tapped-delay-line, non-recursive) filters. The observation we collect at the receiver can be expressed as

$$\begin{aligned} z &= \mathbf{w}^H \mathcal{C}^H(\mathbf{a}_{0,0}) \mathbf{r} \\ &= (\mathbf{w} \otimes \mathbf{a}_{0,0})^H \mathbf{r} \\ &= \mathbf{a}_{0,0}^H \mathcal{C}^H(\mathbf{w}) \mathbf{r} \end{aligned}$$

where \otimes denotes convolution. This explains the relation of the matrix form and vector form of the same equalizer.

In GRAKE receiver $\mathbf{w} = \mathbf{R}_u^{-1}\mathbf{h}$, if each significant path is selected, then

$$\mathbf{R}_u = E_c(\mathcal{C}(\mathbf{g})\mathcal{C}^H(\mathbf{g}) - \mathbf{h}\mathbf{h}^H) + N_0\mathbf{I} = \mathbf{K} - E_c\mathbf{h}\mathbf{h}^H$$

which, provided that \mathbf{K} and \mathbf{R}_u are non-singular, results in

$$\begin{aligned}\mathbf{w} &= \mathbf{R}_u^{-1} \mathbf{h} \\ &= \left(\mathbf{K}^{-1} + \frac{\mathbf{K}^{-1} \mathbf{h} \mathbf{h}^H \mathbf{K}^{-1}}{E_c^{-1} - \mathbf{h}^H \mathbf{K}^{-1} \mathbf{h}} \right) \mathbf{h} \\ &= \frac{\mathbf{K}^{-1} \mathbf{h}}{E_c^{-1} - \mathbf{h}^H \mathbf{K}^{-1} \mathbf{h}},\end{aligned}$$

where the second equation follows from the binomial inverse theorem, or

$$\mathbf{w} = \frac{\mathbf{w}_{lc}}{E_c^{-1} - \mathbf{h}^H \mathbf{K}^{-1} \mathbf{h}}, \quad (6.18)$$

where \mathbf{w}_{lc} is the chip level LMMSE estimator in Equation (6.17).

Now, since [105]

$$\mathbf{w}^H \mathbf{h} = \frac{\mathbf{h}^H \mathbf{K}^{-1} \mathbf{h}}{E_c^{-1} - \mathbf{h}^H \mathbf{K}^{-1} \mathbf{h}} \geq 0,$$

and $\mathbf{h}^H \mathbf{K}^{-1} \mathbf{h}$ is positive, the denominator in the right hand side of Equation (6.18) is also positive. This shows \mathbf{w} and \mathbf{w}_{lc} give the same result for detector decision and therefore establishes the equivalence of GRAKE receiver and LMMSE chip level equalizer.

The equalities

$$\mathbf{w}^H \mathcal{C}^H(\mathbf{a}_{0,0}) \mathbf{r} = (\mathbf{w} \otimes \mathbf{a}_{0,0})^H \mathbf{r} = \mathbf{a}_{0,0}^H \mathcal{C}^H(\mathbf{w}) \mathbf{r}$$

show that despreading the signal in each finger branch is equivalent to despreading signal after been weighted combining and that GRAKE and LMMSE-CE has equivalent structure. It has been shown that under this approximation and using the same finger placement, the weight vectors of GRAKE and LMMSE-CE are equivalent. Furthermore, from the analysis above, we can conclude that the equivalence between GRAKE and LMMSE-CE even without the simplification.

6.6 Finger Placement Algorithms

We have seen that GRAKE and LMMSE-CE are optimal in many aspects when using the same finger placement strategies. The finger placement is shown to be a key factor in determining the system performance [104]. For this reason, a number of finger placement algorithms have recently been proposed, including those employing non-iterative approaches [101] [109] [102] [107]. Some recursive finger placement algorithms have also been developed that perform greedy searches in a J dimensional space [110] which are based on minimizing the non-convex MSE as a function of the finger locations. For channels with fast-time-varying path delays, recursive algorithms are not attractive due to their complexity. In this section we present a new non-iterative solution for the finger placement.

6.6.1 The Greedy Search Algorithm

We suppose that the finger locations are constrained in bounded spaces and use mean square error as our optimization criteria. If the search space is defined as $[a, b]$ for every finger, the whole search space for J fingers is $[a, b]^J$. In [110] an algorithm is proposed that considers the MSE as a function of J finger locations as $\text{MSE}(t_1, t_2, \dots, t_J)$. First L finger are set aligned to the channel paths. The finger location t_{L+1} is chosen in $[a, b]$ to minimize MSE while fixing t_1, \dots, t_L . Finger location t_{L+2} is chosen to minimize MSE while fixing t_1, \dots, t_{L+1} . All other finger locations are chosen in the same fashion until t_J is found. Since the computation of MSE involves matrix inversion, the matrix inversion lemma for partitioned Hermitian matrix can be used to reduce the computational complexity [88].

6.6.2 GRAKE Symmetric Placement Algorithm

This finger placement strategy is based on the following facts and analysis [102]. Let us consider two extreme cases. The first case corresponding to when only inter-cell interference is present. In this case, if the inter-cell interference is assumed to be white and Gaussian, RAKE receiver can have a closed-form optimal finger placement strategy. The reason is that in this case the optimal receivers that maximize signal

power, maximize the likelihood function, or minimize the MSE are equivalent and their common implementation is simply the RAKE receiver, which places fingers on the delays of the most significant incoming paths. In the second case we assume that only intra-cell interference is present. We recall that in this case chip level equalizers cannot utilize the orthogonality of the OVSF codes but they are aware of the path coefficients and delays, as well as the inter-cell noise variance. In this case, the best strategy is to restore the orthogonality of the channel and force the inter-chip interference to be zero by inverting the channel. This way, the interuser interference is totally canceled. Since there is no inter-cell noise, the problem of noise-enhancement for zero-forcing equalizer will not be an issue.

To clarify this point, we present an example. We define τ and $\tau + \Delta\tau$ as two path delays of a two-path channel. In this case, channel inverse filter has to be IIR or can be approximated by an FIR filter with a large number of fingers with delays set at τ , $\tau \pm \Delta\tau$, $\tau \pm 2\Delta\tau$, $\tau \pm 3\Delta\tau$, \dots . This can be visualized by the FIR matrix representation using the pseudo-inverse of the channel matrix. For example, assume that the path search procedure has a time resolution of T_c , equal to the chip duration, and the channel has two paths with path gains 3 and 1 at delays 0 and $2T_c$ respectively, i.e., the channel matrix is

$$\mathbf{H}_1 = \begin{bmatrix} 3 & 0 & 0 & 0 & 0 & 0 & 0 & 0 & 0 \\ 0 & 3 & 0 & 0 & 0 & 0 & 0 & 0 & 0 \\ 1 & 0 & 3 & 0 & 0 & 0 & 0 & 0 & 0 \\ 0 & 1 & 0 & 3 & 0 & 0 & 0 & 0 & 0 \\ 0 & 0 & 1 & 0 & 3 & 0 & 0 & 0 & 0 \\ 0 & 0 & 0 & 1 & 0 & 3 & 0 & 0 & 0 \\ 0 & 0 & 0 & 0 & 1 & 0 & 3 & 0 & 0 \\ 0 & 0 & 0 & 0 & 0 & 1 & 0 & 3 & 0 \\ 0 & 0 & 0 & 0 & 0 & 0 & 1 & 0 & 3 \\ 0 & 0 & 0 & 0 & 0 & 0 & 0 & 1 & 0 \\ 0 & 0 & 0 & 0 & 0 & 0 & 0 & 0 & 1 \end{bmatrix}.$$

The left pseudo-inverse matrix \mathbf{H}_1^{-1} is then

$$\mathbf{H}_1^{-1} = \begin{bmatrix} 0.3333 & 0 & 0.0001 & 0 & -0.0004 & 0 & 0.0012 & 0 & -0.0037 & 0 \\ 0 & 0.3333 & 0 & 0.0001 & 0 & -0.0004 & 0 & 0.0012 & 0 & -0.0037 \\ -0.1110 & 0 & 0.3329 & 0 & 0.0014 & 0 & -0.0041 & 0 & 0.0122 & 0 \\ 0 & -0.1110 & 0 & 0.3329 & 0 & 0.0014 & 0 & -0.0041 & 0 & 0.0122 \\ 0.0366 & 0 & -0.1097 & 0 & 0.3292 & 0 & 0.0123 & 0 & -0.0370 & 0 \\ 0 & 0.0366 & 0 & -0.1097 & 0 & 0.3292 & 0 & 0.0123 & 0 & -0.0370 \\ -0.0110 & 0 & 0.0329 & 0 & -0.0988 & 0 & 0.2963 & 0 & 0.1111 & 0 \\ 0 & -0.0110 & 0 & 0.0329 & 0 & -0.0988 & 0 & 0.2963 & 0 & 0.1111 \end{bmatrix}.$$

If the channel matrix is

$$\mathbf{H}_2 = \begin{bmatrix} 7 & 0 & 0 & 0 & 0 & 0 & 0 & 0 & 0 \\ 0 & 7 & 0 & 0 & 0 & 0 & 0 & 0 & 0 \\ 0 & 0 & 7 & 0 & 0 & 0 & 0 & 0 & 0 \\ 2 & 0 & 0 & 7 & 0 & 0 & 0 & 0 & 0 \\ 0 & 2 & 0 & 0 & 7 & 0 & 0 & 0 & 0 \\ 0 & 0 & 2 & 0 & 0 & 7 & 0 & 0 & 0 \\ 0 & 0 & 0 & 2 & 0 & 0 & 7 & 0 & 0 \\ 0 & 0 & 0 & 0 & 2 & 0 & 0 & 7 & 0 \\ 0 & 0 & 0 & 0 & 0 & 2 & 0 & 0 & 7 \\ 0 & 0 & 0 & 0 & 0 & 0 & 2 & 0 & 0 \\ 0 & 0 & 0 & 0 & 0 & 0 & 0 & 2 & 0 \end{bmatrix},$$

then

$$\mathbf{H}_2^{-1} = \begin{bmatrix} 0.1428 & 0 & 0 & 0.0002 & 0 & 0 & -0.0009 & 0 & 0 & 0.0031 & 0 \\ 0 & 0.1428 & 0 & 0 & 0.0002 & 0 & 0 & -0.0009 & 0 & 0 & 0.0031 \\ 0 & 0 & 0.1420 & 0 & 0 & 0.0031 & 0 & 0 & -0.0107 & 0 & 0 \\ -0.0405 & 0 & 0 & 0.1419 & 0 & 0 & 0.0033 & 0 & 0 & -0.0116 & 0 \\ 0 & -0.0405 & 0 & 0 & 0.1419 & 0 & 0 & 0.0033 & 0 & 0 & -0.0116 \\ 0 & 0 & -0.0375 & 0 & 0 & 0.1313 & 0 & 0 & 0.0406 & 0 & 0 \\ 0.0107 & 0 & 0 & -0.0375 & 0 & 0 & 0.1312 & 0 & 0 & 0.0408 & 0 \\ 0 & 0.0107 & 0 & 0 & -0.0375 & 0 & 0 & 0.1312 & 0 & 0 & 0.0408 \end{bmatrix}.$$

From above examples we notice an interesting characteristic of the pseudo-inverse of the Toeplitz multipath channel matrix. To be more specific let us define the main diagonal as the diagonal with index 0 and the index increases by 1 every time the diagonal shift toward right hand side one element and by -1 every time the diagonal shift toward left hand side one element. The channel matrix \mathbf{H}_1 has constant diagonals at diagonal 0 and -2 and \mathbf{H}_2 has constant diagonals at 0 and -3 . The indices of non-zero diagonals of \mathbf{H}_1^{-1} are $0, \pm 2, \pm 4, \pm 6$ and 8 . The common spacing (2) in indices of these non-zero diagonals equals to the spacing of those in the channel matrix. Similarly, when the channel matrix has spacing 3 in \mathbf{H}_2 case, the common index spacing of the non-zero diagonals of \mathbf{H}_2^{-1} becomes 3 accordingly. This specifies the finger locations of the equalizer for this two-path channel, i.e., to place fingers symmetrically around the first path and the common spacing between consecutive fingers to be set equal to the time difference of the two paths. Further investigation in [102] from empirical study shows that the diagonal indices closer to 0 have higher weights. Therefore, available fingers are placed in the FIR matrix representation starting from 0 diagonal to locations that corresponding to diagonals with larger absolute value of indices until the finger pool is exhausted. Detailed but ad-hoc algorithm of this finger placement strategy, which covers cases when channels have multiple paths with different delays, can be found in the literatures related to GRAKE receiver. For instance, according to the above design considerations, if we have a channel that has path delays as $0, T_c, 2T_c, 3T_c$, the candidate delay set is constructed as $[-6, -4, -3, -2, -1, 0, 1, 2, 3, 4, 5, 6]T_c$.

More details on this method can be found in [111] and [112].

6.6.3 The Maximum Weight Placement Algorithm

In this section we introduce a new finger placement strategy that tries to approximate a MMSE IIR filter using a block matrix FIR equalizer.

In a ZF equalizer, the block form of the equalizer satisfies $\mathbf{W}_{zf}^H \mathcal{C}(\mathbf{g}) = \mathbf{I}$ such that the decision statistic

$$z_{zf} = \mathbf{a}_{0,0}^H \mathbf{W}_{zf}^H \mathcal{C}(\mathbf{g}) \sum_{k=0}^{K-1} \mathbf{a}_{k,0} s_k(0) = s_0(0).$$

Linear transversal implementation of this inverse channel filter requires infinite taps [111]. However, a finite length ZF FIR equalizer can approximate this inverse [112] [113]. In order to orthogonalize the channel, the equalizer has to allocate weights according to the mutual spacing of the paths. Suppose there are only two paths with delays t_1 and t_2 , the ZF FIR equalizer needs to put fingers at the delays of these two paths, as well as delays at $(t_1 + kt_2)$ where $k = 0, \pm 1, \pm 2, \pm 3, \dots$. This is due to the structure of the inverse of a Toeplitz matrix [114]. From the analysis on these two extreme cases it is shown that, when ignoring colored interference, in order to maximize signal power and therefore SINR, RAKE receiver can be used and optimal finger locations are on the path delays. On the other extreme, when ignoring the white noise, in order to nullify the chip interference and interuser interference, fingers should be placed on the path delays and their mirror locations to approximate inverse channel filter, based on which most proposed finger placement algorithms in the current literature about GRAKE implementation are designed. However, neither algorithms is optimal when both white noise and colored interference are present. Adaptive algorithms have been developed to fill the gap between real implementation and the performance bound using gradient greedy search, however, when the number of fingers is large, the required computational load is very high.

The proposed finger placement is based on the LMMSE-CE block form equalizer with above simplification

$$\mathbf{W}_{lc} = (E_c \mathcal{C}(\mathbf{g}) \mathcal{C}^H(\mathbf{g}) + N_0 \mathbf{I})^{-1} \mathcal{C}(\mathbf{g}). \quad (6.19)$$

Assuming a two-path channel with path delays 0 and T_c and the sampling rate of the

RRC filter is R_o , the time resolution between two consecutive elements of \mathbf{g} becomes T_c/R_o seconds. The proposed finger placement follows the following steps.

- The discrete channel delay-coefficient vector \mathbf{g} is constructed in such a way that two complex channel coefficients are inserted into \mathbf{g} at the first and $R_0 + 1$ elements respectively and zeros elsewhere.
- The block form equalizer \mathbf{W} is calculated based on Equation (6.19). Diagonals of this matrix are labeled in the fashion used in the last section, i.e., the main diagonal has index 0 and the index increases by 1 if the diagonal shift toward right hand side.
- The weight function of a diagonal is denoted by α_i , where i is the diagonal index. This weight function α_i can be defined in many ways but one simple example is to use the average of the absolute value of each element on this diagonal, i.e.,

$$\alpha_i^1 = \frac{1}{N_i} \sum_{j=1}^{N_i} |\mathbf{d}_i(j)|,$$

where $\mathbf{d}_i(j)$ denotes the j th element of the diagonal vector \mathbf{d}_i and N_i is the number of elements of the diagonal i . Or α_i can be defined as the norm of the diagonal vector divided by the size of the diagonal vector, i.e.,

$$\alpha_i^2 = \frac{1}{N_i} \sum_{j=1}^{N_i} (\mathbf{d}_i(j))^2.$$

Both weight functions can differentiate the significance of the diagonals.

- Sort the diagonal indices based on their weights. The first J diagonals are those whose corresponding delays constitute the proposed Maximum Weight Placement (MWP) delay vector.

Note that in this way, it is possible that the fingers are not placed at the path delays. For example, one path with large path gain may cause this algorithm to choose finger locations based solely on this path and ignore the existence of other less significant paths. However, this behavior is expected since in this case placing fingers to mitigate

the interference caused by the strong paths is more helpful to increase SINR than just matching fingers with weak paths.

It is easy to verify from Equation (6.19) that when the ACF of the impairment matrix \mathbf{R}_u is approximately a scaled identity matrix, indicating the interferences and noise are close to white, this algorithm results in the finger locations that coincide with the path delays. When there is little white noise presents, the resulting \mathbf{W} converges to the ZF equalizer and the fingers will be placed at the same locations suggested by the ZF equalizer.

6.7 Simulation Results

We have simulated the proposed MWP algorithm in a WCDMA/HSDPA environment. The chip rate is 3.84 Mcps and the spreading factor is $N = 16$. The modulation scheme is QPSK. The scrambling code generation is based on the downlink as described in [103]. Totally $K = 5$ users are active in the cell with relative energy per symbol distributed as $[3, 2, 1, 4, 5]$. The first element in this sequence is the energy per symbol of the user of interest. The total base station energy per symbol is 15. The RRC filter employed here has a roll-off factor of $\alpha = 0.22$ and over sampling rate is $R_o = 8$. The multipath channel in this simulation has $L = 4$ paths with relative path gains $[0, -3, -6, -9]$ dB. The delays of these path gains are then normalized to $[0, 290, 621, 981] \times 10^{-9}$ s, which results in $[0, 9, 19, 30]$ th samples. Maximum Doppler frequency shift is 200Hz. The path coefficients and delays are assumed perfectly known at the receiver. The maximum number of available fingers is $J = 8$. We have used Simulink to carry out these simulations. The performance of MWP with 8 fingers is compared with 8-finger GRAKE and 4-finger RAKE receivers in terms of symbol error probability. In Figure 6.1 the symbol error probability curve at different SNR (E_b/N_0) values shows that the MWP algorithm outperforms the other two techniques. Both MWP and GRAKE achieve the same diversity order but MWP has about 1 dB power gain over the performance of GRAKE with limited added computational complexity due to a sparse matrix inversion.

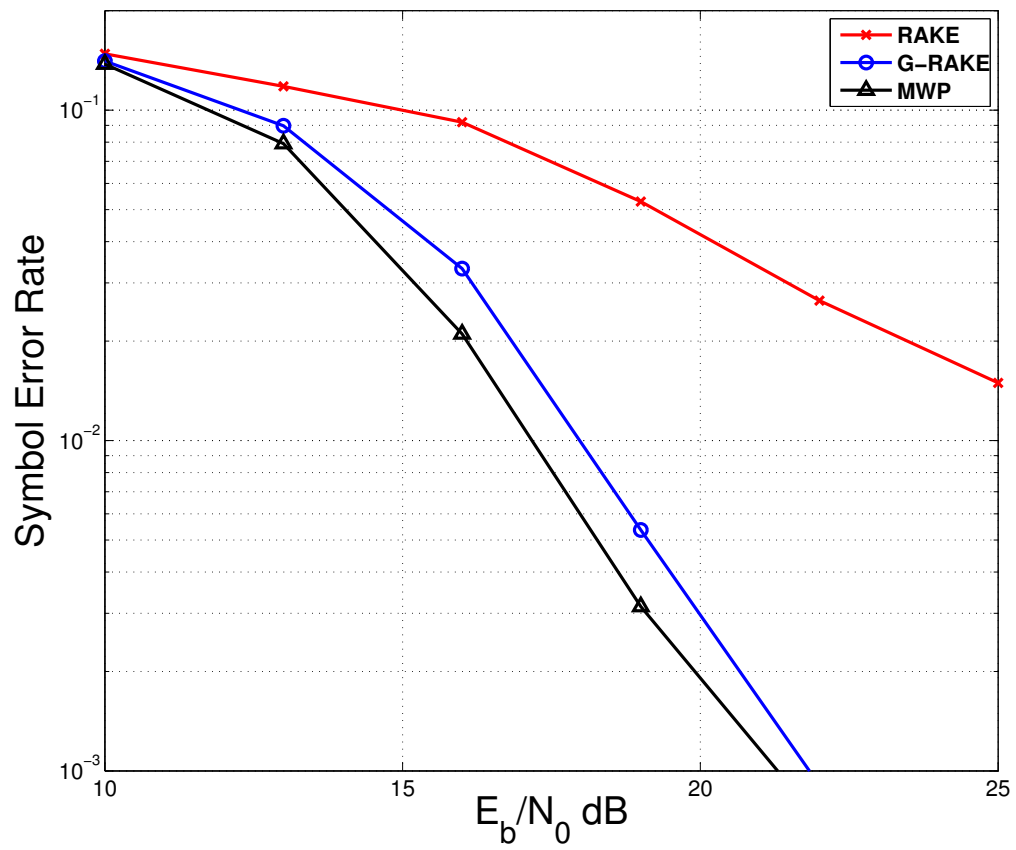


Figure 6.1: Error probability performance with finger placements: RAKE, GRAKE, and MWP

6.8 Conclusions

In this chapter, equalization of spread spectrum signals in slow fading multipath channels is discussed. Particularly, in contrast to the widely used RAKE receiver, the generalized RAKE receiver (GRAKE) is introduced. The implementation issues in real spread spectrum communication systems are illustrated. We show that the GRAKE receiver can be interpreted as a noise whitening filter, and therefore, the SINR of RAKE receiver is a lower bound to the SINR of the GRAKE receiver.

Furthermore, after a brief analysis of LMMSE and other equalizers, the equivalence of GRAKE receiver and the LMMSE chip level equalizer is proved. This equivalence is established under a number of assumptions and a broad range of circumstances.

A preliminary assumption for the equivalence is that both GRAKE receiver and LMMSE chip level equalizer use the same finger placement strategy. Finger placement strategy has a significant impact on the equalizer performance. A novel finger placement strategy, MWP, is proposed in this chapter. This strategy, following similar track of MMSE equalization, balances the signal energy and the noise and interference energy at the finely placed fingers. Simulation results show that MWP has advantages on error rate performance over traditional finger placement algorithms and can be implemented with affordable computational complexity.

Chapter 7

Future Work

In this chapter we are going to present some future possibilities that extend the work of this thesis.

In Chapter 2, we have proposed a linear precoding technique for MIMO broadcast channels that bridges the gap between the channel capacities achieved by channel inversion based and the matched filter based techniques. This technique, i.e., the Coordinated Interference-Aware Beamforming (CIB), works for flat-fading channels and any number of transmit antennas, any number of users and any number of receiver antennas. Although not optimal, it achieves a large region of the sum-capacity and features a low computational complexity. Chapter 3 extends CIB in multiple-antenna frequency-selective spread spectrum channel case. Both applications of CIB assumes perfect CSIT and CSIR. In reality, CSI suffers from estimation errors. Moreover, when CSIT needs to be acquired from the receiver sides, quantization errors also affect the performance. Therefore, in order to implement CIB in these cases, the performance degradation in systems where CSI has errors has to be investigated. The way how the performance degrades with the channel estimation error helps to determine the method and parameters of the channel estimation function. When quantization error presents, the performance degradation with respect to this error should be used to find right quantization order. Therefore, necessary adjustment in the CIB algorithm in the presence of channel estimation error can be made to improve the performance in those cases. Similarly, improvement can be extended to the technique proposed in Chapter 3 too.

For the EDLP technique proposed in Chapter 4, the provided equations for computation of perturbation vector apply for the case when we have spatial multiplexing order equals to 2 and modulation scheme 4-QAM. We can extend the EDLP to systems that can support and demand for higher spatial dimensions and higher modulation rates.

In Chapter 5 we have come up with a low complexity precoding scheme using BDZF and EDLP. However, the perturbation vectors used are optimal for each individual user, instead of for the overall system. We conjecture that using a technique based on the block channel matrix and the optimal perturbation vector for each user, to correct the final perturbation that minimizes the overall transmitted power can achieve the full diversity order for each data stream.

Bibliography

- [1] E. Biglieri, J. Proakis, and S. Shamai, “Fading channels: Information-theoretic and communications aspects,” *IEEE Transactions on Information Theory*, vol. 1, pp. 2619–2692, October 1998.
- [2] A. Goldsmith, S. A. Jafar, N. Jindal, and S. Vishwanath, “Capacity limits of MIMO channels,” *IEEE Journal on Selected Areas in Communications*, vol. 21, pp. 684–702, June 2003.
- [3] S. Diggavi, N. Al-Dhahir, A. Stamoulis, and A. Calderbank, “Great expectations: the value of spatial diversity in wireless networks,” *Proceedings of the IEEE*, vol. 92, pp. 219–270, February 2004.
- [4] G. J. Foschini, Jr., “Layered space-time architecture for wireless communication in a fading environment when using multielement antennas,” *Bell System Technical Journal*, 1996.
- [5] D. Gesbert, M. Shafi, D. shan Shiu, P. J. Smith, and A. Naguib, “From theory to practice: An overview of MIMO space-time coded wireless systems,” *IEEE Journal on Selected Areas in Communications*, vol. 21, pp. 281–302, Apr. 2003.
- [6] D. Tse and P. Viswanath, *Fundamentals of Wireless Communication*. Cambridge University Press, 2005.
- [7] R. G. Gallager, *Information Theory and Reliable Communication*. New York, NY, USA: Wiley, 1968.
- [8] E. Telatar, “Capacity of multi-antenna Gaussian channels,” *AT&T-Bell Labs Internal Technical Memo*, June 1995.

- [9] G. J. Foschini, Jr. and M. J. Gans, "On limits of wireless communication in a fading environment when using multiple antennas," *Wireless Personal Communication*, March 1998.
- [10] L. Zheng and N. C. D. Tse, "Diversity and multiplexing: A fundamental trade-off in multiple-antenna channels," *IEEE Transactions on Information Theory*, vol. 49, no. 5, pp. 1073–1096, 2003.
- [11] V. Tarokh, N. Seshadri, and A. R. Calderbank, "Space-time codes for high data rate wireless communication: Performance criterion and code construction," *IEEE Transactions on Information Theory*, pp. 744–765, March 1998.
- [12] V. Tarokh, H. Jafarkhani, and A. R. Calderbank, "Space-time block codes from orthogonal designs," *IEEE Transactions on Information Theory*, vol. 45, pp. 1456–1467, July 1999.
- [13] H. E. Gamal, G. Caire, and M. O. Damen, "Lattice coding and decoding achieve the optimal diversity-multiplexing tradeoff of MIMO channels," *IEEE Transactions on Information Theory*, vol. 50, pp. 968–985, June 2004.
- [14] P. W. Wolniansky, G. J. Foschini, G. D. Golden, and R. A. Valenzuela, "V-BLAST: An architecture for realizing very high data rates over the rich-scattering wireless channel," in *URSI ISSSE*, pp. 295–300, September 1998.
- [15] M. Sellathurai and S. Haykin, "A simplified diagonal BLAST architecture with iterative parallel-interference cancelation receivers," in *Proceedings of IEEE International Conference on Communications (ICC)*, vol. 10, pp. 3067–3071, IEEE, 2001.
- [16] M. Park, "Performance evaluation of multiuser detectors with V-BLAST to MIMO channel," Master's thesis, Virginia Polytechnic Institute and State University, Blacksburg, Virginia, 2003.
- [17] H. Yao and G. W. Wornell, "Lattice-reduction-aided detectors for MIMO communication systems," in *Proceedings of IEEE Global Communications Conference (GLOBECOM)*, pp. 424–428, IEEE, 2002.

- [18] J. H. Conway and N. J. A. Sloane, *Sphere Packings, Lattices and Groups*. New York, NY, USA: Springer-Verlag, 3rd ed., 1999. ISBN 0-387-98585-9.
- [19] A. K. Lenstra, H. W. Lenstra, and L. Lovsz, “Factoring polynomials with rational coefficients,” *Annals of Mathematics*, vol. 261, pp. 515 – 534, 1982.
- [20] D. Wubben, R. Bohnke, V. Kuhn, and K.-D. Kammeyer, “Near-maximum-likelihood detection of MIMO systems using MMSE-based lattice reduction,” in *Proceedings of IEEE International Conference on Communications (ICC)*, vol. 2, pp. 798–802, June 2004.
- [21] J. G. Proakis and M. Salehi, *Digital Communications*. New York, N.Y.: McGraw-Hill, Inc., fifth ed., 2007.
- [22] M. Tomlinson, “New automatic equalizer employing modulo arithmetic,” *Electronics Letter*, vol. 7, pp. 138–139, March 1971.
- [23] H. Harashima and H. Miyakawa, “Matched-transmission technique for channels with intersymbol interference,” *IEEE Transactions on Communications*, vol. 20, pp. 774–780, August 1972.
- [24] M. H. M. Costa, “Writing on dirty paper,” *IEEE Transactions on Information Theory*, vol. IT-29, pp. 439–441, May 1983.
- [25] S. I. Gelfand and M. S. Pinsker, “Coding for channel with random parameters,” *Problems of Control and Information Theory*, vol. 9, no. 1, pp. 19 – 31, 1980.
- [26] U. Erez, S. Shamai, and R. Zamir, “Capacity and lattice strategies for canceling known interference,” *IEEE Transactions on Information Theory*, vol. 51, no. 11, pp. 3820–3832, 2005.
- [27] U. Erez and S. ten Brink, “A close-to-capacity dirty paper coding scheme,” *IEEE Transactions on Information Theory*, vol. 51, pp. 3417–3432, October 2005.
- [28] W. Yu, D. P. Varodayan, and J. M. Cioffi, “Trellis and convolutional precoding for transmitter-based interference presubtraction,” *trcom*, vol. 53, pp. 1220–1230, November 2005.

- [29] G. Caire and S. Shamai, “On the achievable throughput of a multiantenna Gaussian broadcast channel,” *IEEE Transactions on Information Theory*, vol. 49, pp. 1691–1706, July 2003.
- [30] H. Weingarten, Y. Steinberg, and S. Shamai, “The capacity region of the Gaussian MIMO broadcast channel,” in *Proceedings of IEEE International Symposium on Information Theory (ISIT)*, (Chicago, USA), p. 174, June 2004.
- [31] T. M. Cover and J. Thomas, *Elements of Information Theory*. John Wiley and Sons, 1991.
- [32] G. Caire and S. Shamai, “On achievable rates in a multi-antenna broadcast downlink,” in *Proceedings of the 38th Annu. Allerton Conf. Communication, Control and Computing*, (Monticello, IL), Oct 2000.
- [33] H. Weingarten, Y. Steinberg, and S. Shamai, “The capacity region of the Gaussian multiple-input-multiple-output broadcast channel,” *IEEE Transactions on Information Theory*, vol. 52, pp. 3936 – 3964, September 2006.
- [34] A. Khisti, U. Erez, and G. Wornell, “Writing on many pieces of dirty paper at once: The binary case,” in *Proceedings of IEEE International Symposium on Information Theory (ISIT)*, (Chicago, USA), p. 533, June 2004.
- [35] A. S. Cohen and A. Lapidoth, “Generalized writing on dirty paper,” in *Proceedings of IEEE International Symposium on Information Theory (ISIT)*, (Lausanne, Switzerland), p. 227, June 2002.
- [36] W. Yu, A. Sutivong, D. Julian, T. M. Cover, and M. Chiang, “Writing on colored paper,” in *Proceedings of IEEE International Symposium on Information Theory (ISIT)*, (Washington, DC), p. 302, June 2001.
- [37] I. J. Cox, M. L. Miller, and A. L. McKellips, “Watermarking as communications with side information,” *Proceedings of the IEEE*, vol. 87, no. 7, pp. 1127 – 1141, 1999.
- [38] A. S. Cohen and A. Lapidoth, “The Gaussian watermarking game,” *IEEE Transactions on Information Theory*, vol. 48, pp. 1639–1667, June 2002.

- [39] F. Willems, “On Gaussian channels with side information at the transmitter,” in *Proc. 9th Symp. Inform. Theory*, (Benelux, Mierlo, The Netherlands), pp. 129–135, May 1988.
- [40] W. Yu and J. Cioffi, “Sum capacity of Gaussian vector broadcast channels,” *IEEE Transactions on Information Theory*, vol. 50, pp. 1875 – 1892, 2004.
- [41] R. Choi, M. Ivrlac, R. Murch, and W. Utschick, “On strategies of multiuser MIMO transmit signal processing,” *IEEE Transactions on Wireless Communications*, vol. 3, pp. 1936–1941, November 2004.
- [42] R. Chen, J. Andrews, and J. Health, R.W., “Multiuser space-time block coded MIMO with downlink precoding,” in *Proceedings of IEEE International Conference on Communications (ICC)*, pp. 2689–2693, June 2004.
- [43] T. Yoo and A. Goldsmith, “Optimality of zero-forcing beamforming with multiuser diversity,” in *Proceedings of IEEE International Conference on Communications (ICC)*, pp. 542–546, May 2005.
- [44] C. Peel, Q. Spencer, A. L. Swindlehurst, and B. Hochwald, “Downlink transmit beamforming in multi-user MIMO systems,” in *Proceedings of IEEE Sensor Array and Multichannel Signal Processing Workshop*, pp. 43–51, 2004.
- [45] Y. Xie and C. N. Georghiades, “Some results on the sum-rate capacity of MIMO fading broadcast channels,” *IEEE Transactions on Wireless Communications*, vol. 5, pp. 377 – 383, February 2006.
- [46] Z. Shen, R. Chen, J. G. Andrews, J. Robert W. Heath, and B. L. Evans, “Sum capacity of multiuser MIMO broadcast channels with block diagonalization,” in *Proceedings of IEEE International Symposium on Information Theory (ISIT)*, (Seattle), July 2006.
- [47] N. Jindal, S. Vishwanath, and A. Goldsmith, “On the duality of Gaussian multiple-access and broadcast channel,” *IEEE Transactions on Information Theory*, vol. 50, pp. 768–783, May 2004.

- [48] K.-K. Wong, R. Murch, and K. Letaief, "Performance enhancement of multiuser MIMO wireless communication systems," *IEEE Transactions on Communications*, vol. 50, pp. 1960 – 1970, December 2002.
- [49] A. M. Tulino and S. Verdu, *Random Matrix Theory and Wireless Communications*. now Publishers Inc., 2004.
- [50] S. Verd, *Multiuser Detection*. Cambridge University Press, 1998.
- [51] B. M. Hochwald, C. B. Peel, and A. L. Swindlehurst, "A vector-perturbation technique for near-capacity multiantenna multiuser communication - part ii: Perturbation," *IEEE Transactions on Communications*, vol. 53, pp. 537–544, 2005.
- [52] C.-B. Chae, D. Mazzaresse, N. Jindal, and J. Robert W. Heath, "Coordinated beamforming with limited feedback in the MIMO broadcast channel," *to appear in IEEE Journal on Selected Areas in Communications*, 2008.
- [53] M. Sharif and B. Hassibi, "On the capacity of MIMO broadcast channels with partial side information," *IEEE Transactions on Information Theory*, vol. 51, pp. 506 – 522, February 2005.
- [54] J. Lee and N. Jindal, "Dirty paper coding vs. linear precoding for MIMO broadcast channels," in *Proceedings of the 40th Annual Asilomar Conference on Signals, Systems, and Computers*, (Pacific Grove, CA), Oct. 2006.
- [55] M. Sharif and B. Hassibi, "A comparison of time-sharing, DPC, and beamforming for MIMO broadcast channels with many users," *IEEE Transactions on Communications*, vol. 55, pp. 11 – 15, Jan. 2007.
- [56] M. Sadek, A. Tarighat, and A. H. Sayed, "A leakage-based precoding scheme for downlink multi-user MIMO channels," *IEEE Transactions on Wireless Communications*, vol. 6, pp. 1711–1721, 2007.
- [57] T. R. WG1, "Physical layer aspects of UTRA high speed downlink packet access," tech. rep., 3GPP TR 25.848 v4.0.0(2001), 2005.

- [58] T. R. WG1, "Multiple-input multiple output in UTRA," tech. rep., 3GPP TR 25.876 v1.5.1(2004-05), 2005.
- [59] T. R. WG1, "Spatial channel model for multiple input multiple output (MIMO) simulations," tech. rep., 3GPP TR 25.996 v6.1.0(2003-09), 2003.
- [60] J. He and M. Salehi, "Autonomic coordinated beamforming for multi-user MIMO-GBC," in *Proceedings of Conference on Information Sciences and Systems*, (Princeton, NJ), March 2006.
- [61] K. Hooli, M. Juntti, M. J. Heikkilä, P. Komulainen, M. Latva-aho, and J. Lilleberg, "Chip-level channel equalization in WCDMA downlink," *Journal on Applied Signal Processing (EURASIP)*, vol. 8, pp. 757 – 770, 2002.
- [62] T. Krauss, W. Hillery, and M. Zoltowski, "MMSE equalization for forward link in 3G CDMA: Symbol-level versus chip-level," in *Proceedings of the 10th IEEE Workshop on Statistical Signal and Array Processing, SSAP*, (Pocono Manor, PA), pp. 18 – 22, Aug 14 - 16 2000.
- [63] A. Bastug and D. T. Slock, "Optimization issues in combined chip and symbol level equalization for downlink WCDMA receivers," in *Proceedings of the Thirty-Eighth Asilomar Conference on Signals, Systems and Computers*, 2004.
- [64] L. Mailaender, "Linear MIMO equalization for CDMA downlink signals with code reuse," *IEEE Transactions on Wireless Communications*, vol. 4, no. 5, pp. 2423 – 2434, 2005.
- [65] A. Burg, M. Rupp, D. Perels, S. Haene, N. Felber, and W. Fichter, "Performance of MIMO-extended UMTS-FDD downlink comparing space-time RAKE and linear equalizer," in *Proceedings of the IEEE Vehicular Technology Fall Conference (VTC-Fall)*, (Orlando, Florida), October 2003.
- [66] R. Esmailzadeh and M. Nakagawa, "Pre-RAKE diversity combination for direct sequence spread spectrum mobile communications systems," *IEICE Trans. Commun.*, vol. E76-B, pp. 1008 – 1015, 1993.

- [67] I. Jeong and M. Nakagawa, "A novel transmission diversity system in TDD-CDMA," *IEICE Trans. Commun.*, vol. E81-B, pp. 1409 – 1416, 1998.
- [68] R. Choi, K. Letaief, and R. Murch, "CDMA pre-RAKE diversity system with base station transmit diversity," in *Proceedings of the IEEE Vehicular Technology Conference (VTC)*, pp. 951 – 955, 2000.
- [69] R. Choi, K. Letaief, and R. Murch, "MISO CDMA transmission with simplified receiver for wireless communication handsets," *IEEE Transactions on Communications*, vol. 49, pp. 888 – 898, 2001.
- [70] J. B. Wang, M. Zhao, S. D. Zhou, and Y. Yao, "A novel multipath transmission diversity scheme in TDD-CDMA systems," *IEICE Trans. Commun.*, vol. E82-B, pp. 1706 – 1709, 1999.
- [71] R. Irmer, A. N. Barreto, and G. Fettweis, "Transmitter precoding for spread-spectrum signals in frequency-selective channels," in *Proceedings of 3G Wireless*, (San Francisco, CA), pp. 939 – 944, 2001.
- [72] J. K. Han, M. W. Lee, and H. K. Park, "Principal ratio combining for pre/post-RAKE diversity," *IEEE Communications Letters*, vol. 6, pp. 234 – 236, 2002.
- [73] T. Eng, N. Kong, and L. Milstein, "Comparison of diversity combining techniques for Rayleigh fading channels," *IEEE Transactions on Communications*, vol. 44, pp. 1117 – 1129, 1996.
- [74] J. Winters and M. Win, "Hybrid-selection/optimum combining," in *Proceedings of the IEEE Vehicular Technology Spring Conference (VTC-Spring)*, 2001.
- [75] R. Irmer and G. Fettweis, "Combined transmitter and receiver optimization for multiple-antenna frequency-selective channels," in *Proceedings of WPMC*, 2002.
- [76] J. He and M. Salehi, "Low-complexity coordinated interference-aware beamforming for MIMO broadcast channels," in *Proceedings of the IEEE Vehicular Technology Conference (VTC)*, pp. 685–689, 2007.

- [77] K. Kusume, M. Joham, W. Utschick, and G. Bauch, “Efficient Tomlinson-Harashima precoding for spatial multiplexing on flat MIMO channel,” in *Proceedings of IEEE International Conference on Communications (ICC)*, vol. 3, pp. 2021–2025, May 2005.
- [78] C. Windpassinger and R. F. H. Fischer, “Low-complexity near-maximum-likelihood detection and precoding for MIMO systems using lattice reduction,” in *Proc. of Information Theory Workshop*, (Paris, France), pp. 345 – 348, March 2003.
- [79] C. Windpassinger, R. F. H. Fischer, T. Vencel, and J. B. Huber, “Precoding in multiantenna and multiuser communications,” *IEEE Transactions on Wireless Communications*, vol. 3, pp. 1305 – 1316, 2004.
- [80] M. Taherzadeh, A. Mobasher, and A. K. Khandani, “Communication over MIMO broadcast channels using lattice-basis reduction,” *IEEE Transactions on Information Theory*, vol. 53, pp. 4567 –4582, December 2007.
- [81] S. Shim, C.-B. Chae, and R. W. Heath Jr., “A lattice-based MIMO broadcast precoder with block diagonalization for multi-stream transmission,” in *Proceedings of IEEE Global Communications Conference (GLOBECOM)*, pp. 1–5, 2006.
- [82] E. Agrell, T. Eriksson, A. Vardy, and K. Zeger, “Closest point search in lattices,” *IEEE Transactions on Information Theory*, vol. 48, pp. 2201 – 2214, August 2002.
- [83] L. Babai, “On Lovasz lattice reduction and the nearest lattice point problem,” *Combinatorica*, vol. 6, no. 1, pp. 1–13, 1986.
- [84] M. O. Damen, H. E. Gamal, and G. Caire, “On maximum-likelihood detection and the search for the closest lattice point,” *IEEE Transactions on Information Theory*, vol. 49, pp. 2389 – 2402, October 2003.
- [85] C. Windpassinger, R. Fischer, and J. Huber, “Lattice-reduction-aided broadcast precoding,” *IEEE Transactions on Communications*, vol. 52, pp. 2057–2060, December 2004.

- [86] Y. H. Gan and W. H. Mow, “Complex lattice reduction algorithms for low-complexity MIMO detection,” in *Proceedings of IEEE Global Communications Conference (GLOBECOM)*, 2005.
- [87] J. Cuppen, “A divide and conquer method for the symmetric tridiagonal eigenproblem,” *SIAM J. Sci. Stat. Comp.*, vol. 8, no. 2, pp. 139 – 154, 1981.
- [88] G. H. Golub and C. F. V. Loan, *Matrix Computations*. The John Hopkins Univ. Press, 3rd ed., 1996.
- [89] Z. Chen and J. J. Dongarra, “Condition numbers of Gaussian random matrices,” *SIAM Journal on Matrix Analysis and Applications*, vol. 27, no. 3, pp. 603 – 620, 2005.
- [90] G. Taricco and E. Biglieri, “Space-time decoding with imperfect channel estimation,” *IEEE Transactions on Wireless Communications*, vol. 4, pp. 1874 – 1888, April 2005.
- [91] B. Hassibi and B. M. Hochwald, “How much training is needed in multiple-antenna wireless links?,” *IEEE Transactions on Information Theory*, vol. 49, pp. 951 – 963, April 2003.
- [92] M. Biguesh and A. Gershman, “Training-based MIMO channel estimation: a study of estimator tradeoffs and optimal training signals,” *IEEE Transactions on Signal Processing*, vol. 54, pp. 884 – 893, March 2006.
- [93] J. Niu and I.-T. Lu, “A new lattice-reduction-based receiver for MIMO systems,” in *Proceedings of Conference on Information Sciences and Systems*, 2007.
- [94] B. A. LaMacchia, *Basis Reduction Algorithms and Subset Sum Problems*. PhD thesis, Massachusetts Institute of Technology, 1991.
- [95] C. Windpassinger and R. Fischer, “Low-complexity near-maximum-likelihood detection and precoding for MIMO systems using lattice reduction,” in *Proceedings of Information Theory Workshop*, pp. 345–348, 2003.

- [96] S. Shim, C. Chae, and J. R.W. Heath, “A lattice-based MIMO broadcast precoder with block diagonalization for multi-stream transmission,” in *Proceedings of IEEE Global Communications Conference (GLOBECOM)*, (San Francisco, CA), 2006.
- [97] U. Erez and R. Zamir, “Achieving $1/2 \log(1 + \text{SNR})$ on the AWGN channel with lattice encoding and decoding,” *IEEE Transactions on Information Theory*, vol. 50, no. 10, p. 22932314, 2004.
- [98] J. Forney and G. David, “On the role of MMSE estimation in approaching the information-theoretic limits of linear Gaussian channels: Shannon meets Wiener,” in *Proceedings of Allerton Conference on Communications, Control, and Computing*, (Monticello, IL), p. 430439, 2003.
- [99] R. F. H. Fischer, *Precoding and Signal Shaping for Digital Transmission*. New York: Wiley, 2002.
- [100] J.-K. Zhang, A. Kavcic, and K. M. Wong, “Equal-diagonal QR decomposition and its application to precoder design for successive-cancellation detection,” *IEEE Transactions on Information Theory*, vol. 51, pp. 154–172, 2005.
- [101] S. Grant and K. Molnar, “Reduced complexity joint detection generalized RAKE receiver for WCDMA MIMO systems,” in *Proceedings of the IEEE Vehicular Technology Spring Conference (VTC-Spring)*, pp. 285 – 289, 2005.
- [102] T. Fulghum, D. Cairns, C. Cozzo, Y.-P. Wang, and G. Bottomley, “Adaptive generalized RAKE reception in DS-CDMA systems,” *IEEE Transactions on Wireless Communications*, vol. 8, pp. 3464 – 3474, 2009.
- [103] T. R. WG1, “Spreading and modulation(FDD),” tech. rep., 3GPP TR 25.213 v6.3.0(2005), 2005.
- [104] G. E. Bottomley, T. Ottosson, and Y.-P. E. Wang, “A generalized RAKE receiver for interference suppression,” *IEEE Journal on Selected Areas in Communications*, vol. 18, pp. 1536 – 1545, August 2000.

- [105] H. Hadinejad-Mahram, "On the equivalence of linear MMSE chip-level equalizer and generalized RAKE," *IEEE Communications Letters*, vol. 8, p. 7, January 2004.
- [106] D. A. Cairns, G. E. Bottomley, and Y.-P. E. Wang, "Low complexity parameter estimation for the generalized RAKE receiver," in *IEEE 11th Digital Signal Processing Workshop & IEEE Signal Processing Education Workshop*, 2004.
- [107] G. Kutz and A. Chass, "On the performance of a practical downlink CDMA generalized RAKE receiver," in *Proceedings of the IEEE Vehicular Technology Conference (VTC)*, 2002.
- [108] K. Hooli, M. Juntti, M. Heikkila, P. Komulainen, M. Latva-aho, and J. Lilleberg, "Chip-level channel equalization in WCDMA downlink," *EURASIP Journal on Applied Signal Processing*, pp. 757 – 770, 2002.
- [109] G. Kutz and A. Chass, "Low complexity implementation of a downlink CDMA generalized RAKE receiver," in *Proceedings of the IEEE Vehicular Technology Fall Conference (VTC-Fall)*, pp. 1357 – 1361, 2002.
- [110] H. Sui, E. Masry, and B. Rao, "Chip-level DS-CDMA downlink interference suppression with optimized finger placement," *IEEE Transactions on Signal Processing*, vol. 54, 2006.
- [111] S. Qureshi, "Adaptive equalization," in *Proceedings of IEEE*, vol. 73, no. 9, 1985.
- [112] M. Miyoshi and Y. Kaneda, "Inverse filtering of room acoustics," *IEEE Transactions on acoustics, speech, and signal processing*, vol. 36, no. 2, pp. 145 – 152, 1988.
- [113] T. Tuncer, "Deconvolution and preequalization with best delay LS inverse filters," *Elsevier Signal Processing*, vol. 84, no. 11, pp. 2207 – 2219, 2004.
- [114] W. Ray, "The inverse of a finite Toeplitz matrix," *Technometrics*, vol. 12, no. 1, pp. 153 – 156, 1970.